Tracing the source of anomalous geochemical patterns in soil, water and seepage gas near the Nazko volcanic cone, BC, NTS 93B/13.

Geoscience BC Report 2015-16

By

Ray Lett, Consultant
3956 Ashford Rd, Victoria, BC, Canada, V8P 3S5

Wayne Jackaman, Noble Exploration Services Ltd.
3890 Trailhead Drive, Jordan River, BC, Canada, V9Z 1L1

December, 2015

Executive Summary

Travertine deposits and CO_2-rich gas seepages, known to be indicators of geothermal activity, are common in two wetlands, informally named the North and South Bogs, near the Nazko volcanic cone, BC. Extensive $CaCO_3$ -rich mud deposits mixed with organic soil are an unusual feature of the bogs and are probably formed by a reaction between dissolved Ca in bog surface water and CO_2-rich gas seeping through the water. Although the travertine and CO_2-rich gas seepages may suggest the existence of sub-surface geothermal activity, the bog ground and surface water temperatures are no anomalous. The geochemistry of soil, water, travertine, bedrock, vegetation and CO_2 -rich seepage gas sampled from the Nazko bogs and surrounding area has been studied to detect anomalous geothermal indicator elements. Analysis of ground water, surface water, stream water and lake water samples for trace elements, temperature, pH, alkalinity and dissolved CO_2 found that while geothermal pathfinder elements, Li, Sr, Rb and B are elevated in bog ground and surface water, their concentrations are lower than those reported in the hot springs at geothermal fields where travertine deposits and CO_2-rich gas seepages are abundant. Other geothermal indicators Cl and Hg could not be detected in the bog water. Lithium Sr, Rb and B levels are anomalous in the organic soil near a small travertine cone in the North Bog. Water accumulating at the base of the travertine cone shows vigorous CO_2-rich gas seeping through, an unusually low (<6^{o}C) water temperature and has traces of dissolved As and Ni. The anomalous Li, Rb, Sr and B in the North Bog water and soil may be evidence of a deeper, warmer fluid that has cooled during transport to the surface. However, $\delta^{2}H$ and $\delta^{18}O$ isotope data and absence of Cl suggests the bog water source is mainly meteoric. Aragonite-rich carbonate rock from the travertine cone-CO_2 vent wall suggest a mineralizing water temperature to have been higher in the past. While there are no visible springs the actual point of ground water discharge may be concealed beneath the bog sediment.

High Hg concentrations in soil and rock could reflect past hot spring activity. However, the source of the Hg appears to be cinnabar in a surface boulder and as grains in till. The absence of detectable Hg in bog water suggests that the Hg is not related to current geothermal activity. Carbon dioxide-rich gas, sampled from seepages in the North and South Bog has $^{3}He/^{4}He$ ratios between 2.55 and 5.94 $_{RA}$ and a ^{4}He content of up to 120 ppm. The $^{3}He/^{4}He$ ratios suggest that the He is from mantle degassing and the CO_2 could be derived from the reaction between hot fluids and crustal carbonate rocks. Although there are presently subtle geochemical indicators for sub surface geothermal activity the current heat source is believed to be very deep. The presence of He, the anomalous $^{3}He/^{4}He$ ratios and previously measured $\delta^{13}C$ values between – 6.2 to – 6.9 $^{o}/_{oo}$ PDB in the CO_2 seepage gas are evidence for a mantle heat source in the area beneath the Nazko Cone.

Table of Contents

Figures

Figures con't

Tables

1. Introduction

Two wetlands, informally named the North and South Bogs, near the Nazko volcanic cone, British Columbia have numerous CO_2 gas seepages, travertine deposits and organic soil mixed with calcium carbonate (Figure 1.1, Figure 1.2). Although there are no actual hot springs, the CO_2 seepages, travertine deposits, recent seismic activity (Cassidy et. al, 2007) and Holocene volcanism suggest possible presence of a concealed, geothermal heat source. During exploration in 2012, Alterra Power Corp. confirmed that the seepage gas was predominantly CO_2 with traces of CH_4 and He (Hickson, pers comm, 2013; Vigouroux, pers comm, 2013).

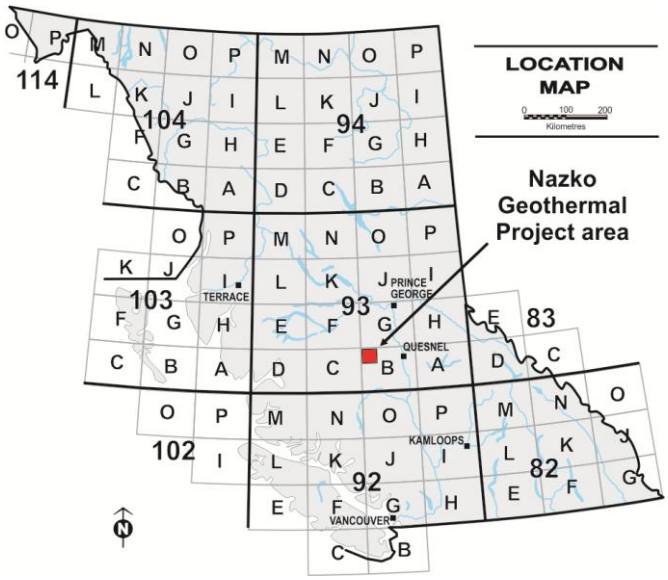

Figure 1.1. Location of study area.

Lett and Jackaman (2013) studied the soil, water and rock geochemistry in the bogs and in the surrounding area to detect the presence of a concealed geothermal heat source. They found the highest bog water temperature is 20.1°C and concluded that the upwelling of thermal water into the bogs from depth is unlikely. The water is typically alkaline with high concentrations of dissolved Ca and CO_2 and elevated dissolved Li, Sr, Rb and B. However, concentrations of Li and B are lower than reported in spring water from known geothermal fields (Pasvanoğlu, 2013).

A vigorous flow of CO_2 through water in a small travertine cone on the edge of the North Bog was observed during field work in 2013. The water accumulating in bottom of the cone has an unusually low temperature (less than 6°C) with elevated dissolved Fe (1000 ppb) and Ni (44 ppb) concentrations. Repeated water sampling of this water over several months revealed little

change in its temperature and trace element chemistry. Ground water flowing through glacial sediment on hill slopes above the bog was considered one source for the elevated Ni.

Calcium carbonate-rich organic soil and travertine on the surface of the North and South Bogs are considered to have formed when dissolved Ca up to 358 ppm in surface water mixes with CO_2 seeping to the bog surface thereby precipitating carbonate minerals. Detailed soil sampling revealed that the B and Li concentrations in well-drained mineral soil and carbonate-rich organic bog soil are similar. However, As, Ni, Ag and Cu sharply increase at the bog margin where the well-drained soil becomes water-saturated and organic rich. High Hg values (> 1 ppm) are also present in the mineral soil north east the North Bog.

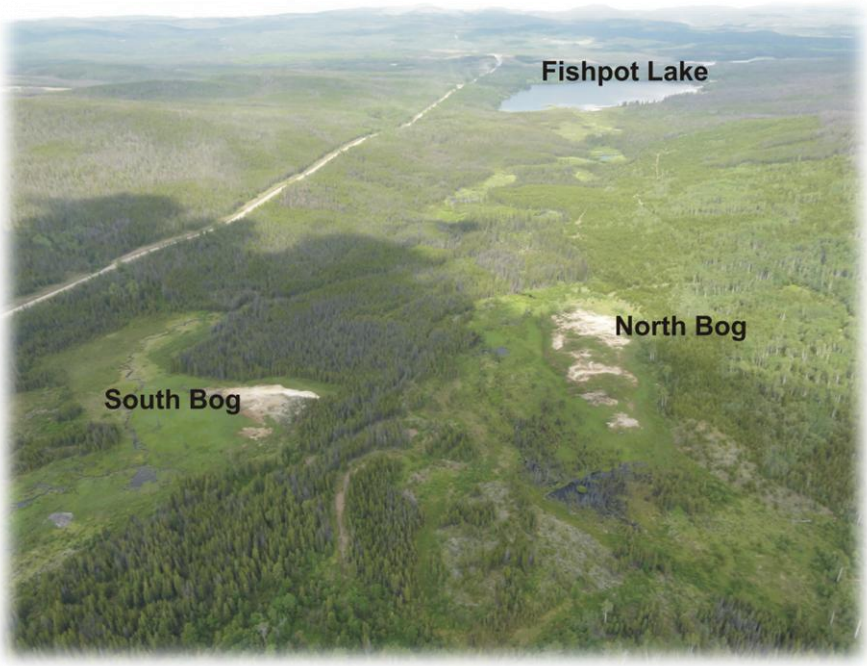

Figure 1.2. Panorama of the North and South Bogs and Fishpot Lake to the west.

While there is presently tenuous evidence for shallow geothermal activity near the Nazko Cone, results of the 2013 geochemical study raise a number of questions including:

- What Hg levels exist in bog and stream water since there is a high Hg concentration in mineral soil at one site near the North Bog? Mercury is not only a potential geothermal pathfinder and at high concentrations in water, soil and soil gas can also be an environmental concern.
- To what extent can the solubility of carbonate and silicate minerals in bog waters be useful as an indicator for geothermal activity?
- To what extent can soil geochemistry be useful for indicating geothermal activity?

- What is the source for the water in the bog, the origin of the travertine and the source for the CO_2?

Preliminary results of field work in 2014 to address some of these questions have been previously reported by Lett and Jackaman, (2015). Geoscience BC Report, 2015-16 compiles all of the geochemical data generated from sampling in 2013, 2014 and 2015 including re-sampling and the analysis of ground and stream water from the North Bog, soil and tree bark sampling around the travertine cone -CO_2 seep in the North bog, and sampling CO_2 -rich seepage gas for $^3He:/^4He$ isotope analysis.

2. Geology and Surface Environment

Geology and the surface environment of the area surrounding the Nazko Cone have been summarized by Lett and Jackaman, (2014, 2015). The North and South bogs lie in the Anahim volcanic belt, an east-trending cluster of Pleistocene-Holocene volcanoes, the most easterly of which is the Nazko cone (Figure 2.1). Bevier et al, (1979) proposed that the volcanism reflects migration of the North American tectonic plate over a mantle hot spot. Much of the surrounding area is underlain by Eocene Ootsa Lake Group, Miocene Endako Group and Pleistocene-Holocene volcanic rocks and by clastic sedimentary rocks of the Cretaceous Taylor Creek formation (Riddell, 2011, Talinga and Calvert, 2014, Angen *et al.* 2015). Glacial deposits covering the bedrock are a combination of till and glacio-fluvial sediments of variable, but unknown thickness.

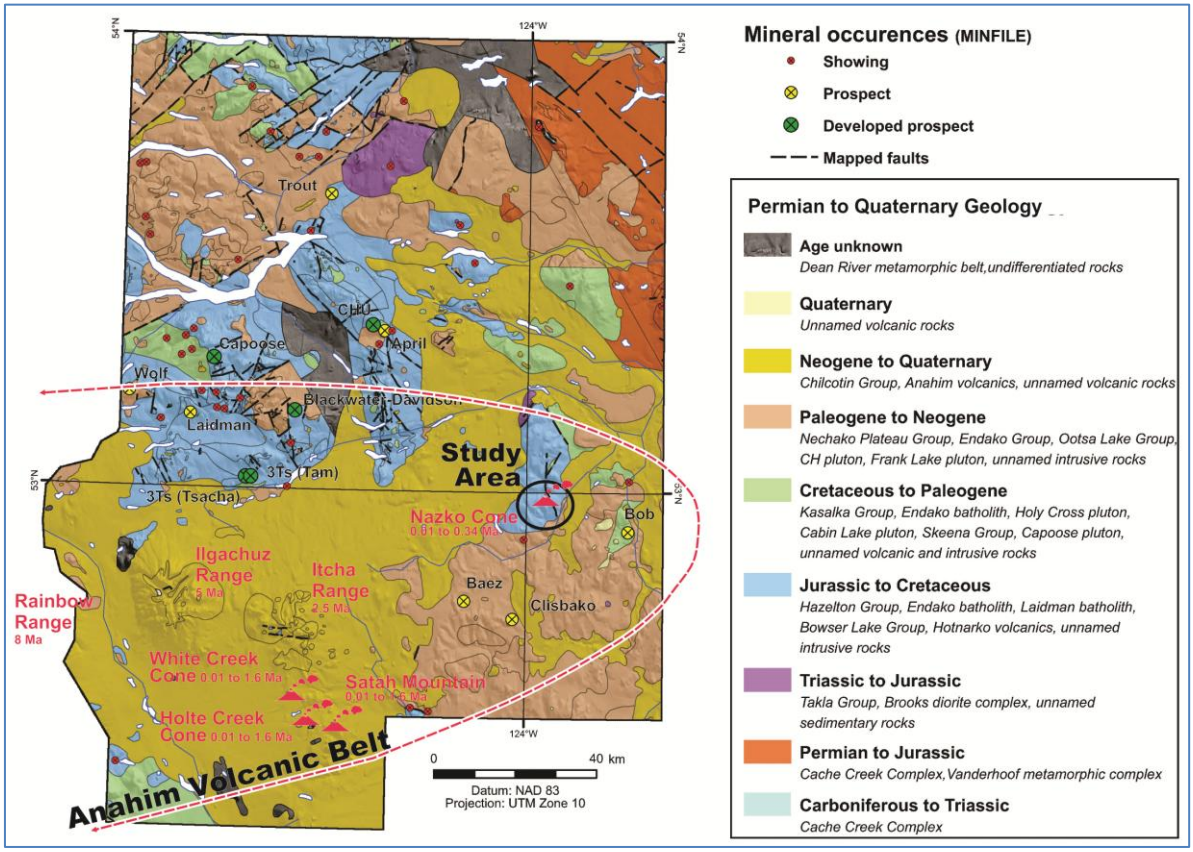

Figure 2.1. Geology of the Anahim Volcanic Belt

Souther *et al.* (1987) estimated the Nazko volcanism to have started during the Fraser Glaciation followed by post glacial ejection of red pyroclastic ash, lapilli and volcanic bombs from the cone. An ash layer, found in a bog near the cone, was interpreted by the authors to have been the result of an eruption around 7200 years BP when, in addition to the ash fall, mafic olivine basalt lava flowed from the volcano to the south and west. Souther et al. (1987) classified this larva as a basanite and concluded that the alkaline basalt was generated from hot spot related mantle sources. There has been no volcanic activity since the cone formed, but an earthquake swarm in 2007 near the Nazko cone (Cassidy *et al.* 2011) and an interpretation of seismic data by Kim et al. (2014) and Hutchinson (2012) suggested the existence of magma in the lower crust between 22 and 36 km depth. Hutchinson (2012) considered that there was strong evidence for Nechako swarm to be generated by the expansion and propagation of magma in the lower crust based on his analysis of the seismic data. He concluded that the two spatially distinct regions of seismic activity identified by his analysis reflected crustal emplacement of two mantle magma bodies with sills and branching dikes between 27 and 29 km depth. The earthquake swarm was interpreted by Hutchinson to be caused by the brittle failure and fracturing of rock in the lower crust by buoyantly rising magma or by an injection of new magma from a mantle source.

Figure 2.2. Fresh carbonate precipitate on the surface of the South Bog.

Hickson *et al.* (2009) identified potential environmental hazards and their impact on the area around the cone if the seismic activity led to an eruption. They also mapped the extent of ash and post glacial larva flows and monitored CO_2 emissions around the cone. The CO_2 was measured with a hand-held Vaisala GM-70 CO_2 system connected via tygon tubing to a 5 mm ID metal probe inserted about 30 cm into the ground (Williams-Jones, pers comm, 2015).

Sedge and scattered wetland shrubs, calcium carbonate-rich mud, stagnant pools or slow moving streams, small, isolated areas of travertine, forest dominated bog, small ponds and meandering streams are features of the North and South bogs (Figure 2.2). Vegetation ranges from scattered willow and spruce stands in the wetland to a second-growth lodge pole pine (*Pinus contorta)* canopy on the surrounding upland. Luvisolic and brunisolic soils have formed on the hill slope above the wetland and gleyoslic soil is typical of the poorly drained bog margin. Peat mixed with a calcium carbonate-rich mud is the most common bog sediment. The depth of the deposit is unknown, but exceeds 3 m. Travertine, typically a rusty to white coloured rubble, forms small, isolated mounds on the bog surface. A small, 35 cm high cone-shaped travertine deposit identified in 2013 on the northern edge of the North bog (Figure 2.3) has a partially submerged vent from which there is a steady flow of CO_2. A second CO_2 seep from the center of a travertine pavement in the South Bog, active in 2013 ceased to have any detectable gas flow in 2015. However, in 2015 several new seepages with an active CO_2-rich gas flow, but no visible travertine deposit were observed in the North Bog.

Figure 2.3. Travertine mound with bubbling carbon dioxide in the North Bog.

3. Field Work

In August 2014 field work in the Nazko bogs and surrounding area included:

- Sampling water from the travertine cone - CO_2 vent, from shallow dug pits and from the stream flowing through the North Bog. An Oakton PCSTestr 35 meter was used to measure the pH, temperature, salinity and conductivity of the water at each site. Water flow, water table depth and other site features were recorded. Eight water samples were collected in 2014 and 6 in 2015 for trace element and stable isotope analysis.
- Sampling Ah (humus), B and C soil horizons and lodge pole pine (*Pinus contorta)* outer bark down vertical profiles at sites in and around the North bog. A total of 20 bark and 67 soil samples were collected. At each site the pH of a minus 2 mm fraction of the mineral soil beneath the humus was measured on a soil - distilled water slurry (1:1 vol:vol) with an Oakton PCSTestr 35 meter.
- Sampling travertine in the North and South bogs (5 samples) for stable isotope and mineral (X-ray diffraction) analysis.
- Re-sampling till at seven sites where TREK regional till samples had been taken in 2013 (Jackaman, 2014). Soil Ah and B horizon and tree bark were also sampled at these sites.
- Sampling the CO_2-rich from four seeps in the North and South Bogs in May 2015 for He isotope analysis. The gas was collected in Cu tubes supplied by Woods Hole Oceanographic Institute using a water displacement system to prevent contamination

by atmospheric He. The Cu tubes were clamped and sealed after the water had been displaced from the tube by the CO_2.-rich gas

Figure 3.1 shows the distribution water, soil, bark, bulk till and travertine sites in 2014.

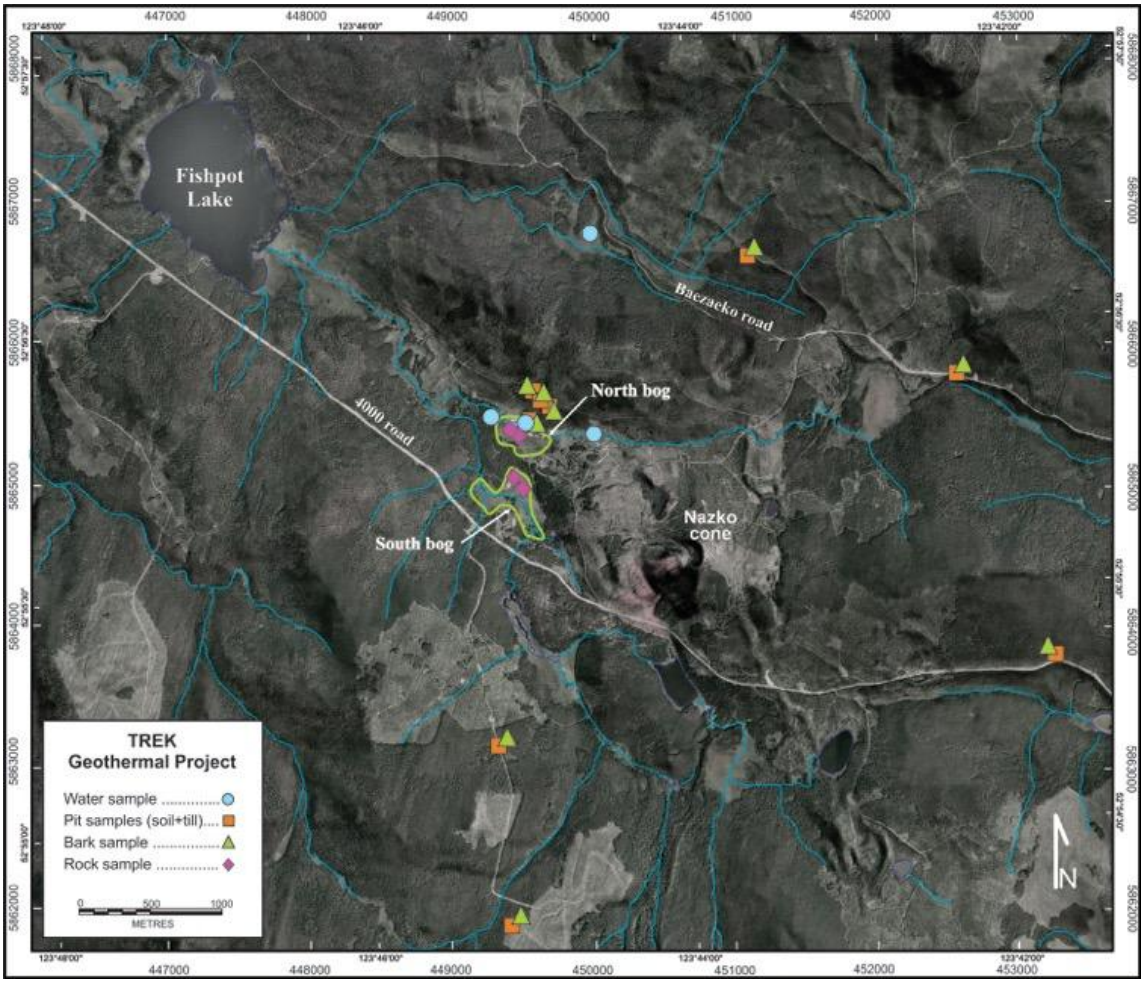

Figure 3.1. Water, soil, tree bark and rock samples collected in 2014.

4. Sample Preparation and Analysis

Four water samples were collected in HDPE bottles at each site for the following analysis:

- Within 6 hours of collection one of the water samples was analysed using Hach field test kits for total alkalinity and dissolved CO_2.

- A second sample was stored at 4°C for later analysis by ALS Environmental, Burnaby for hardness, total alkalinity by titration and for F, Cl, Br, NO_3, NO_2 and SO_4 by ion chromatography.

- A third sample was filtered through a Phenex™ polyethersulfone (*PES*) 0.45 micron membrane filter, acidified with ultrapure nitric acid to pH 1 and later analysed by ALS Environmental, Burnaby, BC, Canada for Ag, Al, As, Ag, Ba, Be, Bi, B, Cd, Ca, Cs, Cr, Co, Cu, Ga, Fe, Pb, Li, Mn, Mo, Ni, Na, P, K, Re, Rb, Sb, Se, Si Sr, Sn, Te, Tl, Ti, U, V, Y, Zn and Zr by high resolution mass spectrometry (ICPMS). A distilled-deionised water sample blank and a sample of the National Research Council Canada (NRCC) river water standard SLRS 3 were also analysed with the water samples.

- A fourth sample, filtered through a Phenex™ polyethersulfone (*PES*) 0.45 micron membrane filter and acidified with ultrapure hydrochloric acid to pH 1 was stored in a glass vial for later analysis by ALS Environmental for dissolved Hg.

- In May 2015 a fifth sample was collected for stable isotope analysis in a tightly capped, 50 ml Nalgen bottle. The samples were analysed at the University of Calgary for $\delta^{18}O$ by CF-GasBench-IRMS, $\delta^{2}H$ by TCEA-CF-IRMS and $\delta^{13}C$ and dissolved inorganic carbon (DIC) CF-GasBench-IRMS. The methods are documented in more detail in Appendix B.

- Soil samples were air dried at <30°C and sieved to –80mesh (<0.177mm) before analysis. A 0.5 g samples of the –80 mesh fraction of the soil was analyzed at Bureau Veritas Commodities Canada Limited, Vancouver (formerly Acme Analytical Laboratories Ltd.) for Ag, Al, As, Au, B, Ba, Be, Bi, Ca, Cd, Co, Cr, Cs, Cu, Fe, Ga, K, Li, Mn, Mo, Na, Ni, P, Pb, Rb, Rh, Sb, Se, Sn, Sr, Te, Th, Ti, Tl, U, V, Y, Zn and Zr by a HNO_3-HCl-H_2O (1:1:1 v/v) (modified aqua regia) digestion followed by inductively coupled plasma–mass spectrometry (AR-ICPMS).

- Tree-bark samples were analysed for trace elements at Bureau Veritas Commodities Canada Limited, Vancouver. The samples were washed with de-mineralized water, air-dried at <30°C, macerated and 1 g of the macerated bark digested in HNO_3 then in aqua regia before analysis for Ag, Al, As, Au, B, Ba, Be, Bi, Ca, Cd, Ce Co, Cr, Cs, Cu, Fe, Ga, Hf, Hg, In, K, Li, Mn, Mg, Mo, Na, Nb, Ni, P, Pb, Pb, Pt, Rb, Rh, Re, Sb, Se, Sn, Sr, Ta, Te, Th, Ti, Tl, U, V, Y, Zn and Zr by Ar-ICPMS.

- Travertine and soil samples were analysed for major oxides and minor elements at Bureau Veritas Commodities Canada Limited, Vancouver. The travertine samples were air dried at < 30°C and milled to –150 mesh (<0.050mm). A 0.1 g the –150 mesh fraction

of the travertine or - 80 mesh fraction of the soil was analyzed for Al_2O_3, SiO_2, Fe_2O_3, CaO, MgO, MnO, P_2O_5, Ba, Ce, Co, Cu, Nb, Ni, Sc, Sr, Y, Zn and Zr by lithium borate fusion–ICP-ES/MS. The samples were also analysed for loss-on-ignition at 1100°C; and for total C and total S by LECO combustion.

- The travertine samples were also analysed for $\delta^{18}O$ and $\delta^{13}C$ ratios in calcite at Queen's University, Ontario, Facility for Isotope Research by reacting approximately 1 mg of powdered material with 100% anhydrous phosphoric acid at 72°C for 4 hours. The CO_2 released was analyzed using a Thermo-Finnigan Gas Bench coupled to a Thermo-Finnigan Delta^{Plus} XP Continuous-Flow Isotope-Ratio Mass Spectrometer (CF-IRMS). The $\delta^{18}O$ and $\delta^{13}C$ values are reported using the delta (δ) notation in per mil (‰), relative to Vienna Pee Dee Belemnite (VPDB) and Vienna Standard Mean Ocean Water (VSMOW) respectively, with precisions of 0.2 ‰.

- Modal mineralogy analysis of the travertine samples (e.g. percentage calcite, magnesite) was carried out at Department of Earth Ocean Atmospheric Sciences, University of British Columbia. The samples were reduced to the optimum grain-size range for quantitative X-ray diffraction analysis (<10 µm) by grinding under ethanol in a vibratory McCrone Micronising Mill for 10 minutes. Step-scan X-ray powder-diffraction data were collected over a range 3-80°2θ with CoKα radiation on a Bruker D8 Advance Bragg-Brentano diffractometer equipped with an Fe monochromator foil, 0.6 mm (0.3°) divergence slit, incident- and diffracted beam Soller slits and a LynxEye-XE detector. The long fine-focus Co X-ray tube was operated at 35 kV and 40 mA, using a take-off angle of 6°.

- Seepage gas samples were analysed for $^3He/^4He$ ratio and ^4He content. Helium was extracted and measured by mass spectrometry in the Isotope Geochemistry Facility at Woods Hole Oceanographic Institution (Kurz et al. 2004). Details of the procedure are in Appendix B.

5. Water Geochemistry

5.1 Water Data Quality

An ultrapure water sample and two samples of the National Research Council Canada (NRCC) water standard SLRS 3 were analysed with water samples collected in 2014 and 2015 to monitor potential contamination during filtering and to assess the reliability of the results. Ultrapure water, supplied by ALS Global, was filtered at the sample site and then acidified with nitric acid to produce the blanks. The ALS reported detection limits and duplicate results of the blank water and the standard SLRS 3 analysed with the samples collected in 2014 and in 2015 are listed in Table 1. Only the samples collected in 2014 were analysed for Hg. Analyses of the filtered water blanks reveal that only Sr was detectable in the blanks at a concentration above the detection limit. The %RSD (percent relative standard deviation) calculated from duplicate SLRS 3 standard As, B, Be, Li, Rb, Th, Zn and Zr analyses range from more that 10 percent to 48 percent (B). While several of these elements (B, Li) are geothermal pathfinders their large variability based on duplicate analyses reflects a concentration in the standard close to the detection limit. Where NRCC do report a recommended value for an element in SLRS 3, it is within 10 percent of the recommended value.

Analyte	DL	2014 Blank	2015 Blank	2014 - SLRS 3	2015 - SLRS 3	% RSD	SLRS 3*	Analyte	DL	2014 Blank	2015 Blank	2014 - SLRS 3	2015 - SLRS 3	% RSD	SLRS 3*
Al ppb	1	-1.0	-1.0	30.60	29.50	2.588	31	Na ppm	2	-2	-2	2.600	2.700	2.668	2.3
Ag ppb	0.005	-0.005	-0.005	-0.005	-0.005	0.000		Ni ppb	0.2	-0.2	-0.2	0.770	0.780	0.912	0.83
As ppb	0.05	-0.05	-0.05	0.970	0.742	18.834	0.72	P ppm	0.3	-0.3	-0.3	-0.300	-0.300	0.000	
B ppb	5.00	-5.00	-5.00	13.100	6.400	48.591		Pb ppb	0.05	-0.05	-0.05	0.070	0.072	1.992	0.068
Ba ppb	0.1	-0.1	-0.1	15.600	14.700	4.201	13.4	Rb ppb	0.02	-0.02	-0.02	1.720	2.190	16.999	
Be ppb	0.005	-0.005	-0.005	0.008	0.012	29.159	0.005	Re ppb	0.005	-0.005	-0.005	-0.005	-0.005	0.000	
Bi ppb	0.05	-0.05	-0.05	-0.050	-0.050	0.000		Sb ppb	0.01	-0.01	-0.01	0.170	0.167	1.259	0.12
Ca ppm	0.050	-0.05	-0.05	6.280	6.000	3.225	6	Se ppb	0.2	-0.2	-0.2	-0.200	-0.200	0.000	
Cd ppb	0.005	-0.005	-0.005	0.015	0.017	8.730	0.013	Si ppm	0.05	-0.05	-0.05	1.800	1.760	1.589	
Co ppm	0.05	-0.05	-0.05	-0.050	-0.050	0.000	0.027	Sn ppb	0.2	-0.2	-0.2	-0.200	-0.200	0.000	
Cr ppb	0.5	-0.5	-0.5	-0.500	-0.500	0.000	0.3	Sr ppm	0.001	-0.00005	0.00014	0.033	0.035	5.036	0.028
Cs ppb	0.005	-0.005	-0.005	0.007	0.007	7.226		Te ppb	0.010	-0.010	-0.010	-0.010	-0.010	0.000	
Cu ppb	0.2	-0.2	-0.2	1.550	1.420	6.190	1.35	Th ppb	0.005	-0.005	-0.005	0.037	0.017	51.663	
Fe ppb	30.0	-30.0	-30.0	104.0	102.0	1.373	100	Ti ppb	0.2	-0.2	-0.2	0.680	0.710	3.052	
Ga ppb	0.05	-0.05	-0.05	-0.050	-0.050	0.000		Tl ppb	0.002	-0.002	-0.002	0.007	0.008	5.657	
Hg ppb	0.1	-0.1	nm	-0.050	nm			U ppb	0.002	-0.002	-0.002	0.044	0.043	1.942	0.045
K ppm	2	-2	-2	-2.000	-2.000	0.000	0.7	V ppb	0.05	-0.05	-0.05	0.301	0.311	2.311	0.3
Li ppb	0.2	-0.2	-0.2	0.850	0.530	32.793		W ppb	0.01	-0.01	-0.01	-0.010	-0.010	0.000	
Mg ppm	0.1	-0.1	-0.1	1.690	1.710	0.832	1.6	Y ppb	0.005	-0.005	-0.005	0.122	0.120	1.169	
Mn ppb	0.2	-0.2	-0.2	4.050	3.750	5.439	3.9	Zn ppb	1.00	-1.00	-1.00	1.700	1.200	24.383	1.04
Mo ppb	0.05	-0.05	-0.05	0.188	0.218	10.450	0.19	Zr ppb	0.05	-0.050	-0.050	0.118	0.070	36.108	

Table 1. Analytical detection limits (DL), 2014 and 2015 sampling blank and National Research Council Canada river water standard SLRS 3 analyses. SLRS 3* - NRCC recommended values. nm - not measured.

Sample	2013-1013	2013-1038	2014-1003	2014-2004	15 TREKGT1	Mean	% RSD
Date	29-Jul-09	6-Aug-13	23-Jun-14	26-Aug-14	29-May-15		
Temp	5.6	5.9	5.8	5.5	5.7	5.7	2.8
pH	6.48	6.37	6.31	6.44	6.32	6.4	1.2
CO_2	400	600	1450	1210	500	832	56.2
Tot Alk ppm	2400	2410	4600	2720	1400	2706	43.2
F ppm	0.48	0.45	nm	0.57	nm		
SO_4 ppm	18	18	nm	19	nm		
Al ppb	-1.0	-1.0	-30.0	2.4	-1.000	-6.1	-220
As ppb	2.02	2.56	1.79	2.51	1.13	2.0	29.3
B ppb	380	343	369	353	331	355	5.5
Ba ppb	174	187	159	232	198	190	14.5
Be ppb	0.040	0.044	0.054	0.059	0.040	0.0	18.2
Ca ppm	231	235	207	231	207	222	6.3
Cd ppb	0.092	0.0376	0.044	0.025	0.053	0.1	50.2
Co ppb	2.23	2.24	1.95	2.07	1.900	2.1	7.5
Cs ppb	1.77	1.73	1.73	2.18	2.130	1.9	11.9
Cu ppb	-0.20	-0.2	0.50	-0.20	-0.200	-0.1	-521
Fe ppb	446	3920	1330	5240	130	2213	102
Hg ppb	nm	nm	nm	-0.050	nm	-0.1	
K ppm	31.1	31.5	30	32.1	28.0	30.5	5.3

Sample	2013-1013	2013-1038	2014-1003	2014-2004	15 TREKGT1	Mean	% RSD
Date	29-Jul-09	6-Aug-13	23-Jun-14	26-Aug-14	29-May-15		
Li ppb	342	323	378	436	329	362	12.9
Mg ppm	221.0	239	267	295	259	256.2	11
Mn ppb	197	193	142	194	145	174	16.1
Mo ppb	0.574	0.459	0.38	0.4210	0.350	0.4	19.9
Na ppm	298	307	275	304	264	290	6.6
Ni ppb	43.8	44	36.5	40.8	40.6	41.1	7.4
Rb ppb	39.6	39.3	37.1	39.1	39.5	38.9	2.7
Re ppb	0.0069	0.0064	0.007	-0.0050	0.007	0.0	120
Sb ppb	0.055	0.039	0.05	0.032	0.023	0.0	32.7
Si ppm	9.75	9.63	9.3	8.54	10.3	9.5	6.8
Sr ppm	7.53	7.68	7.16	9.37	7.16	7.8	11.8
Te ppb	-0.010	-0.01	-0.010	0.013	-0.010	0.0	-190
Ti ppb	0.35	0.23	0.3	0.37	-0.200	0.2	112
Tl ppb	0.335	0.323	0.36	0.340	0.401	0.4	8.6
U ppb	0.113	0.12	0.125	0.159	0.102	0.1	17.3
V ppb	1.230	1.08	0.81	1.560	0.322	1.0	46.6
Y ppb	0.270	0.358	0.185	0.478	0.129	0.3	48.9
Zn ppb	11.2	10.5	12	11	7.800	10.4	15.2
Zr ppb	2.43	1.73	0.38	1.73	1.950	1.6	46.4

Table 2. Analytical results for North Bog travertine-carbon dioxide vent water sampled in 2013, 2014 and 2015. Chloride, Br, Cr, Ga, P, Th, Sn and Pb are not reported here because values in all samples are below detection limit. nm - not measured.

5.2 Water Results - Trace and minor element chemistry

Figure 5.1 and 5.2 show locations of the water samples collected in 2013, 2014 and 2015 in and from the region around the Nazko Bogs. A map in Appendix G shows the site of a water sample collected from a seep near Redwater Creek.

Lithium B, As, Rb, Sr, Si and Hg are recognised geochemical pathfinders for geothermal activity and in hot spring and thermal well waters where their concentration may reach several hundred parts per million. For example, water from wells in Eastern Turkey, analysed by Pasvanoğlu (2013), has up to 138 ppm Si, 2.7 ppm Li, 37 ppm B, 2820 ppm Sr, 5070 ppb As and 0.3 ppb Hg and a water temperature up to 78^{o}C. The area is also seismically active, has CO_2-rich gas seepages that carry other gases including He. However, the ground and surface water in the Nazko bogs sampled by Lett and Jackaman (2013) only has up to 637 ppb B, 2.6 ppb As, 547 ppb Li, 56.1 ppb Rb and 15.9 ppm Sr. Figure 5.3 compares the Li and B range and median values for the two studies.

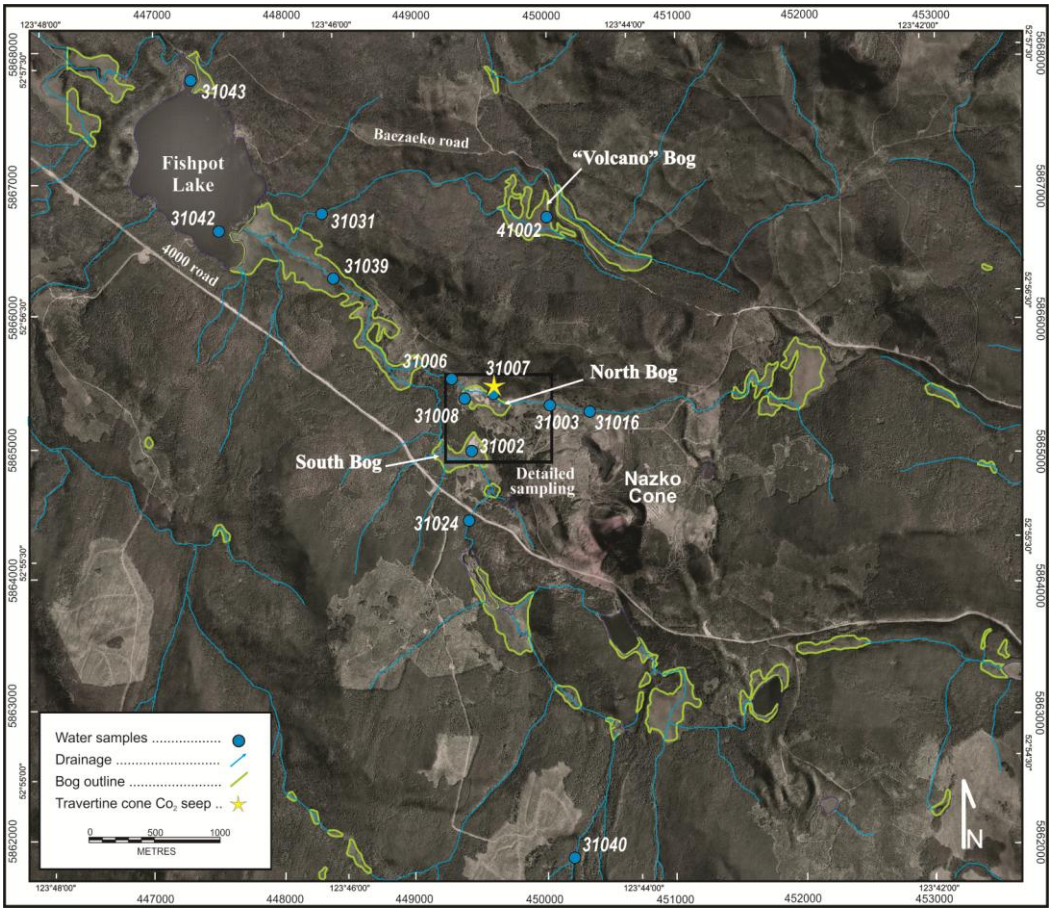

Figure 5.1. Nazko wetlands area water sample sites.

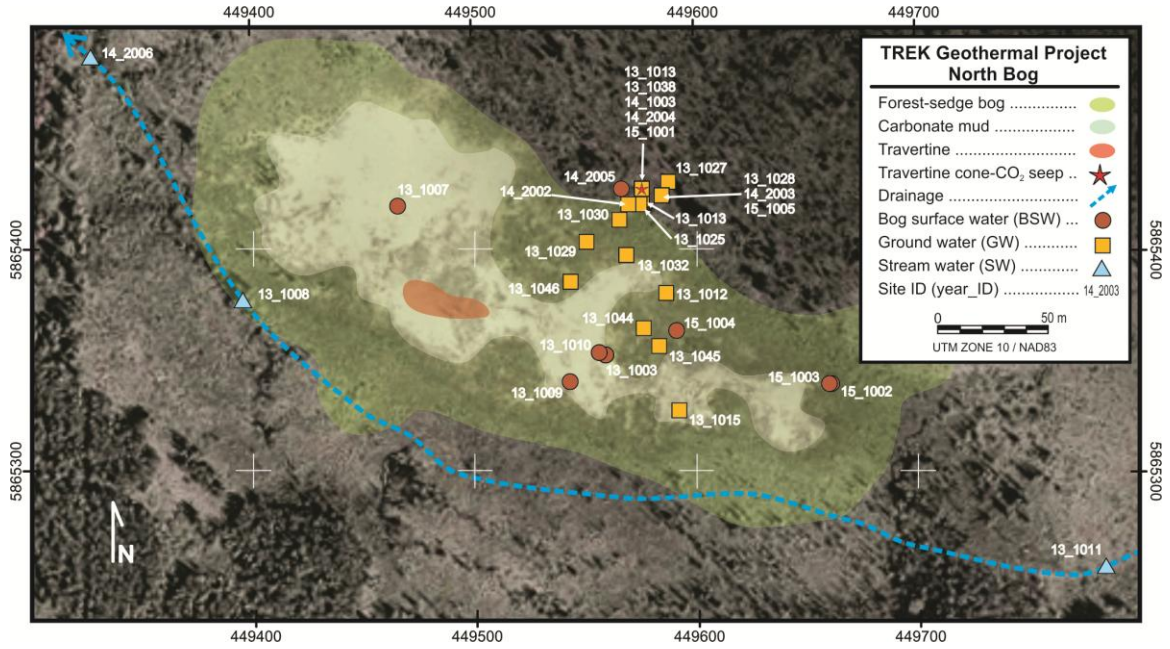

Figure 5.2. North Bog water sample sites.

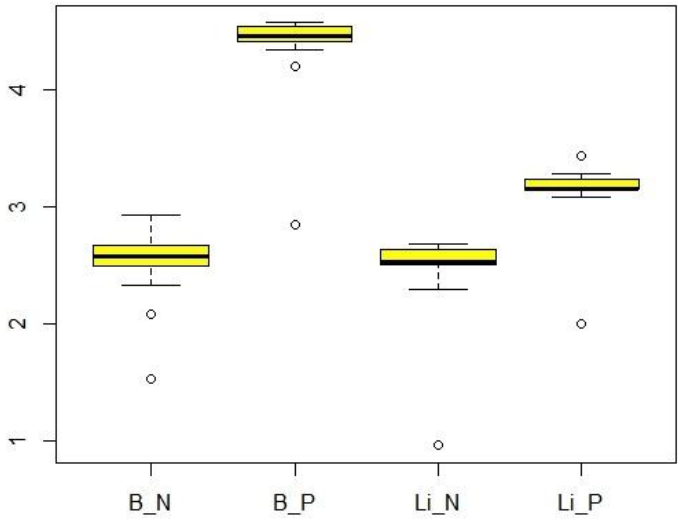

Figure 5.3. Lithium and B in Nazko (N) ground water and thermal water (P) sampled by Pasvanoğlu (2013). Units in parts per billion (ppb)

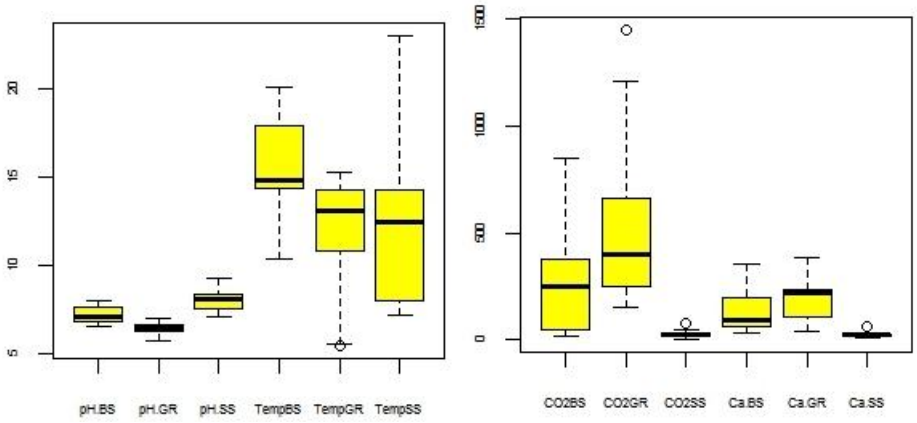

Figure 5.4. Temperature, pH, Ca and CO_2 in Nazko wetland system (GR) bog surface water (BS) and stream water (SS). Temperature units are in ^{o}C; Ca and CO_2 are in ppm.

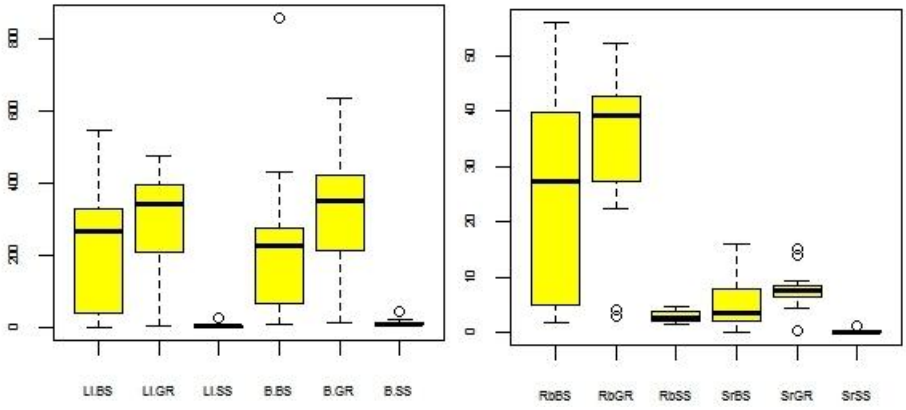

Figure 5.5. Lithium, B, Sr and Rb in Nazko wetland system (GR) bog surface water (BS) and stream water (SS). Boron, Rb and Li units are in ppb; Sr is in ppm.

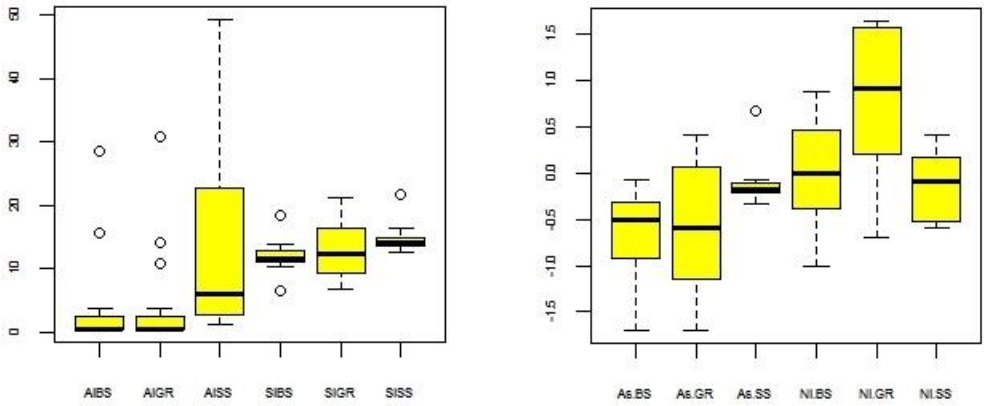

Figure 5.6. Aluminum, Si, As and Ni in Nazko wetland system (GR) bog surface water (BS) and stream water (SS). Aluminium, As and Ni units are in ppb; Si is in ppm.

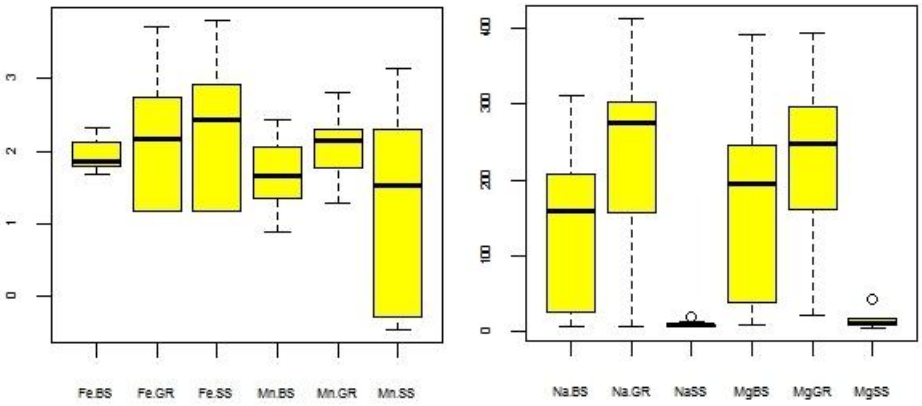

Figure 5.7. Fe, Mn, Na and Mg in Nazko wetland system (GR) bog surface water (BS) and stream water (SS). Fe and Mn units are in Log ppb; Na and Mg are in ppm.

Differences between ground and surface water chemistry reflect the mixing of stream and spring water from different sources. For example, the box plot in Figures 5.4 shows that the Nazko North and South Bog ground water is cooler, more acid, has a higher dissolved CO_2 and Ca content compared to surface and stream water. The water in Fishpot Lake is the most alkaline (pH 9.26) and has the highest temperature (23^{o}C) of all waters. Median and interquartile range for Li, Sr , Rb and B values in bog ground water are higher than those in bog surface water and are, in turn, much higher in stream water (Figure 5.5). However, Li, Sr, Rb and B maximum and outliner values for surface water are higher than ground and stream water. Compared to Li, Sr, Rb and B, Al is much higher in the stream water than in bog water, but Si levels in Figure 5.6, are similar in all three water types. Silicon concentrations are slightly higher in stream water with lower values in ground and surface water. The highest As and Ni values found are in water from the travertine cone-CO_2 vent (Figure 5.6), but 4.7 ppb As was measured in water sampled in 2014 from the stream flowing through the North Bog. However, in 2013, the stream water at this site was found to contain less than 1 ppb As. Figure 5.7

compares Fe with Mn and Na with Mg. Stream water has the highest Fe and Mn values, although Table 2 reveals that the ground water from the travertine cone-CO_2 vent has more than 5000 ppb Fe. The distribution of Na is similar to Mg in bog waters and while these elements are highest in ground water they are very low in stream water. While there are insufficient water samples to fully determine element variations across the North Bog, Figures 5.8, 5.9 and 5.10 suggest that higher Li, B and Mg values are found in the travertine cone-CO_2 vent water and in nearby ground and surface water.

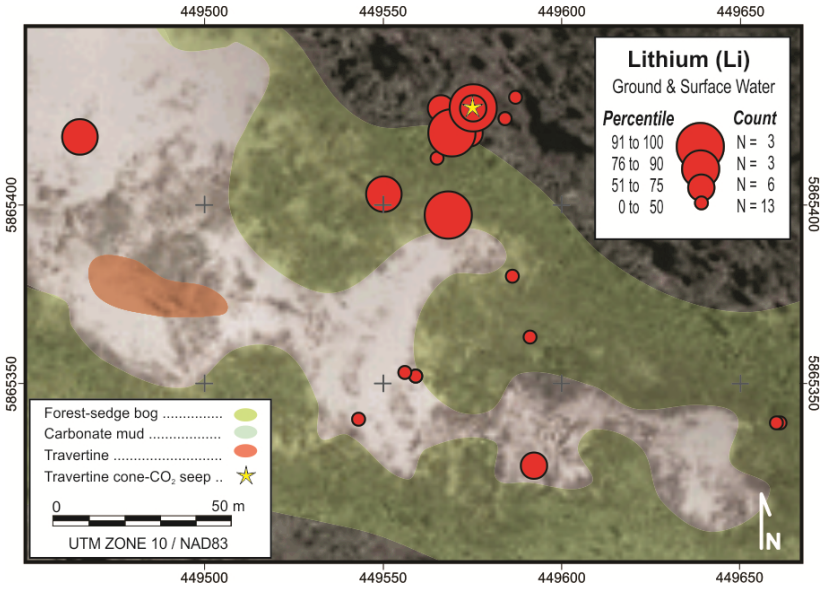

Figure 5.8. Lithium in North Bog ground and surface water (50 percentile = 84 ppb; 75 percentile = 341 ppb; 90 percentile = 434 ppb; maximum = 547 ppb).

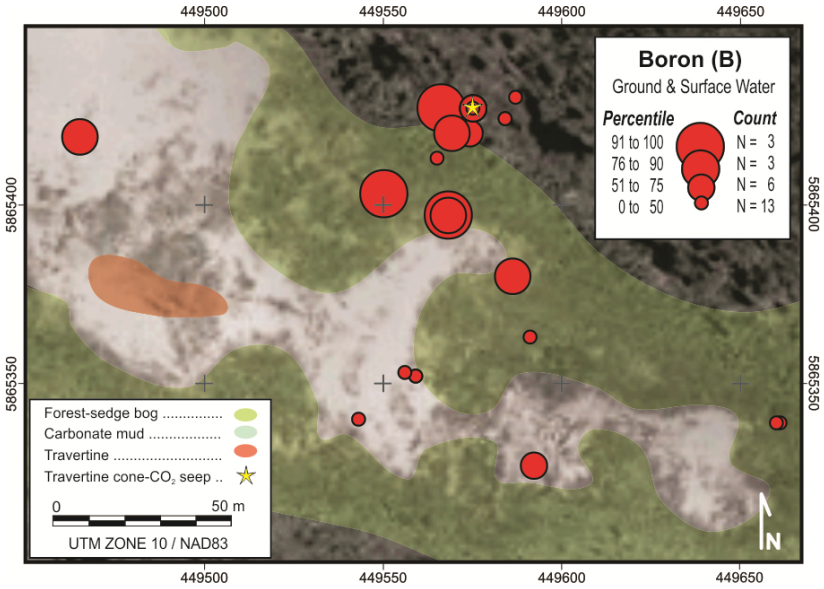

Figure 5.9. Boron in ground and surface water (50 percentile = 173 ppb; 75 percentile = 343 ppb; 90 percentile = 438 ppb; maximum - 860 ppb).

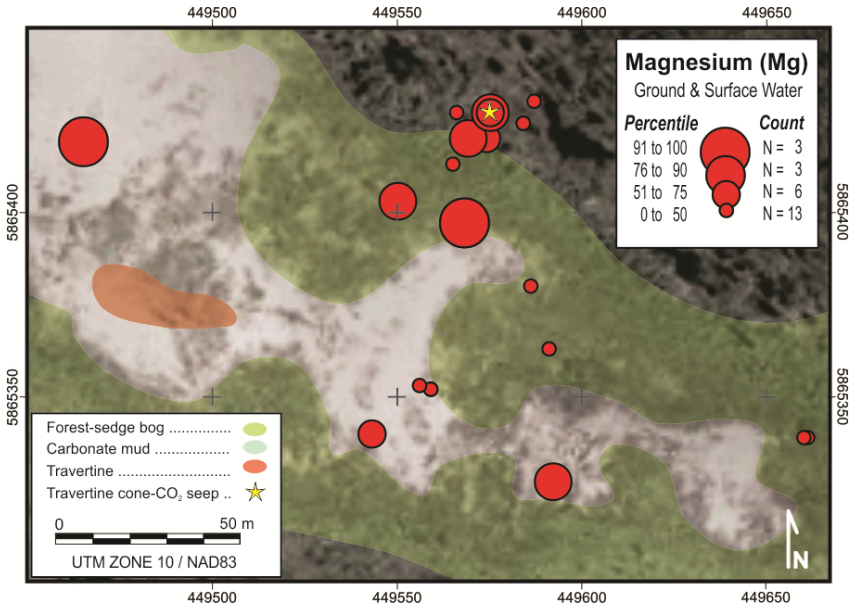

Figure 5.10. Magnesium in ground and surface water (50 percentile = 84 ppm; 75 percentile = 263 ppm; 90 percentile = 325 ppm; maximum = 393 ppm).

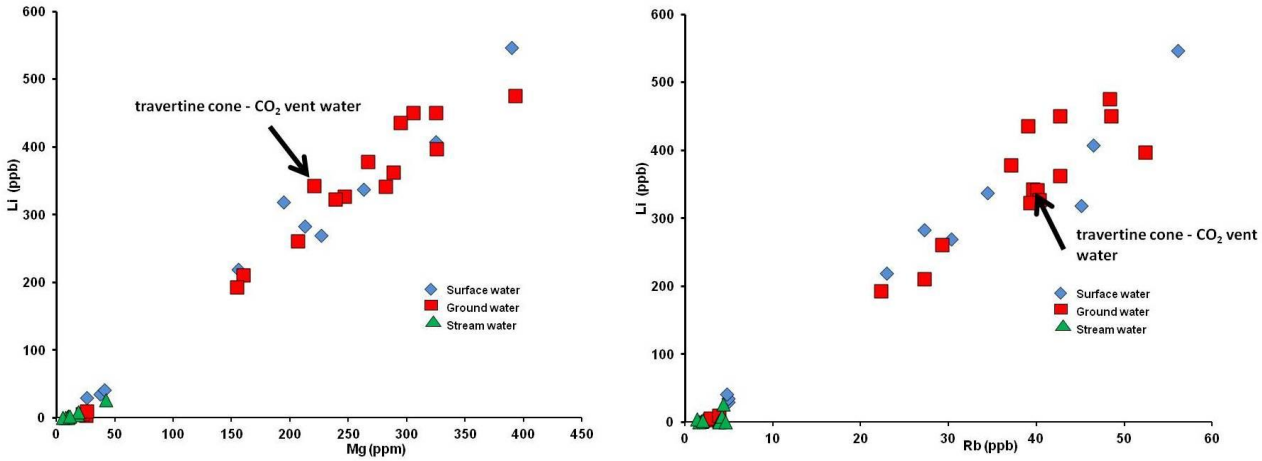

Figure 5.11. Lithium vs Mg and Li vs Rb in bog ground, bog surface and stream water.

A concomitant increase of two elements in natural water may indicate that they have a common source or released simultaneously from rock-water reactions. Scatter plots in Figure 5.11 show that there is a strong, positive correlation between Li vs Mg and between Li vs Rb in the North Bog ground and surface water. There is a weaker correlation between other geothermal pathfinder elements such as Li and B in the North Bog water. The travertine cone - CO_2 vent water chemistry, identified on Figure 5.11, corresponds to the Li-Mg and Li-Rb trends. Ground and surface water appears to have similar Li and Mg concentrations and this may reflect a similar water chemistry and/or mixing of ground and surface water. The low

temperature and distinct chemistry of water in the travertine cone - CO_2 vent (Figure 5.11) suggest a distinct ground water source. Table 2 lists trace element data for samples collected in 2013, 2014 and 2015 from the North Bog travertine-CO_2 vent water (Figure 5.2) and % RSD (relative standard deviation) values calculated from the repeated analysed. Percent RSD values below 12% for pH, water temperature, B, Li, Ca, Mg, Sr and Si indicate that these parameters remain constant from month the month and from 2013 to 2015. Larger % RSD values in Table 2 for Sb, Al, As, Cd, Cu, Fe, Re, Sb, Te, Ti, V, Y and Zr may reflect element concentrations below or near instrument detections limit. Iron is unusual because there are large seasonal and annual variations that may be weathering of Fe minerals (e.g. pyrite) in contact with a changing ground water hydrology. A copious Fe oxide precipitate commonly coats the base of the travertine cone and forms a matrix of travertine rubble one metre southwest of the cone. The cool water (< 6^{o}C) and almost constant chemistry (except for Fe) over time suggests that the travertine-CO_2 vent water may be discharging from a confined aquifer or that the low temperature reflects the endothermic reaction when CO_2 reacts with water to form H_2CO_3.

In 2014 surface water was sampled in the "Volcano" bog (Figure 5.1) described by Souther *et al*. (1987) to compare the water chemistry of a bog with no visible CO_2 seeps to the North and South Bog where CO_2 seeps are common. The "Volcano" bog surface water temperature of 14.2^{o}C is similar to the North Bog surface water median temperature (14.5^{o}C)and the ground water median temperature (13.5^{o}C). Data in Table 3 compares the chemistry of the "Volcano" bog with the chemistry of several North Bog sites. The temperature difference between the travertine cone-CO_2 vent water (< 6^{o}C), the water in a nearby dug pit (11.26^{o}C)and the stream water leaving the bog (11.4^{o}C) is clearly emphasised by data in Table 3. The North Bog water also has higher Li, B and Mg concentrations compared to those in the "Volcano" bog water. No Hg was detected in any of the water samples collected in 2014 from North and "Volcano" bogs. Only one water sample from a stream has detectable Cl (2.4 ppm). Since geothermal fluids typically have high Cl and Hg concentrations the absence of detectable Cl and Hg in the bog water suggests that it is unlikely the water has a thermal source.

Table 3 shows significant changes in the water chemistry near the travertine cone-CO_2 vent and the edge of the North Bog. The bar graphs in Figures 5.12 and 5.13 reveal much higher B, Li, Mg, Ni and Rb in ground water northeast (up slope) from the travertine-CO_2 vent compared to those in the vent water and in the water from a pit to the southwest whereas Al and Si, however, decrease. This variation in water chemistry suggest inflow of ground water into the North Bog in the area near the travertine cone-CO_2 vent.

Sample	14-2002	14-2004	14-2003	14-2006	14-2007	14-1002
Date	24-Aug-14	26-Aug-14	24-Aug-14	26-Aug-14	26-Aug-14	23-Jun-14
UTM E	449569	449575	449881	449328	450046	450071
UTM N	5865420	5865426	5865428	5865493	5865431	5866752
Notes	3 m SW from CO_2 vent	CO_2 vent water	3 m NE from CO_2 vent	Stream flowing into N. Bog	Stream leaving N. Bog	"Volcano" Bog
Temp	14.1	5.5	11.26	14.3	11.2	14.20
pH	6.46	6.44	5.76	7.14	8.12	7.51
CO_2	990	1210	660	80	30	20
Tot Alk ppm	2670	2720	249	375	123	160
F ppm	0.57	0.57	0.159	0.240	0.194	nm
NO_3 ppm	-0.1	-0.1	-0.005	0.0058	0.0212	nm
SO_4 ppm	19	19	10.3	-0.5	3.98	nm
Ag ppb	-0.005	-0.005	-0.005	0.027	-0.005	-0.005
Al ppb	1.1	2.4	30.7	8.5	2.2	-30
As ppb	1.17	2.51	0.21	4.73	0.66	0.83
B ppb	429	353	34	44	21	8
Ba ppb	241.0	232.0	29.2	99.9	61.5	69.6
Be ppb	-0.005	0.059	0.025	0.006	-0.005	-0.005
Ca ppm	231	231	47.1	65.1	25.2	30.1
Cd ppb	0.007	0.025	0.219	-0.005	-0.005	-0.005
Co ppb	5.16	2.07	1.03	2.51	-0.05	-0.05
Cs ppb	2.58	2.18	0.01	0.08	0.01	0.008
Cu ppb	0.47	-0.20	2.79	-0.20	0.23	-0.5
Fe ppb	1750	5240	-30	6390	-30	190
Hg ppb	-0.050	-0.050	-0.050	-0.050	-0.050	-0.050
K ppm	31.8	32.1	3.9	4.2	3.0	3
Li ppb	450	436	9	26	2	0.5
Mg ppm	306	295	26.3	42.6	11.9	9.9
Mn ppb	471	194	60	1400	1	49.1
Mo ppb	0.0990	0.4210	0.6310	1.7500	1.2600	0.09
Na ppm	303	304	8.0	18.9	7.2	8
Ni ppb	37.30	40.80	12.00	2.62	0.26	-0.2
Rb ppb	42.70	39.10	3.93	4.37	2.08	1.62
Re ppb	-0.0050	-0.0050	0.0152	-0.0050	0.0308	-0.005
Sb ppb	0.0280	0.0320	0.4900	0.0420	0.0640	0.01
Se ppb	-0.20	-0.20	0.55	0.72	3.22	-0.2
Si ppm	9.26	8.54	21.3	21.6	14.0	13.9
Sr ppm	8.05	9.37	0.278	1.05	0.149	0.148
Te ppb	0.014	0.013	-0.010	-0.010	-0.010	-0.0100
Ti ppb	2.320	0.370	1.370	0.540	-0.200	-0.2
Tl ppb	0.318	0.340	0.594	0.003	-0.002	-0.002
U ppb	0.220	0.159	0.255	0.124	0.150	-0.002
V ppb	0.119	1.560	0.374	1.450	1.690	-0.05
Y ppb	0.017	0.478	0.839	0.051	0.010	-0.005
Zn ppb	5	11	10	-1	-1	-3
Zr ppb	0.960	1.730	0.515	0.227	-0.050	-0.05

Table 3. Analyses of "Volcano" bog, North Bog travertine cone-CO_2 vent water and a North Bog stream. Chloride, Br, Cr, Ga, P, Th, Sn and Pb are not reported here because values are below detection limit. nm - not measured. Sample sites shown on Figure 5.1 and 5.2.

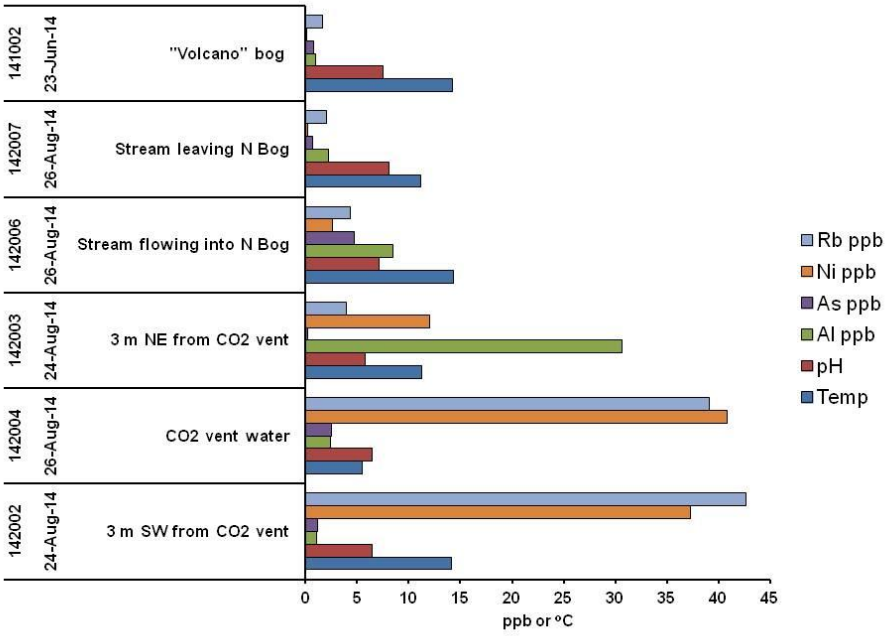

Figure 5.12. Temperature, pH and As, Al, Ni and Rb in North Bog and "Volcano" bog water sites.

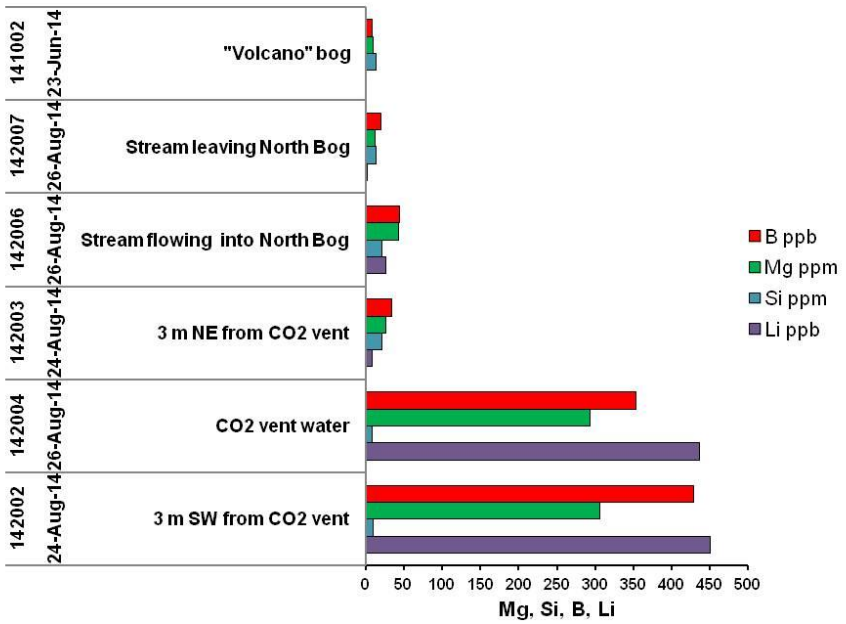

Figure 5.13. Dissolved B, Li, Si and Mg in North Bog and "Volcano" bog water sample sites.

5.3 Mineral solubility modelling

Mineral solubility modelling can help interpreting water chemistry, but the results must be interpreted with caution because computer simulated thermodynamic modelling can oversimplify complex natural water systems (Leybourne and Cameron, 2007). The abundant mineral carbonate mud and travertine in the North Bog are clearly predicted by the oversaturation of calcite and aragonite carbonate most likely when the CO_2-rich gas seeping from beneath the bog reacts with dissolved Ca and Mg in the ground and surface pool water. Table 4 lists pH, temperature, bicarbonate, sulphate and element concentrations in the water sampled at six locations in the North Bog. The samples are from the stream flowing through the bog, the travertine cone - CO_2 vent water, a bog surface pool and ground water sampled in two pits adjacent to the travertine cone - CO_2 vent. The minerals that could precipitate from the water and mineral saturation indices predicted by a PHREEQC thermodynamic simulation (Parkhust and Appelo, 1999) using the water data in Table 4 are also listed.

Sample	13-1009	14-2006	14-2007	14-2002	14-2004	14-2003
Type	Pool	Stream	Stream	Ground	Ground*	Ground
pH	7.8	7.14	8.12	6.5	6.37	5.76
Temp. °C	19.3	14.3	11.2	5.8	5.9	11.26
HCO_3^- ppm	1590	375	123	2670	2410	249
Al ppb	0.5	8.5	2.12	1.1	0.5	30.7
Ca ppm	90.8	65.1	25.2	231	235	47.1
Mg ppm	213	42.6	11.9	306	239	26.3
Fe ppb	65	6390	15	1750	3920	15
Ni ppb	0.34	2.62	0.26	37.3	44	12
B ppb	234	44	21	429	343	34
Li ppb	283	26.4	2.27	450	323	9
Si ppm	10.4	21.6	14	9.26	9.63	21.3
Sr ppm	3.6	1.05	0.149	8.05	9.37	0.278
SO_4 ppm	1	1	4	19	18	10.3
Aragonite	1.02	-0.27	-0.15	0.42	0.04	-1.97
Calcite	1.17	-0.12	0.01	0.57	0.18	-1.82
Chalcedony	-0.14	0.24	0.08	-0.12	-0.04	0.27
Dolomite	2.99	-0.23	-0.17	1.19	0.49	-0.45
$Fe(OH)_3$	2	4.1	1.91	3.04	3.93	0.52
Illite	-2.05	2.85	0.02	0.06	3.23	1.58
Magnesite	1.26	-0.65	-0.71	0.08	-0.19	-2.46

Table 4. Chemistry and mineral saturation indices for ground, surface pool and stream water sites in the North Bog. Ground* indicates the chemistry of the travertine cone-CO_2 vent water (sample 14-2004). HCO_3^- ppm = ppm $CaCO_3$.

The positive saturation indices predict that aragonite, calcite, magnesite and dolomite should precipitate from the North Bog surface and the travertine cone-CO_2 vent ground water, but not in the stream water and in the ground water upslope from the bog. Conversely, the saturation indices predict that chalcedony and illite precipitate from the stream water and in the upslope ground water reflecting higher dissolved silica. Oversaturation of Fe $(OH)_3$ in several of the water samples explains visible iron oxide deposits around several of the seeps.

5.4 Water Results - Stable isotope chemistry

Trace element analyses of water samples collected on May 29th, 2015 at North and South Bogs sites are listed in Table 5. All of the water samples were analysed for $\delta^{18}O$, $\delta^{2}H$ and $\delta^{14}C$. and sample locations are shown on Figure 6.26.

Depending on the sample latitude δO^{18} values of meteoric water range from - 20 to - 25 $^{o}/_{oo}$ whereas isotopic values of around 0 $^{o}/_{oo}$ for geothermal water are closer to those of sea water. Since the water samples from the Nasko bogs have δO^{18} values ranging from - 17 to - 19.8 $^{o}/_{oo}$ is likely the water is meteoric and not from a source of deeper ground water. Figure 5.14 shows the variation of $\delta^{2}H$ and $\delta^{18}O$ in the samples from six sites ranging from the travertine cone-CO_2 seep water in the North Bog (TREKGT 1) to surface water from the South Bog (TREKGT 6) with the standard Marine Ocean Water (SMOW) line calculated from a relationship $\delta D = 8\ \delta O^{18} + 10$ proposed by Faure, (1992). In Figure 5.14 the Nazko δO^{18} values diverge from the SMOW trend line and this may reflect a change in the isotopic composition of the North Bog travertine cone-CO_2 seep water compared to surface water. Natural δC^{13} ranges from a large negative value where there has been a biogenic influence on the isotopic composition to - 7 $^{o}/_{oo}$ for carbonate dominated alkaline water to δC^{13} values near 0 for more acid bicarbonate dominated water. Since the Nazko δC^{13} values range from 1.5 to -7.1 the water does not have a biogenic signature and the isotopic composition is likely due to the inorganic chemistry of the carbonate-bicarbonate system.

Site	15 TREKGT 1	15 TREKGT 2	15 TREKGT 3	15 TREKGT 4	15 TREKGT 5	15 TREKGT 6
Number	15-1001	15-1002	15-1003	15-1004	15-1005	15-1006
Types	Water & gas	Water & gas	Water & gas	Water & gas	Water	Water & gas
Date	29-May-15	29-May-15	29-May-15	29-May-15	29-May-15	29-May-15
UTM E	449575	449661	449660	449591	449881	449411
UTM N	5865426	5865339	586540	5865363	5865428	5865012
Site Notes	North Bog main CO2 vent water	North Bog surface water	North Bog surface water	North Bog surface water	N. Bog - Pit water 3 m NE from main CO2 vent	South Bog surface water
Temp	5.7	15.2	14.5	15.2	11.8	16.1
pH	6.32	5.75	5.56	5.99	5.97	6.64
TDS ppm	2180	469	365	751	202	2780
Salinity ppt	1570	317	244	517	130	2050
Alk	1400	600	600	800	500	2000
CO_2	500	350	750	600	200	300
Tot. Alk. ppm	1400	600	600	800	500	2000
Al_ppb	-1.0	1.0	2.3	1.3	nm	-1.0
As_ppb	1.13	0.33	0.43	0.16	nm	0.08
B_ppb	331.0	173.0	100.0	235.0	nm	330.0
Ba_ppb	198.00	70.10	56.80	41.60	nm	128.00
Be_ppb	0.040	0.019	0.131	-0.005	nm	-0.005
Ca_ppm	207.0	55.6	51.3	64.2	nm	140.0
Cd_ppb	0.053	0.013	0.010	0.005	nm	0.011
Co_ppb	1.90	-0.05	-0.05	-0.05	nm	0.20
Cs_ppb	2.130	0.434	0.240	0.291	nm	3.520
Cu_ppb	-0.20	-0.20	0.28	0.27	nm	0.84
Fe_ppb	130.0	297.0	714.0	369.0	nm	-30.0
K_ppm	28.0	5.1	3.4	8.1	nm	26.2
Li_ppb	329.00	31.30	16.30	84.40	nm	376.00
Mg_ppm	259.0	43.0	28.4	83.7	nm	285.0
Mn_ppb	145.0	35.5	37.8	41.5	nm	6.7
Mo_ppb	0.35	0.05	-0.05	0.09	nm	0.07
Na_ppm	264.0	26.8	16.6	57.7	nm	196.0
Ni_ppb	40.60	1.77	0.87	0.47	nm	3.32
Rb_ppb	39.50	6.13	5.44	11.00	nm	40.00
Re_ppb	0.007	-0.005	-0.005	-0.005	nm	-0.005
Sb_ppb	0.02	0.01	0.01	0.02	nm	0.02
Si_ppm	10.30	11.50	11.70	11.70	nm	9.24
Sr_ppm	7.160	1.860	1.530	2.070	nm	6.460
Ti_ppb	-0.20	-0.20	-0.20	-0.20	nm	0.41
Tl_ppb	0.401	-0.002	-0.002	-0.002	nm	0.022
U_ppb	0.102	-0.002	-0.002	-0.002	nm	0.084
V_ppb	0.322	-0.050	0.397	0.088	nm	0.296
Y_ppb	0.129	0.111	0.285	-0.005	nm	0.040
Zn_ppb	7.80	4.30	4.10	3.60	nm	19.10
Zr_ppb	1.95	-0.05	0.08	-0.05	nm	1.39
$\delta^{18}O$ water	-19.8	-18.2	-17.8	-18.4	-18.9	-17.0
$\delta^{2}H$ water	-152	-144	-141	-145	-148	-138
$\delta^{13}C$-DIC	-1.6	-5.8	-5.2	-3.3	-7.1	1.5

Table 5. Analyses of water samples collected in 2015 in the North and South Bogs. Silver, Bi, Cr, Ga, P, Pb, Th, Se, Sn, Te and W are not reported because values in all samples are below detection limit. nm - not measured. The $\delta^{2}H$ and $\delta^{18}O$ are in $_{o}/^{oo}$ (per mil). Sample sites are shown on Figure 6.26.

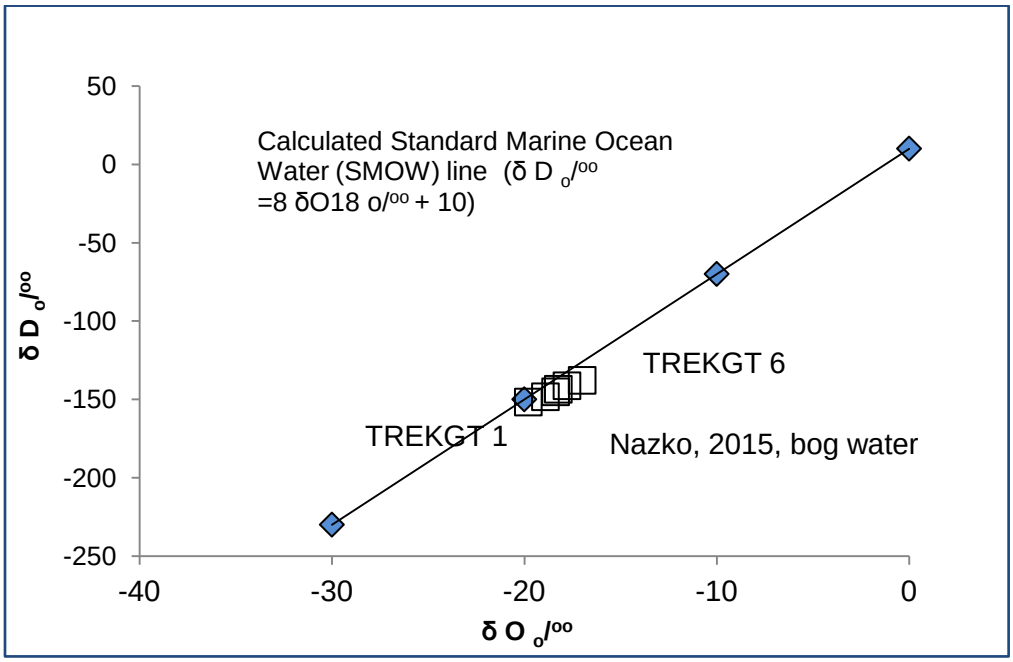

Figure 5.14. δ^2H and $\delta^{18}O$ in North and South Bog water sample sites. The sigma error for δ^2H is 1 and the sigma error for $\delta^{18}O$ is 0.1.

6 Soil and tree bark geochemistry

6.1 Soil and tree bark data quality

Sampling and analytical precision is calculated from the results of trace, minor and major element analysis of CANMET standard TILL 1 and field and analytical duplicate samples inserted randomly with the soil samples.

A method for calculating precision from duplicate sample analyses has been developed by Heberlein (2015) where precision is the total measurement error expressed as the average coefficient of variation, or CV_{av} calculated from formula proposed by Abzalov, (2008).

$$CV_{AVR}(\%) = 100 \times \sqrt{\frac{2}{N}\sum_{i=1}^{N}\left(\frac{(a_i - b_i)^2}{(a_i + b_i)^2}\right)}$$

In the formula the terms a and b represent the original and duplicate analyses and N the number of duplicate pairs. Values can range from 0%, when duplicate pairs have identical concentrations, to an upper value above 141.21% (i.e. the square root of 2) when duplicate results exhibit maximum differences.

Elements are sorted in order of increasing field duplicate CV_{AVG} value (i.e. improved precision) in Figure 6.1. Over 75 percent of the elements determined, including the geothermal pathfinders Li and As have CV_{AVG} value less than 10 percent and the data can be confidently used for further statistical analysis and interpretation. However, analytical duplicate CV_{AVG} values for 24 of the elements are larger than the field duplicate CV_{AVG} value and this reveals a potential quality control problem since the field duplicate precision is the sum of all of the factors responsible for variation (e.g. sampling, preparation, analysis) and, hence, should be larger than the analytical precision. Precision can be also expressed as percent relative standard deviation (%RSD) calculated here from repeated analysis of the CANMET TILL 1. In Figure 6.1 most % RSD values for CANMET TILL 1 are smaller than the field and analytical CV_{AVG} values indicating acceptable analytical precision for an element. A possible cause of analytical duplicate precision being larger than field analytical duplicate precision may be incomplete mixing of a field duplicate before splitting into two analytical duplicate samples. Detection limits for soil samples analysed for elements by aqua regia-ICPMS and by lithium borate-ICPES/MS are listed in Appendix A with a statistical summary. Tables 6 and 7 list element

detection limits, reported and accepted value for a vegetation standard from Saskatchewan analysed with the humus and lodge pole pine (*Pinus contorta)* tree bark samples.

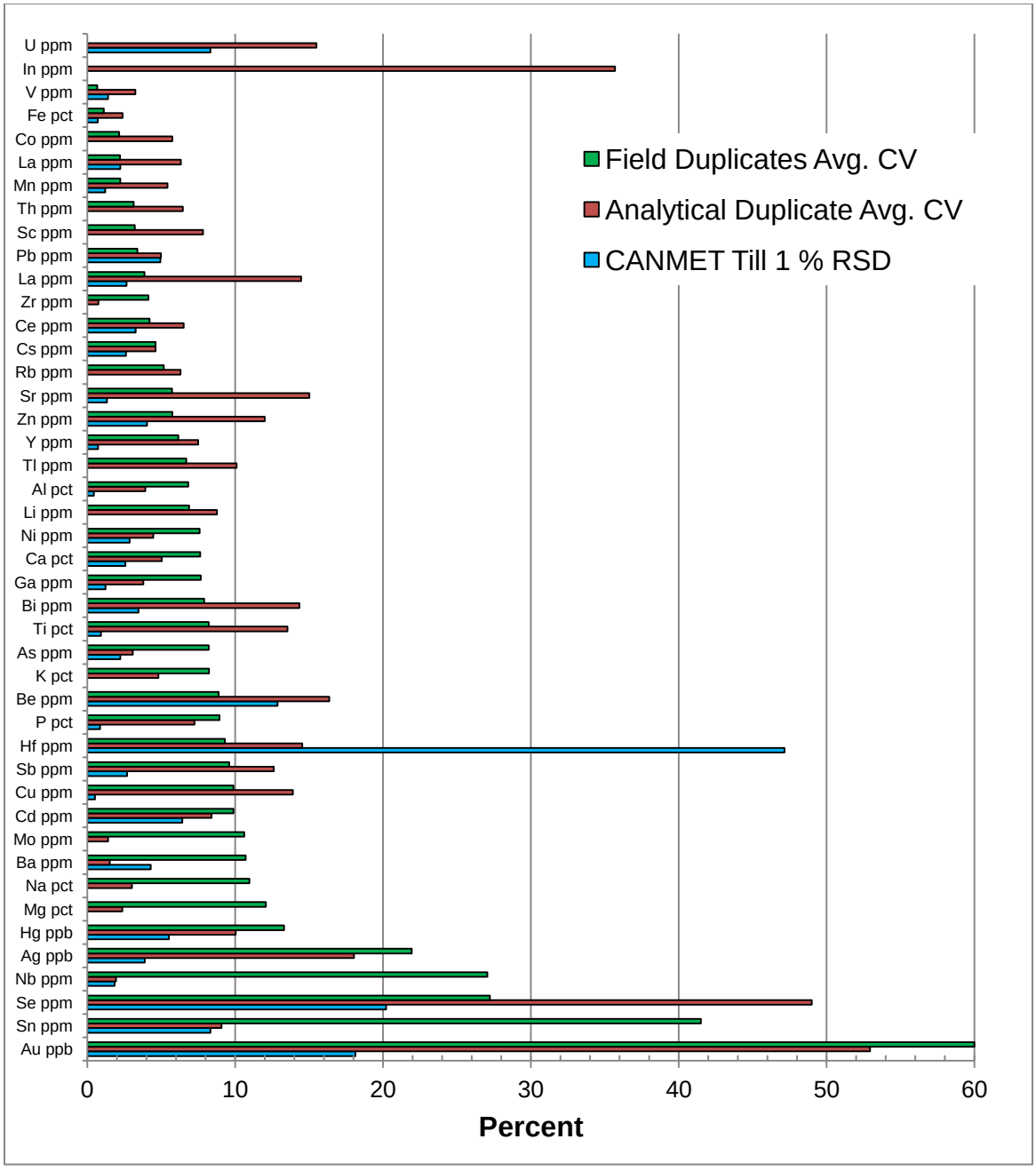

Figure 6.1. Aqua regia - ICPMS analysis field and analytical duplicates samples (3) and CANMET TILL 1 standard (2). The bar graph displays the average coefficient of variation (ACM) from the duplicate data and the percent relative standard deviation (%RSD) from the CANMET data. Boron & Pt is not included because all for duplicate values are less than detection limit.

Major oxide and minor element (e.g. Zr, Ce) precision estimates from the field and analytical and standard duplicate analyses are shown on Figure 6.2. The major oxide field duplicate CV_{AVG} values are typically less than 5 percent indicating that the data can be used with confidence. Phosphorus oxide, Co, Ce and Nb have field duplicate CV_{AVG} values greater than 10 percent and the larger variation reflects that the duplicate analyses close to the detection limit.

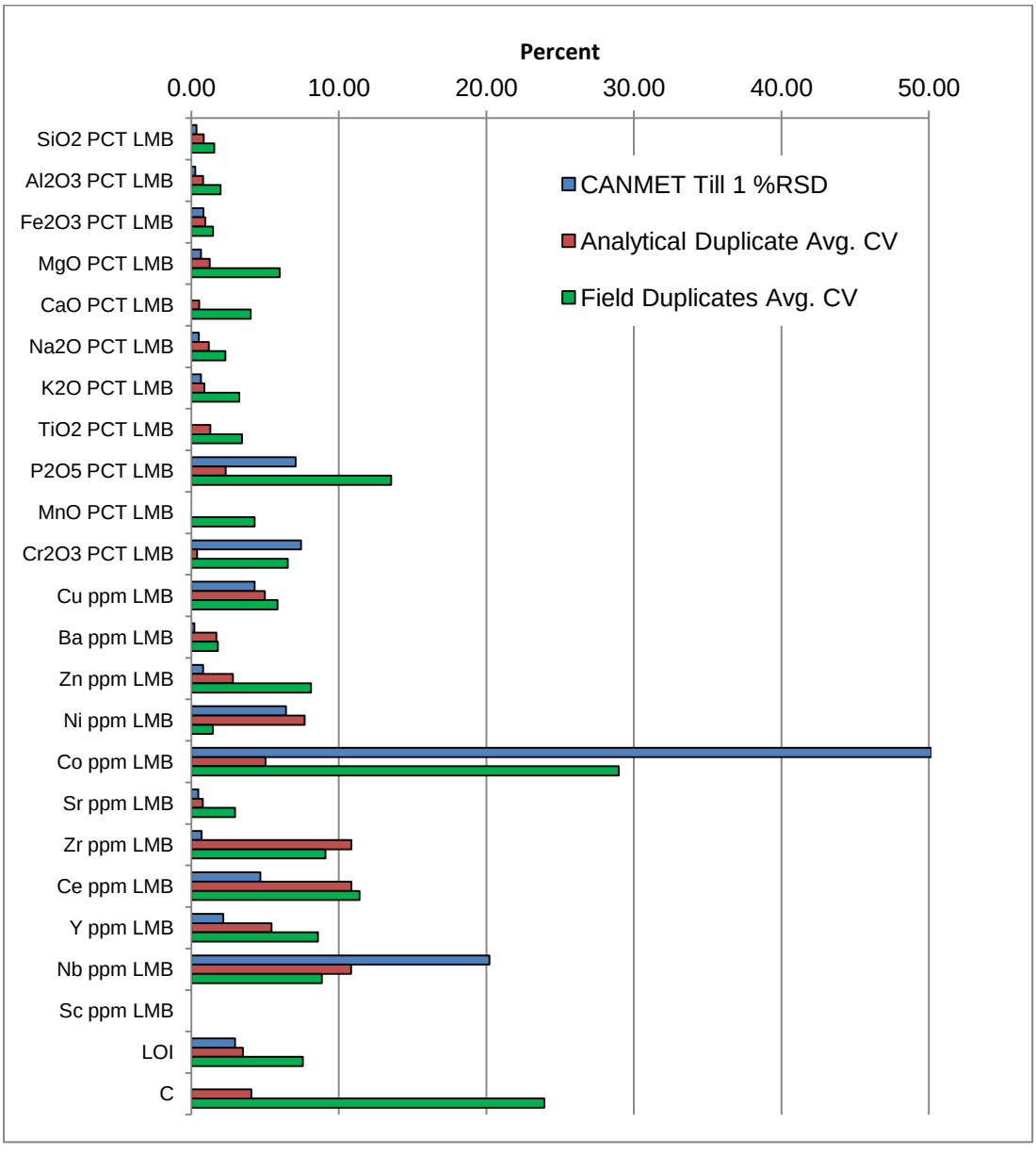

Figure 6.2. Lithium borate fusion - ICPMS analysis field and analytical duplicates samples (3) and CANMET TILL 1 standard (2). The bar graph displays the average coefficient of variation (ACM) from the duplicate data and the percent relative standard deviation (%RSD) from the CANMET data.

Element	MDL	Reported Values	Accepted value	Element	MDL	Reported Values	Accepted value
Ag ppb	2	17	14	Na pct	0.001	0.001	0.002
Al pct	0.01	-0.01	0.01	Nb ppm	0.01	-0.01	0.01
As ppm	0.1	0.3	0.2	Ni ppm	0.1	0.4	0.4
Au ppb	0.2	-0.2	0.2	P pct	0.001	0.015	0.016
B ppm	1	14	6	Pb ppm	0.01	1.53	1.54
Ba ppm	0.1	95.3	88.3	Pd ppb	2	-2	2
Be ppm	0.1	-0.1	0.1	Pt ppb	1	-1	1
Bi ppm	0.02	-0.02	0.02	Rb ppm	0.1	0.7	0.6
Ca pct	0.01	1.04	1.08	Re ppm	1	-1	1
Cd ppm	0.01	0.19	0.2	S pct	0.01	0.06	0.06
Ce ppm	0.01	0.22	0.17	Sb ppm	0.02	0.03	0.03
Co ppm	0.01	0.19	0.18	Sc ppm	0.1	0.3	0.2
Cr ppm	0.1	1.3	1.05	Se ppm	0.1	-0.1	0.2
Cs ppm	0.005	0.015	0.014	Sn ppm	0.02	0.02	0.02
Cu ppm	0.01	3.02	3.13	Sr ppm	0.5	9.4	10.2
Fe %	0.001	0.016	0.012	Ta ppm	0.001	-0.001	0.001
Ga ppm	0.1	-0.1	0.1	Te ppm	0.02	-0.02	0.02
Ge ppm	0.01	-0.01	0.01	Th ppm	0.01	0.01	0.01
Hf ppm	0.001	0.003	0.003	Ti pct	1	4	3
Hg ppb	1	155	135	Tl ppm	0.02	-0.02	0.02
In ppm	0.02	-0.02	0.02	U ppm	0.01	-0.01	0.01
K pct	0.01	0.04	0.05	V ppm	2	-2	2
La ppm	0.01	0.10	0.09	W ppm	0.1	-0.1	0.1
Li ppm	0.01	0.02	0.04	Y ppm	0.001	0.074	0.062
Mg pct	0.001	0.021	0.021	Zn ppm	0.1	39.1	40.7
Mn ppm	1	201	211	Zr ppm	0.01	0.10	0.09
Mo ppm	0.01	0.02	0.02				

Table 6. Detection limits for humus samples analysed by aqua regia - ICPMS , reported value and accepted value for a Central Canada vegetation standard.

Element	MDL	Reported Value	Accepted value	Element	MDL	Reported Value	Accepted value
Ag ppb	2	16	14	Na pct	0.001	-0.001	0.002
Al pct	0.01	-0.01	0.01	Nb ppm	0.01	-0.01	0.01
As ppm	0.1	-0.1	0.2	Ni ppm	0.1	0.5	0.4
Au ppb	0.2	-0.2	0.2	P pct	0.001	0.015	0.016
B ppm	1	11	6	Pb ppm	0.01	1.48	1.54
Ba ppm	0.1	96.9	88.3	Pd ppb	2	-2	2
Be ppm	0.1	-0.1	0.1	Pt ppb	1	-1	1
Bi ppm	0.02	-0.02	0.02	Rb ppm	0.1	0.7	0.6
Ca pct	0.01	1.05	1.08	Re ppm	1	-1	1
Cd ppm	0.01	0.19	0.2	S pct	0.01	0.04	0.06
Ce ppm	0.01	0.23	0.17	Sb ppm	0.02	0.03	0.03
Co ppm	0.01	0.19	0.18	Sc ppm	0.1	0.3	0.2
Cr ppm	0.1	1.5	1.05	Se ppm	0.1	0.1	0.2
Cs ppm	0.005	0.015	0.014	Sn ppm	0.02	0.02	0.02
Cu ppm	0.01	3.23	3.13	Sr ppm	0.5	9.7	10.2
Fe pct	0.001	0.015	0.012	Ta ppm	0.001	-0.001	0.001
Ga ppm	0.1	-0.1	0.1	Te ppm	0.02	-0.02	0.02
Ge ppm	0.01	-0.01	0.01	Th ppm	0.01	-0.01	0.01
Hf ppm	0.001	0.005	0.003	Ti pct	1	4	3
Hg ppb	1	155	135	Tl ppm	0.02	-0.02	0.02
In ppm	0.02	-0.02	0.02	U ppm	0.01	-0.01	0.01
K pct	0.01	0.04	0.05	V ppm	2	-2	2
La ppm	0.01	0.1	0.09	W ppm	0.1	-0.1	0.1
Li ppm	0.01	0.03	0.04	Y ppm	0.001	0.072	0.062
Mg pct	0.001	0.021	0.021	Zn ppm	0.1	39.5	40.7
Mn ppm	1	199	211	Zr ppm	0.01	0.09	0.09
Mo ppm	0.01	0.02	0.02				

Table 7. Detection limits for tree bark samples analysed by aqua regia- ICPMS with reported and accepted value for a vegetation standard from Central Canada analysed with the samples.

6.2 Soil and tree bark statistics

Statistics (median, mean, 3rd Quartile, 95th percentile, the 3rd quartile + 1.5 interquartile range, maximum, minimum) for elements in the B, C and Ah soil horizon (humus) and in lodge pole pine (*Pinus contorta)* outer bark samples are listed in Appendix A. The data are summarized by box plots that compare the element populations in each soil horizon and in the tree the bark. In Figure 6.3, the C soil horizon has the highest Li values and the tree bark the lowest Li whereas the B soil horizon has the highest B level with lower concentrations in the Ah horizon and the C horizon

Figure 6.4 compares Hg and Ni in the soil and tree bark. The C soil horizon has the highest median Hg value with lower medians for the Ah and B soil horizons and the tree bark. However, there are Hg outlier values in the C and B horizon above 2 ppm. Nickel median and interquartile range for the B and C horizons are similar, but are higher than the Ah horizon median and much higher than for the tree bark median. There are also Ni outliers up to 688 ppm that can be explained by Ni accumulation in the organic-rich bog soil. Mercury values over 2000 ppm in the C and B soil horizons compare with much lower median and interquartile range for Hg the Ah horizon and the tree bark. These low values suggest limited Hg dispersion through the upper soil profile and in vegetation from the parent till. Figure 6.5 shows that the C soil horizon has the highest As content with lower values in the B and Ah horizons and no detectable As tree bark. The Ca outliers in the entire horizon reflect bias from few carbonate-organic samples with high Ca. Distributions of Rb and Ce in the Ah, B and C horizons are similar, but medians and interquartile ranges are much higher than those for the tree bark (Figure 6.6).

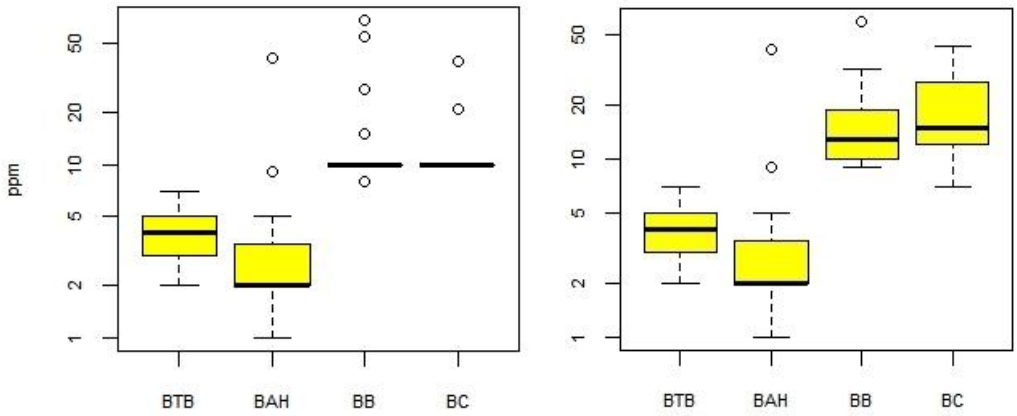

Figure 6.3. Box plots for ppm Li by aqua regia-ICPMS and ppm B by Na_2O_2 fusion - ICPMS analysis in 19Ah, 22 B, 21 C soil samples and 15 lodge pole pine (*Pinus contorta)* outer bark samples.

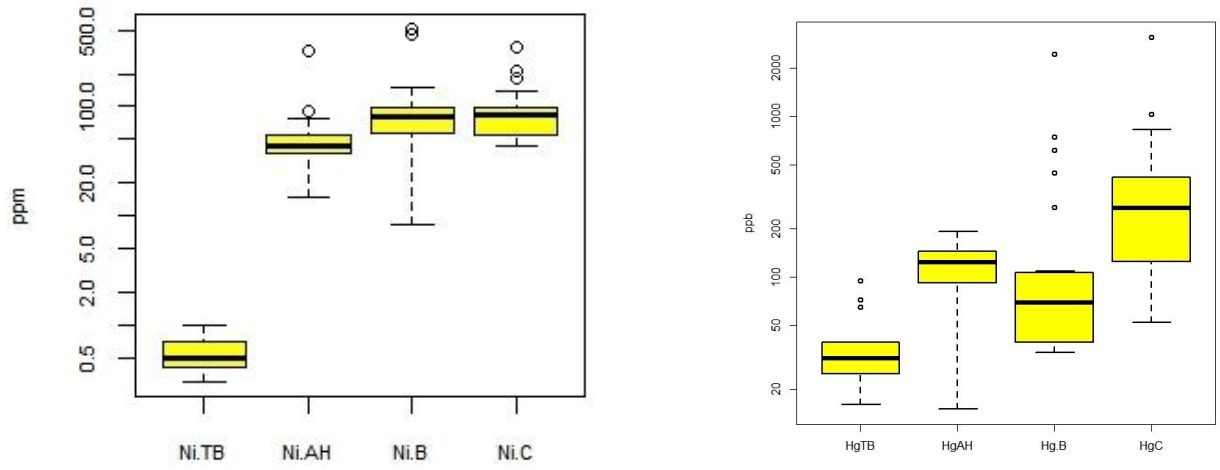

Figure 6.4. Box plots for Ni and Hg by aqua regia-ICPMS analysis in 19Ah, 22 B, 21 C soil samples and 15 lodge pole pine (*Pinus contorta)* outer bark samples.

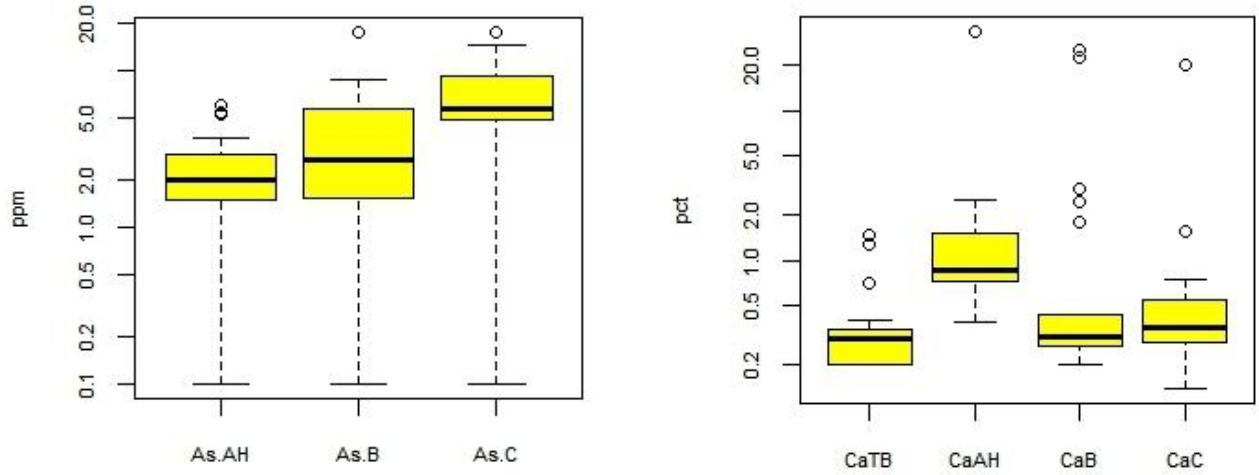

Figure 6.5. Box plots for As and Ca by aqua regia-ICPMS analysis in 19Ah, 22 B, 21 C soil samples and 15 lodge pole pine (*Pinus contorta)* outer bark samples.

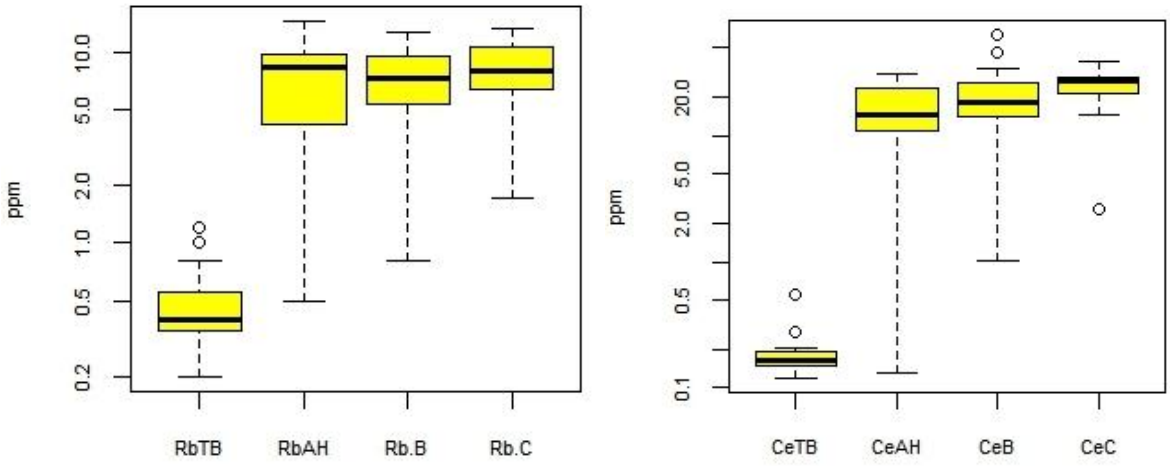

Figure 6.6. Box plots for Rb and Ce by aqua regia-ICPMS analysis in 19Ah, 22 B, 21 C soil samples and 15 lodge pole pine (*Pinus contorta)* outer bark samples.

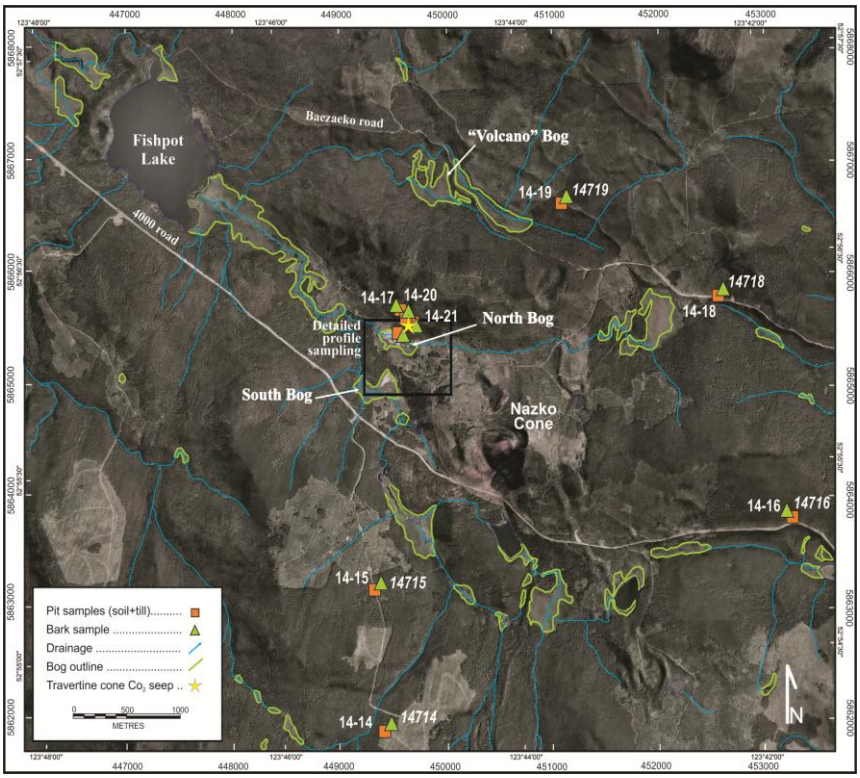

Figure 6.7. Location of Soil Profiles (e.g. 14-15) and tree bark samples *(e.g. 14715)*.

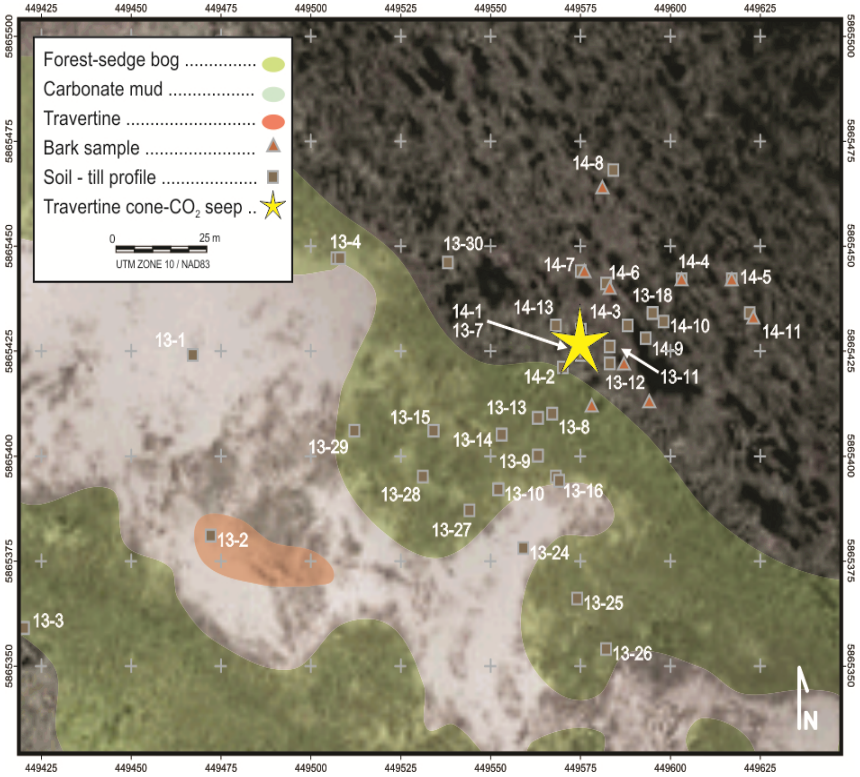

Figure 6.8. Soil Profile and tree bark samples sites in North Bog.

6.3 B soil horizon geochemistry

Soil profile locations are shown in Figures 6.7 and 6.8. Figures 6.9 to 6.16 display the spatial variation of elements in the B soil horizon as bubble plots from combined 2013 and 2014 geochemical data for the B soil horizon and the organic soil intermediate (50 -70 cm) depth data. The B soil horizon data was chosen for the plots because it is the most continuous geochemical layer of the three horizons sampled.

Figures 6.9 and 6.10 show the distribution of Li and B in the North Bog soil. The highest Li levels up to 51 ppm are in B horizon samples from two well-drained soil profiles near the travertine cone-CO_2 vent. There are lower Li values (<25 ppm) in the organic soil to the southwest towards the center of the bog. There is a similar pattern of higher B in the soil, but there are more organic soil samples with anomalous (> 74) B that extend along a south east trend in the bog. Figure 6.11 shows that soil samples with Hg up to 3600 ppb are from well-drained profiles north east from the travertine cone-CO_2 vent. There are also isolated organic soil profiles near the edge of the bog with lower Hg (> 250 ppb) content. Most of the organic soil samples typically have less than 250 ppb Hg.

In Figures 6.12 and 6.13 Ca and total C show the marked change in soil chemistry from the well-drained hill slope into the water-saturated organic-carbonate soil. The organic soil typically has more than 30 percent total C and a similar content compared to levels below 5 percent in the B soil horizon of well-drained soil. Sampling in the North Bog during 2013 revealed several elements including Ag, As and Ni enriched in organic soil compared to their content well drained mineral soil. For example, Figure 6.14 shows the distribution Ni values in the soil including a sample near the edge of the bog that has 688 ppm Ni and 33 percent C. The C soil horizon north east of the North Bog also has higher (> 77 ppm) Ni content, although values are much lower than in the organic soil.

Figure 6-15 shows that the well-drained, mineral B horizon soil samples near the travertine cone-CO_2 vent has an elevated As content compared to As levels in organic soil. However, the highest As value of 18.8 ppm was detected in the C soil horizon of Profile 14-17 located 400 m north of the North Bog. The geochemistry of this profile is shown in more detail in Table. 7. Figure 6.16 shows a cluster of elevated Mo values in well drained mineral soil near the travertine cone-CO_2 vent, but organic soil with 32 percent C from a profile near the middle of the North Bog has 8.9 ppm Mo. This soil also has 82 ppb Re, an element commonly associated with Mo. The source for the elevated Mo and Re is presently unknown.

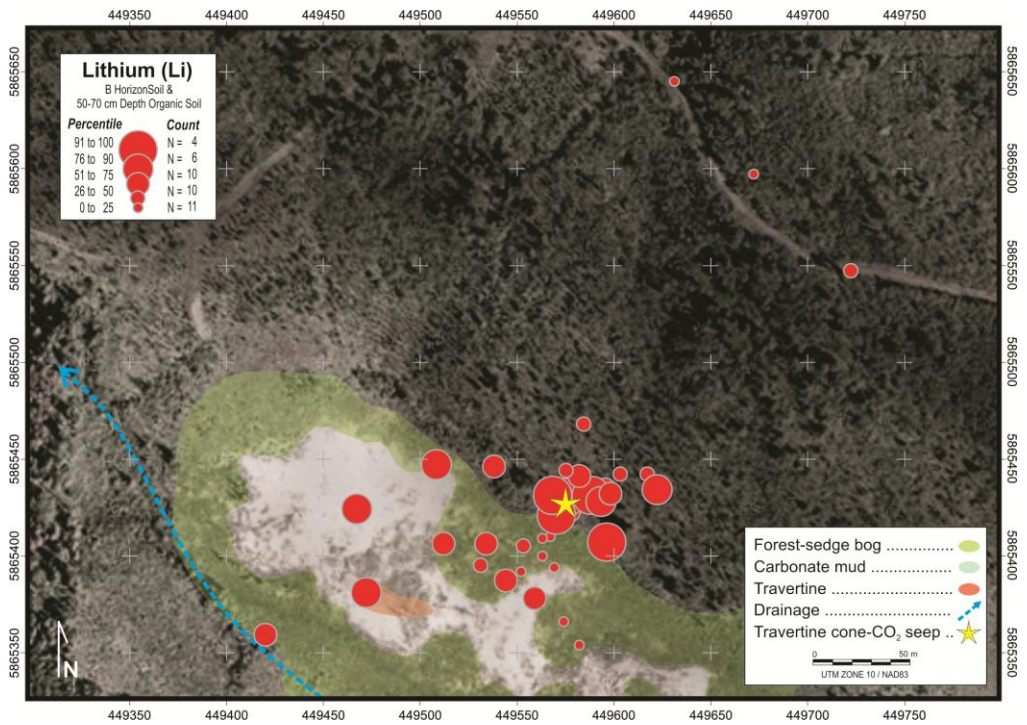

Figure 6.9. Percentile bubble-plot of Li by AR-ICPMS in North Bog B soil horizon and 50-70 cm depth organic soil (25 %ile = 4.6 ppm; 50 %ile = 6.1 ppm; 75 %ile = 8.5 ppm; 90 %ile = 10.7 ppm; maximum = 30 ppm).

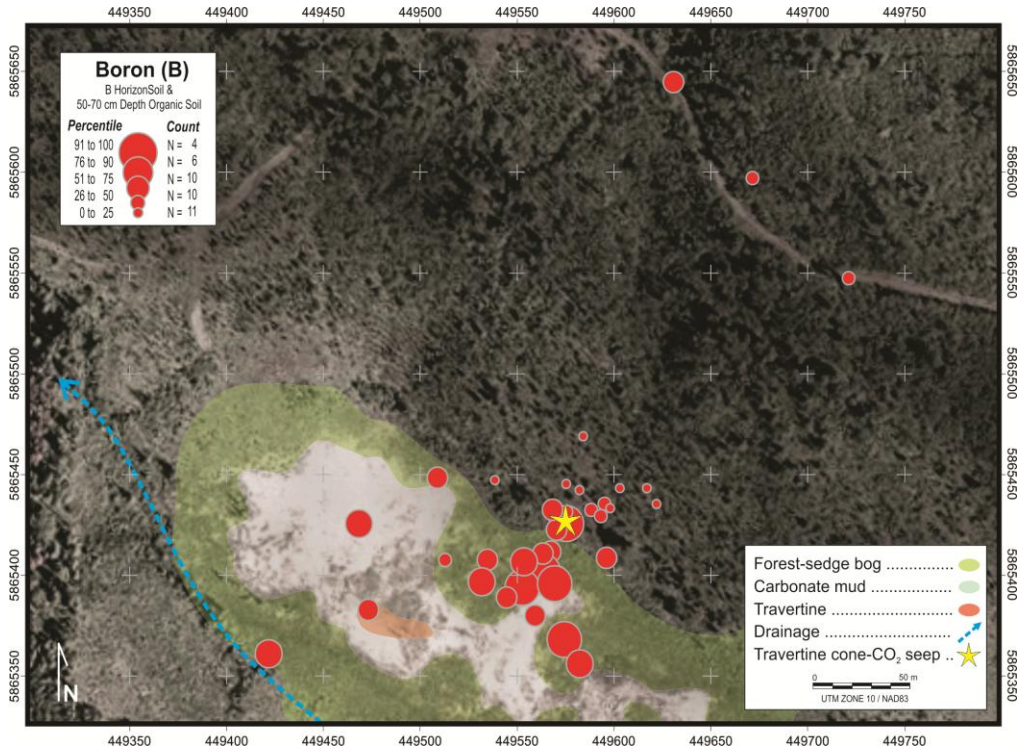

Figure 6.10. Boron by Na_2O_2 fusion-ICPMS in North Bog B soil horizon and 50-70 cm depth organic soil (25 %ile = 11 ppm; 50 %ile = 22 ppm; 75 %ile = 33 ppm; 90 %ile = 64 ppm; maximum = 80 ppm).

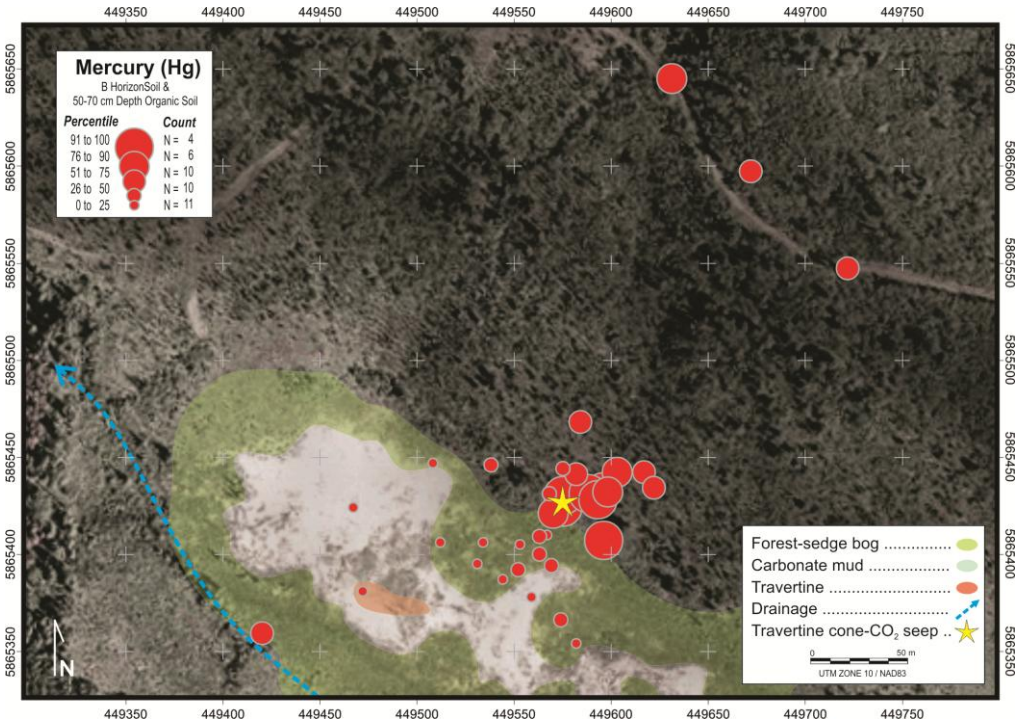

Figure 6.11. Mercury by AR-ICPMS in North Bog B soil horizon and 50-70 cm depth organic soil (25 %ile = 10 ppb; 50 %ile = 38 ppb ; 75 %ile = 88 ppb; 90 %ile = 348 ppb ; maximum = 2461 ppb).

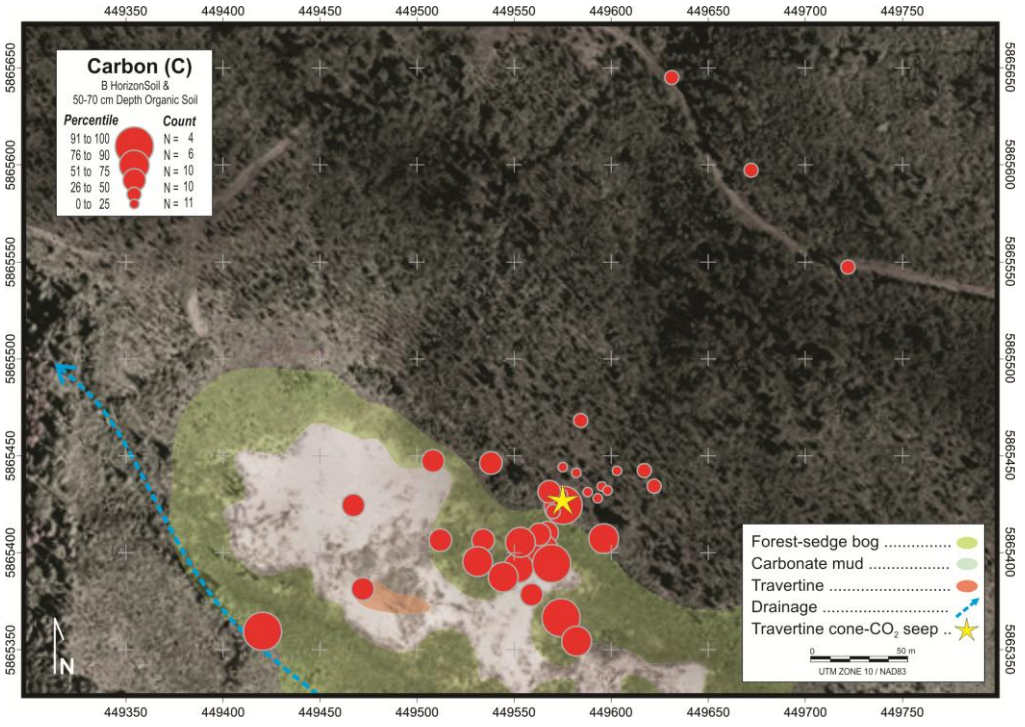

Figure 6.12. Total carbon by Leco in North Bog B soil horizon and 50-70 cm depth organic soil (25 %ile = 1.68 pct; 50 %ile = 12.9 pct; 75 %ile = 18.5 pct; 90 %ile = 31.6 pct; maximum =37 pct).

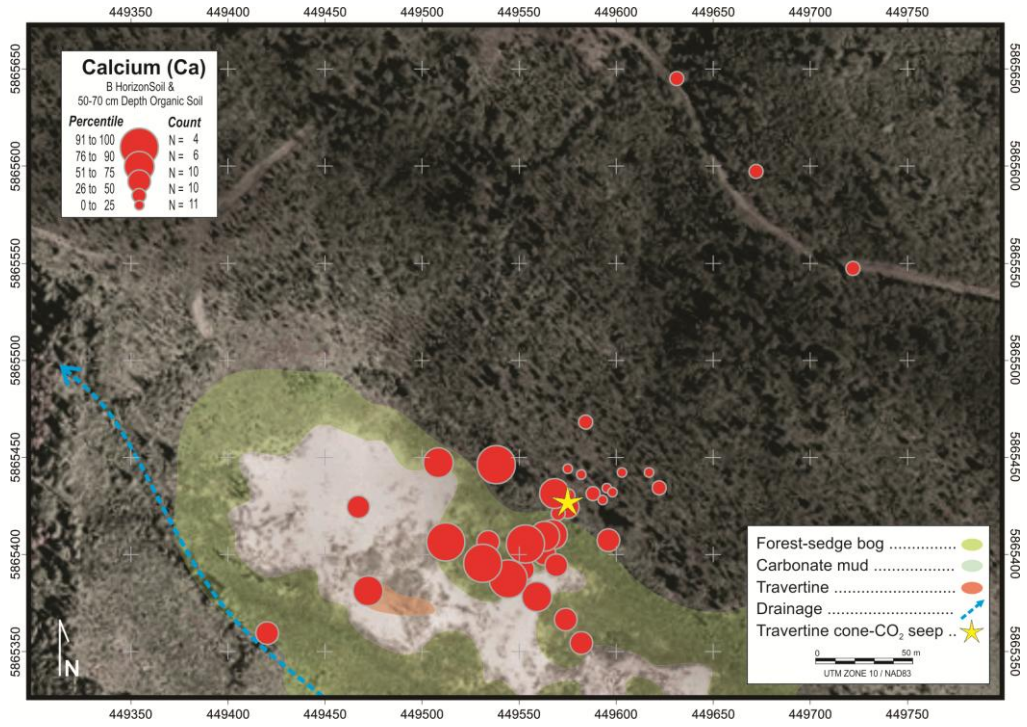

Figure 6.13. Calcium by AR-ICPMS in North Bog B soil horizon and 50-70 cm depth organic soil. (25 %ile = 0.3 pct; 50 %ile = 1.83 pct; 75 %ile = 22.79 pct; 90 %ile = 27.12 pct ; maximum = 33 pct).

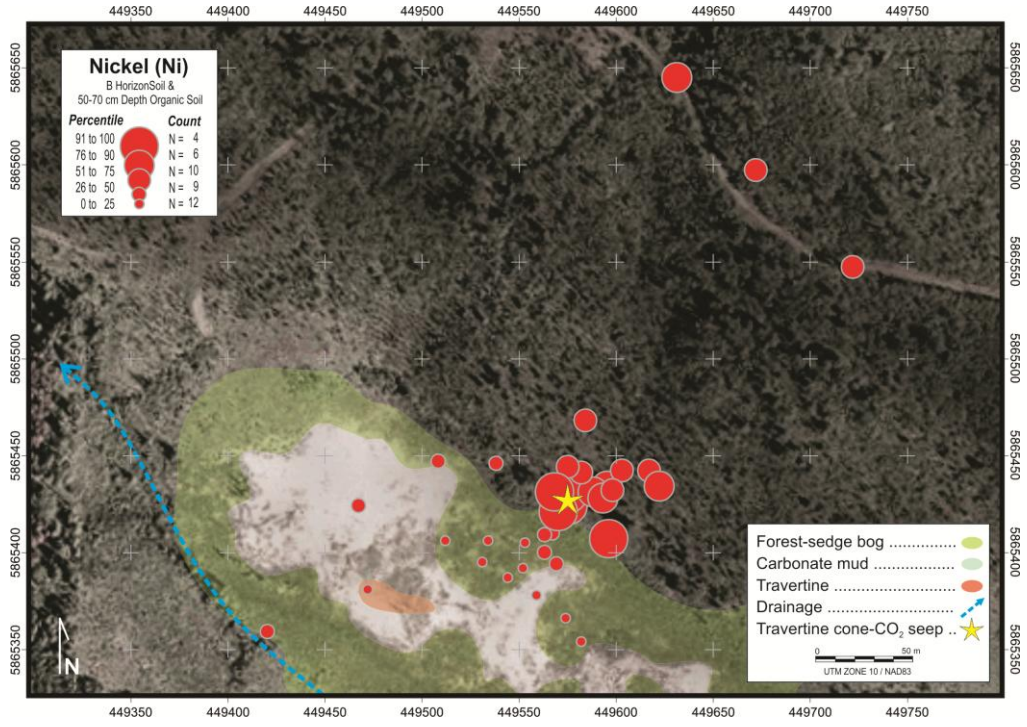

Figure 6.14. Nickel by AR-ICPMS in North Bog B soil horizon and 50-70 cm depth organic soil (25 %ile = 3.4 ppm; 50 %ile = 43.7 ppm; 75 %ile = 83.2 ppm; 90 %ile = 102.6 ppm ; maximum = 688 ppm).

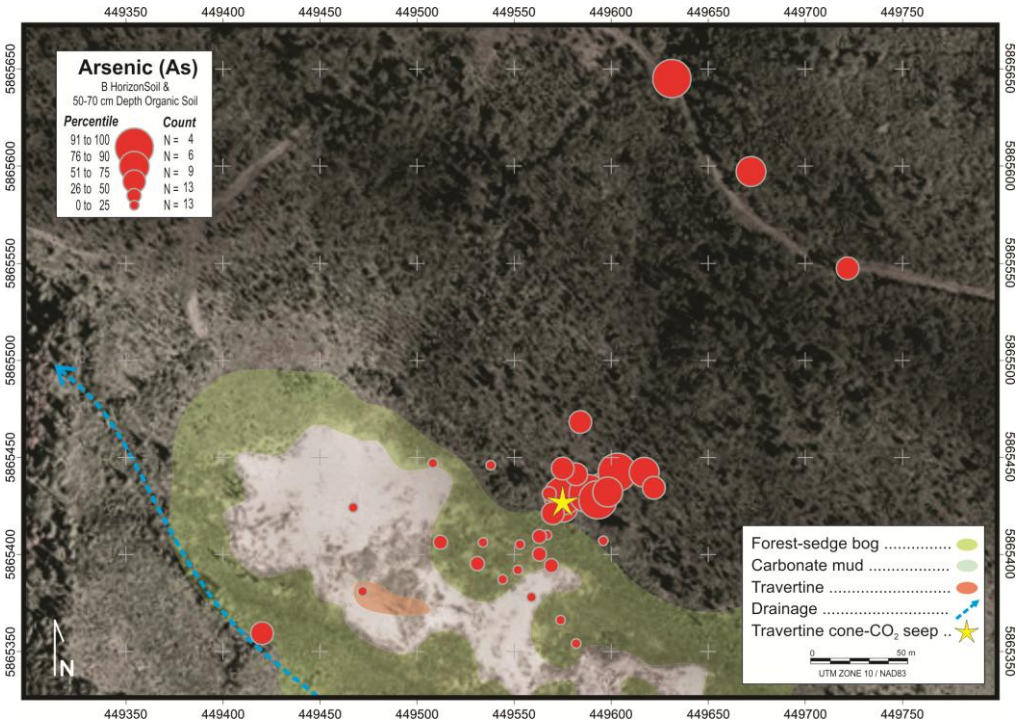

Figure 6.15. Arsenic by AR-ICPMS in North Bog B soil horizon and 50-70 cm depth organic soil (25 %ile = 0.05 ppm; 50 %ile = 1.4 ppm; 75 %ile = 4.2 ppm; 90 %ile = 6.4 ppm ; maximum = 18 ppm)

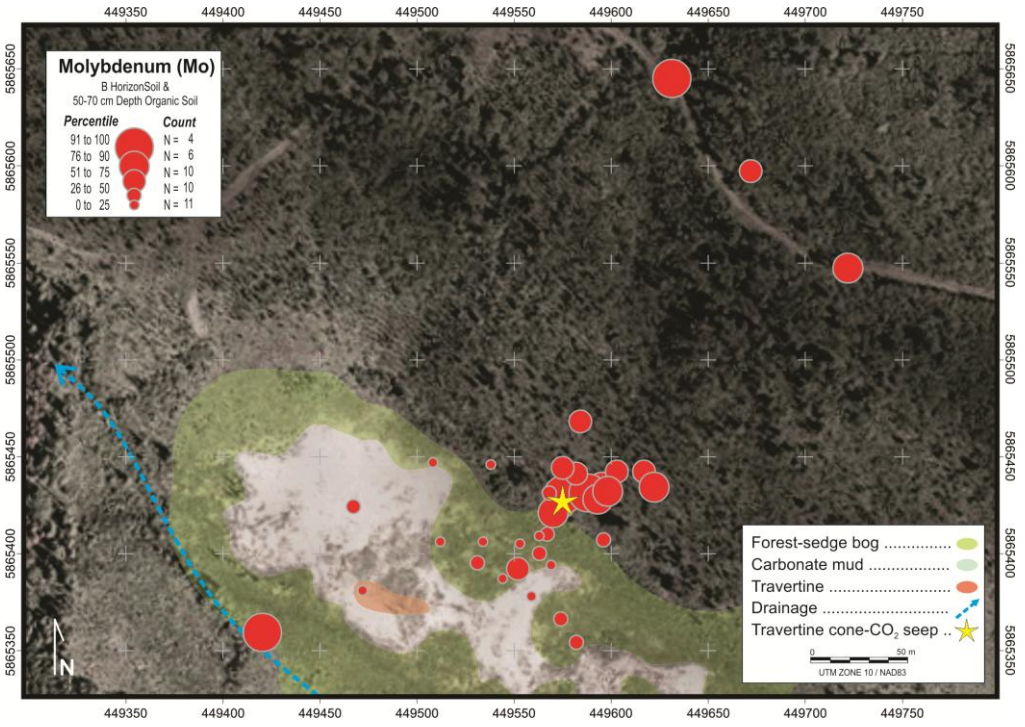

Figure 6.16. Molybdenum by AR-ICPMS in North Bog B soil horizon and 50-70 cm depth organic soil (25 %ile = 0.29 ppm; 50 %ile = 0.87 ppm; 75 %ile = 2.04 ppm; 90 %ile = 2.94 ppm ; maximum = 9 ppm)

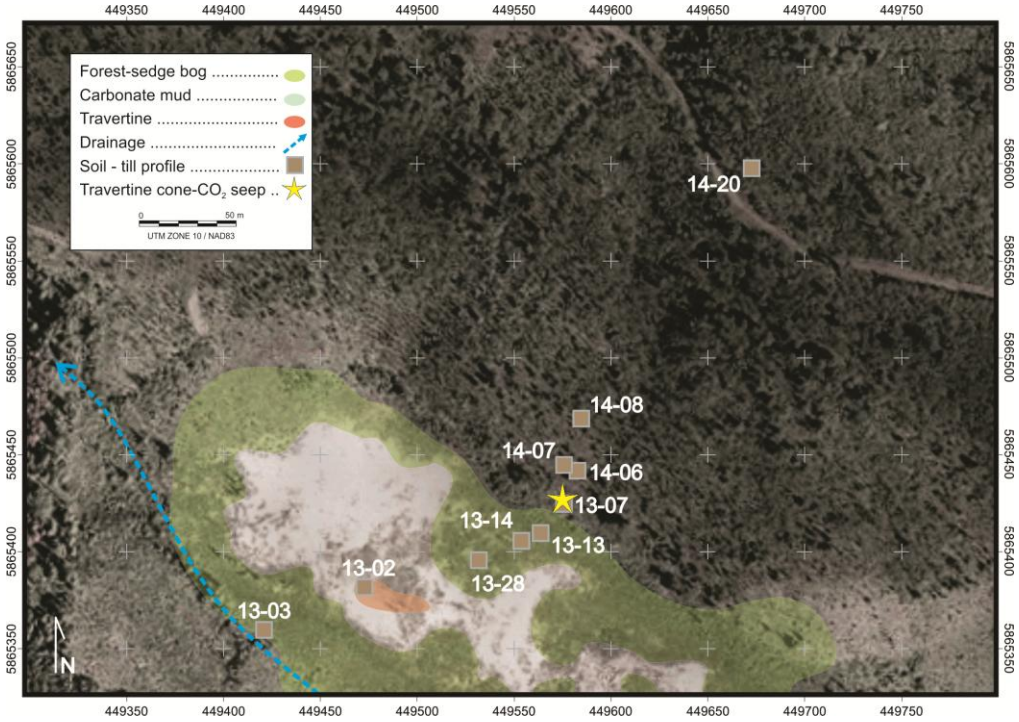

Figure 6.17. Profile locations used to create the North Bog line geochemistry graphs

Geochemical relationships in the different soil horizons are displayed by line graphs showing element variations along profiles beginning in the well-drained mineral soil on the hill side above the North Bog (Profile 14-20), through the bog margin and into the poorly drained organic-carbonate-rich soil in the North Bog (Profile 13-03). Figure 6.17 shows the location of the profiles along a northeast -southwest transect with the site of the travertine cone-CO_2 vent near the edge of the bog and the areas dominated by poorly drained organic and well-drained mineral soil indicated by the dark grey forested and green shaded area on Figure 6.17 . The "A" horizon values plotted on the graphs are show elements in the Ah horizon or in the upper (fibrous) layer of the organic soil. Figure 6.18 shows a Li peak for the C soil and organic soil near the bog edge, but a sharp B peak in the B soil horizon. Figure 16.19 shows sharp Hg and Ni peaks in the B and C soil horizons near the bog boundary, but whereas the Hg peak is in the mineral soil horizons, the Ni peak is the organic soil. Clearly, there is a different dispersion mechanism for Hg and Ni and/or different sources for the two elements. Mercury content of organic soil decreases towards the center of the bog. There were insufficient samples collected in 2013 to fully estimate the size of the Hg soil anomaly, but more sampling in 2014 indicates that the high Hg values are confined to a relatively small area less than 100 m^2 size in the well-drained mineral soils northeast of the travertine cone-CO_2 vent.

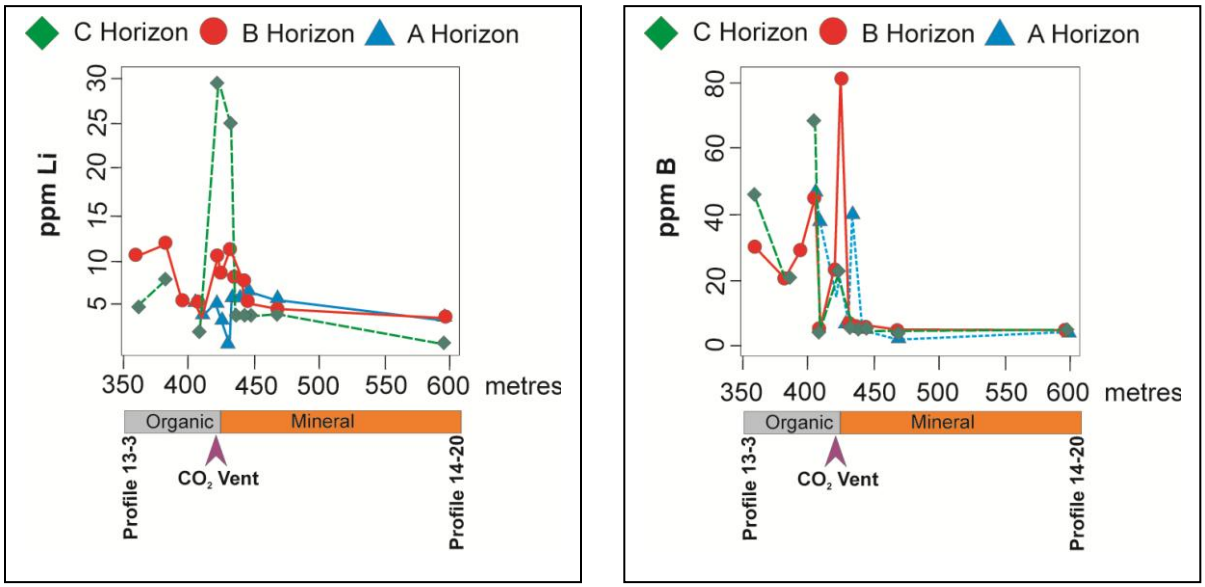

Figure 6.18. North Bog Li and B graphs for A, B and C soil horizons.

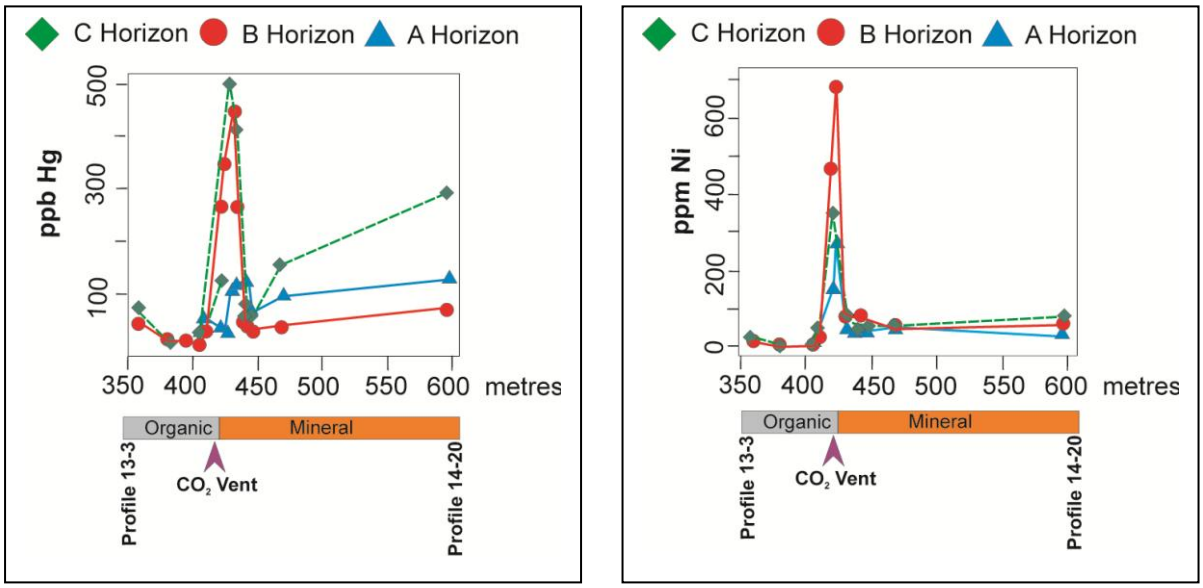

Figure 6.19. North Bog Hg and Ni graphs for A, B and C soil horizons.

6.4 Regional soil-till profile geochemistry

Table 8 compares lodge pole pine (*Pinus contorta*) outer tree bark, Ah, B and C soil horizon geochemistry, the number of sulphide mineral grains in C soil horizon (till) heavy mineral concentrates (HMC) and the soil pH in 6 profiles, identified in Figure 6.7. Profiles most distant from the bogs were sampled to estimate geochemical backgrounds for geothermal pathfinder

and other elements and to determine Hg dispersion in soil and vegetation near a known source of Hg minerals (cinnabar). Table 7 shows that the highest Li detected in the tree bark and samples at Profile 14-16, located 4 km south east from the bogs, is respectively 0.95 ppm and 6.58 ppm. These values compare to North Bog soil that has up to 59.1 ppm Li. Profile 14-17 located 400 m north of the North Bog has 806 ppb Hg in the C soil horizon, but only 34 ppb in tree bark and no cinnabar grains in the C soil horizon (till) HMC. The C soil horizon also has 14.5 ppm As. While the C soil horizon has no cinnabar there are 40 pyrite and 3 gold grains identified in the HMC. Profile 14-18, has 200 cinnabar grains, 400 ppm Hg in the - 80 mesh fraction of the C soil horizon and 206 ppb Hg in tree bark. Mercury is clearly elevated in the C soil horizon and in tree bark, but not in the Ah and B soil horizons despite presence of cinnabar. It is likely that the cinnabar had been transported in the till from an up-ice source. The C soil horizon at Profiles 14-16 to 14-19, north and east of the Nazko Cone, has up to 100 ppm Ni compared to less than 46 ppm at Profiles 14-14 and 14-15 south of the cone. The elevated Ni suggests that the till covering the area northwest of the North Bog has a high Ni geochemical background confirming the Ni results reported by Jackaman et al. (2014) for a regional till survey. The high Ni background in the till may explain the elevated Ni concentrations found in the North Bog organic soil and in the water

Prof.14-14	Type	Depth	As_ppm	B_ppm	Ca_pct	Fe_pct	Hg_ppb	Li_ppm	Ni_ppm	Rb_ppm	Sr_ppm	Total C	Soil pH	Cinnabar
147014	Bark	cm	0.01		1.33	0.015	65	0.02	0.3	1	68.7			grains
149047	Ah	8-10	1.0	1	0.39	1.69	141	2.94	14.8	4.1	54.7		5.18	
149048	B	15-18	1.4	1	0.21	2.40	41	5.60	23.0	6.4	31.9	1.76		
149049	C	85-100	4.9	1	0.47	3.02	228	4.50	43.6	10.5	60.5	0.39		50
Prof. 14-15	**Type**	**Depth**	**As_ppm**	**B_ppm**	**Ca_pct**	**Fe_pct**	**Hg_ppb**	**Li_ppm**	**Ni_ppm**	**Rb_ppm**	**Sr_ppm**	**Total C**	**Soil pH**	**Cinnabar**
147015	Bark	cm	0.1		0.71	0.027	72	0.07	0.8	1.2	89.9			grains
149051	Ah	0.5-1	1.5	2	0.65	1.76	141	3.35	18.9	5.0	76.0		5.01	
149052	B	8-10	2.7	10	0.20	2.76	34	5.20	27.0	6.2	30.5	1.33		
149053	C	180-190	5.0	10	0.50	3.27	140	3.80	46.3	7.7	44.9	0.10		10
Prof. 14-16	**Type**	**Depth**	**As_ppm**	**B_ppm**	**Ca_pct**	**Fe_pct**	**Hg_ppb**	**Li_ppm**	**Ni_ppm**	**Rb_ppm**	**Sr_ppm**	**Total C pct**	**Soil pH**	**Cinnabar**
147016	Bark	cm	1.4	3	0.57	0.551	252	0.95	15.6	2.1	29.4			grains
149055	Ah	0.5-1	5.3	2	0.84	3.89	191	6.58	77.8	8.9	72.4		6.24	
149056	B	15-18	1.0	1	0.44	5.84	51	6.50	91.2	8.4	46.2	3.48		
149057	C	140-150	6.9	1	0.74	3.19	148	6.20	88.3	7.4	43.7	0.15		10
Prof. 14-17	**Type**	**Depth**	**As_ppm**	**B_ppm**	**Ca_pct**	**Fe_pct**	**Hg_ppb**	**Li_ppm**	**Ni_ppm**	**Rb_ppm**	**Sr_ppm**	**C pct**	**Soil pH**	**Cinnabar**
147017	Bark	cm	-0.1	3	0.21	0.014	34	0.02	0.9	0.3	7.2			grains
149058	Ah	10-15	2.0	2	1.60	1.28	186	1.87	39.8	2.5	148.8		5.74	
149059	B	28-30	8.7	1	0.31	3.92	91	4.50	96.3	4.7	31.8	2.65		
149060	C	105-110	14.5	1	0.26	3.70	806	4.10	99.5	5.0	29.7	0.21		0
Prof. 14-18	**Type**	**Depth**	**As_ppm**	**B_ppm**	**Ca_pct**	**Fe_pct**	**Hg_ppb**	**Li_ppm**	**Ni_ppm**	**Rb_ppm**	**Sr_ppm**	**Total C pct**	**Soil pH**	**Cinnabar**
147018	Bark	cm	1	2	0.47	0.408	213	0.6	9.6	2	24			grains
149062	Ah	3-5	3.1	2	0.65	2.06	167	3.09	36.2	4.3	56.8		5.31	
149063	Soil	15-18	1.4	1	0.35	6.40	88	5.40	75.3	5.5	42.1	7.52		
149064	Till	140-150	9.3	1	0.38	2.93	400	4.40	82.5	5.5	37.2	0.11		200
Prof. 14-19	**Type**	**Depth**	**As_ppm**	**B_ppm**	**Ca_pct**	**Fe_pct**	**Hg_ppb**	**Li_ppm**	**Ni_ppm**	**Rb_ppm**	**Sr_ppm**	**Total C pct**	**Soil pH**	**Cinnabar**
147019	Bark	cm	-0.1	5	0.25	0.013	27	0.01	0.6	0.4	13.4			grains
149065	Ah	0.5-1	2.8	3	0.78	2.09	149	3.71	37.6	6.5	76.8		4.86	
149066	B	10-12	4.2	1	0.28	2.82	35	4.00	49.4	5.2	33.4	-0.02		
149067	C	160-170	5.8	1	0.59	3.41	86	5.80	93.7	6.4	48.6	-0.02		20

Table 8. Profiles 14-14 to 14-19.

6.5 Sequential extraction of selected elements from soil samples

Table 9 list ICPMS data for selected elements determined by a sequential extraction analysis of 8 soil samples with elevated Hg using 0.25 M hydroxylamine hydrochloride (NH_2Cl_2) at pH 3.0 followed by a HCl-HNO_3-H_2O_2 acid digestion (modified aqua regia). All of the data is listed in Appendix D. The table also list the results of a separate ICPMS analysis by HCl-HNO_3-H_2O_2 acid digestion (modified aqua regia). The percent hydroxylamine hydrochloride extracted element concentrations are highlighted in **bold** type in the table and the separate aqua regia - ICPMS analyses shown in *italics*. Table 8 reveals that there is a wide range of 0.25 M hydroxylamine hydrochloride extractable values depending on the element and the type of sample. Hydroxylamine hydrochloride primarily dissolves secondary Mn oxides to release trace metals absorbed to the oxide surface whereas the aqua regia dissolves many of the remaining minerals forming the sample matrix. Over 50 percent of Mn, Sr and Ca content is extracted by the hydroxylamine hydrochloride, but the amount dissolved varies with the sample type. Less than 1 percent of Hg is dissolved by hydroxylamine hydrochloride from samples that can have over

3000 ppb aqua regia extractable Hg whereas the samples have more than 30 percent hydroxylamine hydrochloride extractable Ca and more than 14 percent hydroxylamine hydrochloride extractable Mn. The small amount of hydroxylamine hydrochloride extractable Hg can be explained by the predominance of Hg as cinnabar in the soil, a sulphide mineral that is resistant to solution by the weakly acid hydroxylamine hydrochloride. Hence Hg, is most likely geochemically immobile during weathering and soil formation.

The results also illustrate how different soil types have affect the partitioning of elements into the hydroxylamine hydrochloride and aqua regia. All of the soil samples are from the B, BC or C soil horizons except 149042 with a higher carbon content (26%) suggesting that it is organic soil on the edge of the North Bog. This sample has a high Ag, Ba, Cu, Co, Fe and Ni content, but less than 8 percent of the metal is extracted by hydroxylamine hydrochloride suggesting that the metals are strongly bound to organic matter and are geochemically immobile in the near surface environment.

Sample	149004	149009	149010	149031	149032	149036	149042	149060
Pit number	1	3	3	9	9	10	12	17
Depth	50	20	50	5	50	50	28	105
Type	C hoz.	B-C hoz.	B-C hoz.	B-Hoz.	B-C hoz.	B-C hoz.	Bm Hoz.	C hoz. (till)
LAT	52.9361	52.9361	52.9361	52.9361	52.9361	52.9362	52.9359	52.9381
LONG	-123.7503	-123.7501	-123.7501	-123.75	-123.75	-123.7499	-123.75	-123.7495
Ag_NH2Cl2 %	**40.7**	**46.0**	**50.6**	**47.3**	**35.2**	**35.3**	**0.3**	**56.2**
Ag_ppb_total	*140*	*224*	*245*	*165*	*159*	*51*	*335*	*121*
Ba_NH2Cl2 %	**8.7**	**10.4**	**9.9**	**14.2**	**13.0**	**13.3**	**2.8**	**12.8**
Ba_ppm_total	*91.370*	*76.760*	*65.730*	*62.690*	*68.840*	*73.610*	*163.430*	*67.320*
Ca_NH2Cl2 %	**71.5**	**49.3**	**47.2**	**69.6**	**66.5**	**51.7**	**60.1**	**38.1**
Ca_pct_total	*0.46*	*0.45*	*0.42*	*0.26*	*0.33*	*0.31*	*1.96*	*0.27*
Co_NH2Cl2 %	**12.6**	**11.3**	**15.6**	**7.6**	**7.8**	**6.5**	**8.5**	**15.6**
Co_ppm_total	*18.88*	*19.95*	*18.24*	*16.88*	*14.20*	*15.08*	*72.82*	*17.90*
Cu_NH2Cl2 %	**1.1**	**1.8**	**2.6**	**2.4**	**1.4**	**1.3**	**0.8**	**0.3**
Cu_ppm_total	*55.74*	*46.01*	*46.96*	*37.86*	*39.70*	*46.04*	*34.93*	*40.75*
Fe_NH2Cl2 %	**4.5**	**2.3**	**2.4**	**3.3**	**3.1**	**2.3**	**3.7**	**2.3**
Fe_pct_total	*4.38*	*4.81*	*4.67*	*4.44*	*4.19*	*4.20*	*0.97*	*3.66*
Hg_NH2Cl2 %	**0.7**	**0.1**	**0.1**	**0.4**	**0.3**	**0.4**	**0.5**	**0.4**
Hg_ppb_total	*441*	*2544*	*3039*	*688*	*1023*	*742*	*628*	*857*
Mg_NH2Cl2 %	**15.3**	**8.5**	**10.4**	**6.4**	**10.1**	**7.3**	**74.0**	**10.8**
Mg_pct_total	*0.543*	*1.038*	*0.792*	*0.545*	*0.556*	*0.658*	*0.615*	*0.829*
Mn_NH2Cl2 %	**54.1**	**25.7**	**29.0**	**13.7**	**24.9**	**14.7**	**55.9**	**31.4**
Mn_ppm_total	*739*	*482*	*442*	*323*	*345*	*296*	*277*	*447*
Mo_NH2Cl2 %	**3.2**	**3.4**	**2.7**	**2.2**	**1.5**	**0.8**	**4.1**	**1.6**
Mo_ppm_total	*5.88*	*3.25*	*4.34*	*2.90*	*2.81*	*2.66*	*0.54*	*3.61*
Ni_NH2Cl2 %	**5.5**	**2.9**	**3.6**	**1.2**	**2.4**	**1.2**	**4.6**	**7.8**
Ni_ppm_total	*131.05*	*97.30*	*86.63*	*76.73*	*71.02*	*82.20*	*488.29*	*98.17*
Sr_NH2Cl2 %	**46.1**	**38.5**	**33.9**	**56.4**	**50.1**	**49.6**	**48.4**	**27.7**
Sr_ppm_total	*46.78*	*38.51*	*39.04*	*28.42*	*32.64*	*44.24*	*597.36*	*35.01*
V_NH2Cl2 %	**10.5**	**7.4**	**7.8**	**11.6**	**11.4**	**10.4**	**3.9**	**4.9**
V_ppm_total	*92*	*84*	*82*	*103*	*94*	*77*	*18*	*61*
Zn_NH2Cl2 %	**3.0**	**3.4**	**3.7**	**0.8**	**2.3**	**1.2**	**11.8**	**1.4**
Zn_ppm_total	*103*	*93*	*82*	*109*	*97*	*81*	*48*	*83*

Table 9. Sequential extraction of elements by 0.25 M NH_2Cl_2 at pH 3 and HCl-HNO_3-H_2O - ICPMS

Sample	Profile	Hg_ARICPMS_2015	Hg_ARICPMS_2014	Hg_CVAAS_ppb
149004	1	486	488	370
149009	3	2835	2461	2320
149010	3	3400	3137	2890
149031	9	729	749	620
149032	9	1120	1035	850
149036	10	780	831	710
149042	12	500	618	960
149060	17	798	806	730

Table 10. Reanalysis of select soil samples for Hg in ppb by aqua regia followed ICPMS (ARICPMS) and cold vapour atomic absorption spectrometry (CVAAS)

Table 10 lists Hg values in 8 soil samples analysed in 2014 and 2015 by modified aqua regia-ICPMS and in 2015 by aqua regia-cold vapour atomic absorption spectrometry (CVAAS). These data show a close comparison between the 2014 and 2015 Hg values. However, there are larger differences between Hg determined by modified aqua regia-ICPMS and CVAAS and the CVAAS Hg values are lower than those by modified aqua regia-ICPMS. The percentage difference between the results ranges from less than 20 percent for 6 of the 8 samples to 43 percent in two of the samples.

6.6 Lodgepole pine (*Pinus contorta*) bark chemistry

There are several potential geothermal pathfinder elements (e.g. Li, B, Hg) determined in the lodgepole pine (*Pinus contorta)* outer bark sampled at sites near the North Bog. Table 7 lists analyses of the bark sampled at sites some distance from the North Bog showing that Ba, Zn, Mn and Hg appear elevated at several of these sites, but the values should be treated with caution becasue of proximity to logging roads and the possibility of sample contaimination despite washing of the ash before prearation and analysis. There is a smaller contamination potential for the outer bark samples from trees closer to the North Bog because the roads are seldom used by vehicals. Figures 6.20 and 6.21 indicate that outer bark samples close to the travertine cone-CO_2 vent have over 6 ppm B and 72 ppb Hg. There is liitle variation of Li in the outer bark and values range from 0.2 to 0.7 ppm. In addition, the outer bark has 89.9 ppb Sr, 1.2 ppm Li and 0.28 ppm Li. Elevated Hg levels in the Lodgepole pine bark may be signifcant because of there are high Hg concentrations in the soil near the North Bog, but while bark from one tree is 72 ppb Hg, this value should be compared the 5000 ppb measured in the lodgepole pine bark near the Pinchi Hg mine in Central BC (Dunn, 2007).

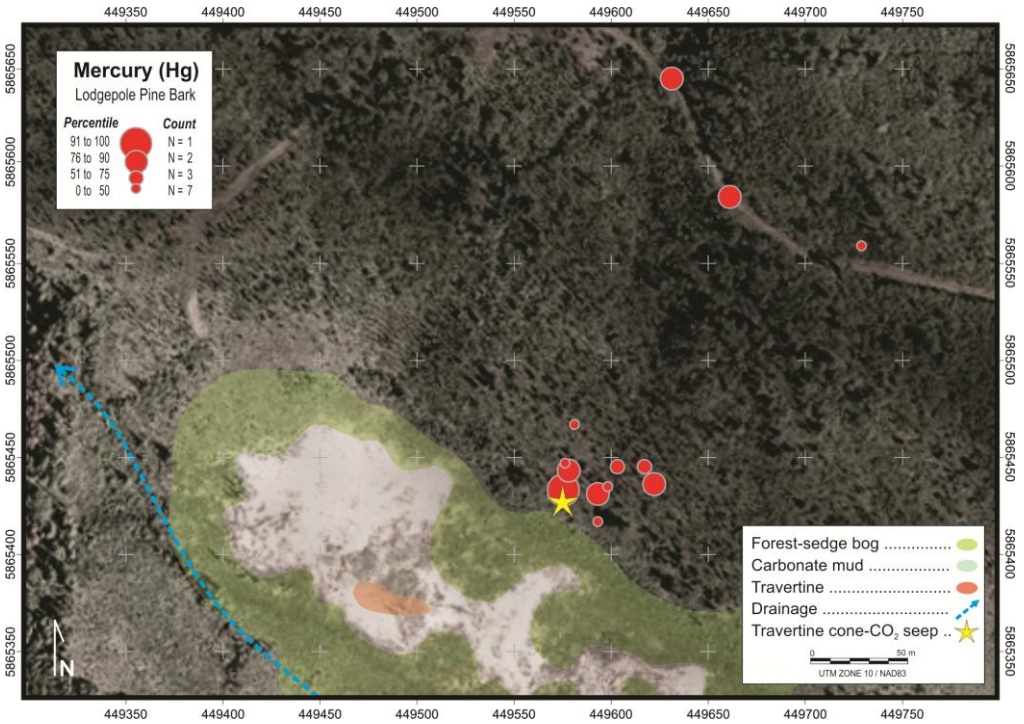

Figure 6.20. Mercury in Lodgepole pine (*Pinus contorta)* bark, North Bog (50 percentile = 33 ppb; 75 percentile = 39 ppb; 90 percentile = 69 ppb; maximum = 95 ppb).

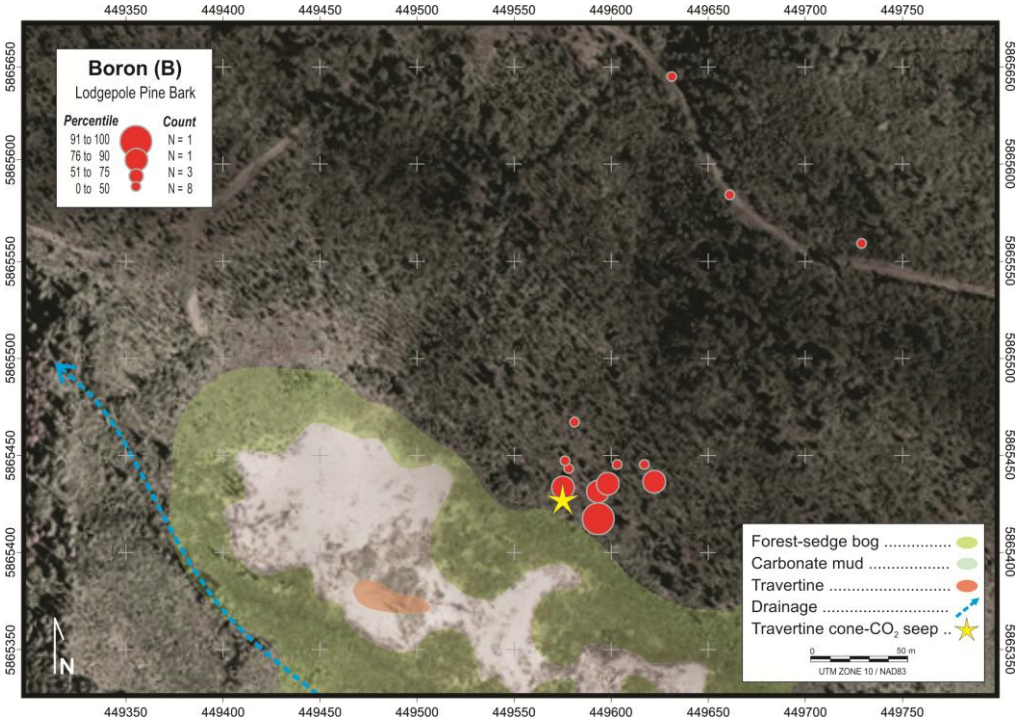

Figure 6.21. Boron in Lodgepole pine (*Pinus contorta)* bark, North Bog (50 percentile = 3.5 ppm; 75 percentile = 5.0 ppm; 90 percentile = 5.5 ppm; maximum = 7 ppm).

6.7 Soil pH

Variation in the pH of the upper B soil horizon and upper layer of the organic soil is displayed in Figure 6.22. There is a marked difference in more acid pH of the well-drained soils on the hill slope above the bog compared to more alkaline Ca-rich organic soil in the North Bog. There are, however, no systematic changes in soil pH that would suggest an influence of a subsurface effect (e.g. gas leakage) on the soil chemistry.

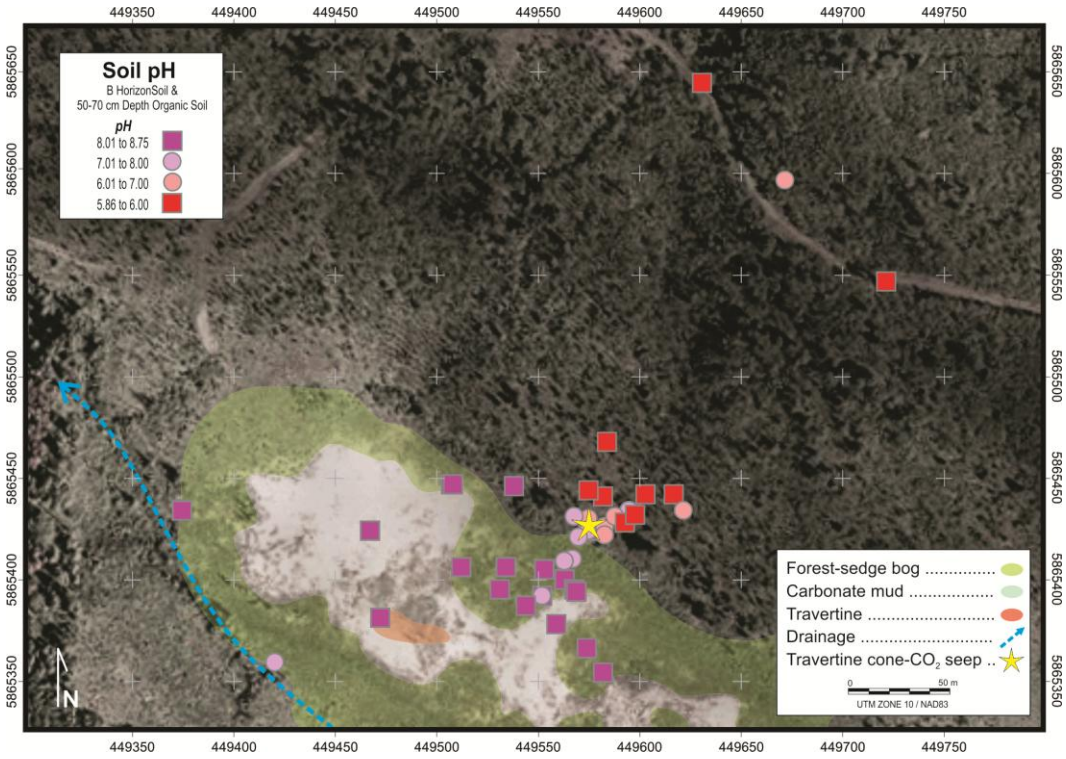

Figure 6.22. B horizon soil or upper layer organic soil pH, North Bog.

7 Rock Geochemistry

Trace elements in 8 rock samples collected in 2014 and described in Table 11 are listed in Table 12. The results confirm the travertine chemistry reported in 2013. Seven of the samples are from the North and South Bogs (Figure 6.23) and one (148009) is from Marmot Falls, a large travertine deposit located 12 km south from the village of Nazko. This deposit has no obvious hot spring association and was sampled to generate background data for comparison to the Nazko bog travertine chemistry. Contents of most minor and trace elements in the travertine are very low or below detection limit, but a conglomerate boulder (sample 148002) from the hill slope north of the North Bog contains over 8000 ppb Hg. There are lower Hg (539 ppb) levels with Ni (49 ppm) in the travertine (sample 148007) from the wall of the travertine cone-CO_2 vent. Major oxides, in Table 13, reveal that that travertine is largely of Ca and Mg carbonates and the travertine mineralogy (determined by quantitative X-ray diffraction) near the active CO_2 seepages is predominantly aragonite whereas travertine from the bog surface and the Marmot Falls carbonate is mainly calcite. Table 14 lists results of the quantitative X-ray diffraction and stable isotope analysis. A graph of $\delta^{13}C$ and $\delta^{18}O$ in the travertine samples from the North Bog, South Bog and Marmot Falls is shown in Figure 6.24. Also displayed on the graph are $\delta^{13}C$ and $\delta^{18}O$ for two travertine sites from Italy associated with warm spring (> 50°C) water reported by Pentecost (1995). All of the bog and Italy sites have very different $\delta^{13}C$ and $\delta^{18}O$ values than the Marmot Falls carbonate, but the is no clear trend that would suggest that the North and South Bog travertine has an isotopic signature attributable to a thermal water source.

Sample	UTM-East	UTM-North	Description
148002	449604	5865443	Float ~ 2 m from Profile 4. Sub angular blocks of dense, red, chert conglomerate. Cinnabar or barite possible in matrix.
148003	449478	5865379	North Bog. Large (20 cm x 30 cm x 10cm) travertine slabs along N-S ridge in bog center.
148004	449498	5865372	North Bog. Rusty travertine slabs along at S end on N-S ridge in bog center.
148005	449530	5865016	South Bog. Remnant, inactive seep - travertine slabs around inactive CO_2 seep.
148006	449487	5865051	South Bog. Travertine blocks scattered on surface near area of wetland.
148007	449579	5865428	North Bog. Travertine from the wall of the cone surrounding active CO_2 seep in the North Bog.
148008	449574	5865425	North Bog. Very iron stained travertine rubble mixed with organic soil. 3.8 m from 148007.
148009	460200	5858500	Marmot Falls. Travertine cementing boulders on the south face of a cliff ~ 1 m from foot of falls.
158002	449555	5865463	Sub angular (0.5 m x0.5m) boulder of cherty conglomerate with a bright red matrix from hill slope above the North Bog.

Table 11. Description of rock samples collected in 2014 and 2015.

Sample	148002	148003	148004	148005	148006	148007	148008	148009	158002
Ag ppb	150	4	-2	4	3	3	-2	8	147
As ppm	9.9	-0.1	-0.1	0.3	0.5	12	0.7	1.8	95.9
B ppm	20	-20	-20	113	30	-20	22	25	-20
Ba ppm	156.6	321.3	374.9	206.7	158.7	349.3	372.9	392.1	164
Ca pct	0.01	34.57	37.46	28.11	36.17	28.72	35.24	32.93	0.01
Ce ppm		-0.1	-0.1	0.3	0.7	0.6	0.5	3.1	1.9
Co ppm	0.8	-0.1	-0.1	-0.1	4.6	7.9	23.8	1.8	1.1
Cr ppm	25.1	0.9	0.8	1	-0.5	-0.5	1	3.3	21.4
Cu ppm	7.69	1.46	0.47	0.59	0.56	0.49	1	3.35	20.61
Fe pct	1.85	0.03	2.46	1.12	0.02	3.44	0.85	0.23	6.35
Hg ppb	8213	-5	-5	7	8	539	16	14	4589
La ppm	1.2	-0.5	-0.5	-0.5	-0.5	-0.5	-0.5	1.2	0.9
Li ppm		5.5	4.9	17.5	5.3	1.8	4	18.4	0.6
Mn ppm	26	276	494	73	331	303	1405	160	49
Mo ppm	2.08	0.1	0.1	0.06	0.07	0.33	0.15	0.67	1.71
Ni ppm	3.6	1.8	1	3.1	4.6	48.8	83.7	7.7	6.3
P pct	0.008	0.006	0.014	0.021	0.003	0.015	0.005	0.016	0.033
Pb ppm	1.95	0.38	0.08	0.2	0.11	0.08	0.12	0.66	17.32
Te ppm	0.03	1.01	0.67	0.94	0.38	0.4	0.47	0.04	0.04
V ppm	17	-2	-2	4	-2	7	-2	6	26
Zn ppm	3.8	5.7	0.9	4.9	1.8	36.7	7.5	6.2	2.1

Table 12. Rock samples analysed for trace elements by aqua regia - ICPMS.

Sample	**148002**	**148003**	**148004**	**148005**	**148006**	**148007**	**148008**	**148009**
Al_2O_3 PCT	3.47	-0.01	-0.01	0.08	-0.01	0.02	0.02	1.1
CaO PCT	0.02	51.23	48.14	36.56	50.49	46.11	48.78	44.34
Cr_2O_3PCT	0.015	-0.002	-0.002	-0.002	-0.002	-0.002	-0.002	-0.002
Fe_2O_3 PCT	3.03	-0.04	3.41	1.65	-0.04	7.56	1.55	0.53
K_2O PCT	0.46	0.01	0.01	0.13	-0.01	0.02	0.02	0.31
MgO PCT	0.17	0.93	2	3.98	2.13	0.4	1.55	4.45
MnO PCT	-0.01	0.04	0.06	0.01	0.05	0.06	0.22	0.03
Na_2O PCT	0.03	0.15	0.1	0.73	0.1	0.15	0.21	0.84
P_2O_5 PCT	0.07	-0.01	0.02	0.04	-0.01	0.05	0.01	0.03
SiO_2 PCT	89.62	0.14	0.37	0.7	0.07	0.75	0.36	5.53
TiO_2 PCT	0.17	-0.01	-0.01	-0.01	-0.01	-0.01	-0.01	0.09
LOI PCT	2.9	45.7	44.8	54.7	45.9	43.3	45.8	42.5
Total C PCT	0.05	13.72	13.11	18.74	13.51	12.28	13.54	11.88
Total S PCT	-0.02	0.02	0.03	0.05	-0.02	-0.02	-0.02	0.09
Ba ppm	632	333	354	199	165	418	415	443
Nb ppm	-5	6	-5	-5	-5	-5	-5	6
Sc ppm	4	-1	2	8	2	9	-1	1
Sr ppm	111	14564	8233	10964	9717	12439	11993	1455
Y ppm	6	-3	-3	5	-3	4	-3	-3
Zr ppm	46	5	7	-5	-5	10	-5	16

Table 13. Rocks analysed for major oxides and minor element by lithium borate fusion-ICPES, total C and S by Leco combustion; loss on ignition (LOI) results at 1100^{o}C.

Isotope	148003	148005	148006	148007	148009
d18O ‰ vs. VMSOW	5.6	6	4.7	6.8	2.4
d13C ‰ vs. VPDP	15.3	16.4	15.4	14.9	14.8
Mineral					
Calcite Magnesian, (Ca, Mg) CO_3	31.9	13.3	81.1	18.2	88
Aragonite, $CaCO_3$	67.5	75.5	18.5	81.3	4.1
Nesquehonite, ($Mg(HCO_3)$ (OH $2H_2O$)		9.2			
Vaterite, CaCO3		0.4			
Ankerite-Dolomite, $Ca(Fe^{2+}$, Mg,Mn)$(CO_3)2/CaMg(CO_3)_2$					2.4
Magnesite, $MgCO_3$					1.1
Plagioclase					2.7
Quartz	0.7	1.3	0.4	0.6	1.7
Total	100	100	100	100	100

Table 14. Results of rock samples analysed for stable isotope and minerals by quantitative X-ray diffraction (XRD).

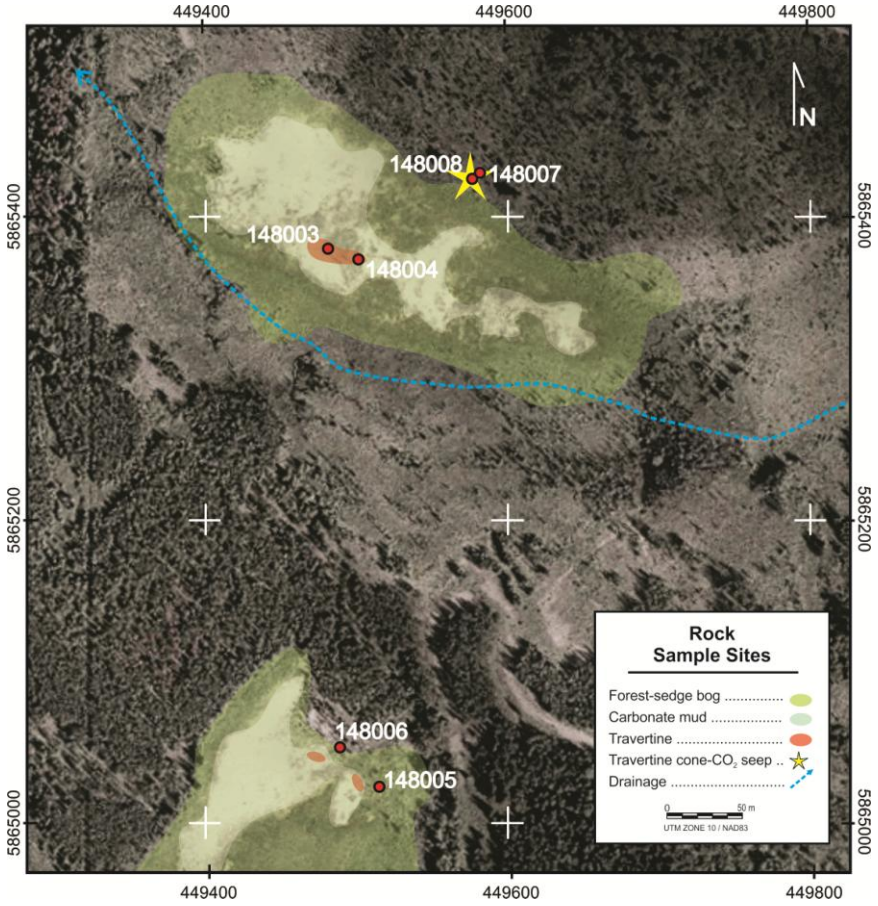

Figure 6.23 Location of rock samples collected in 2014.

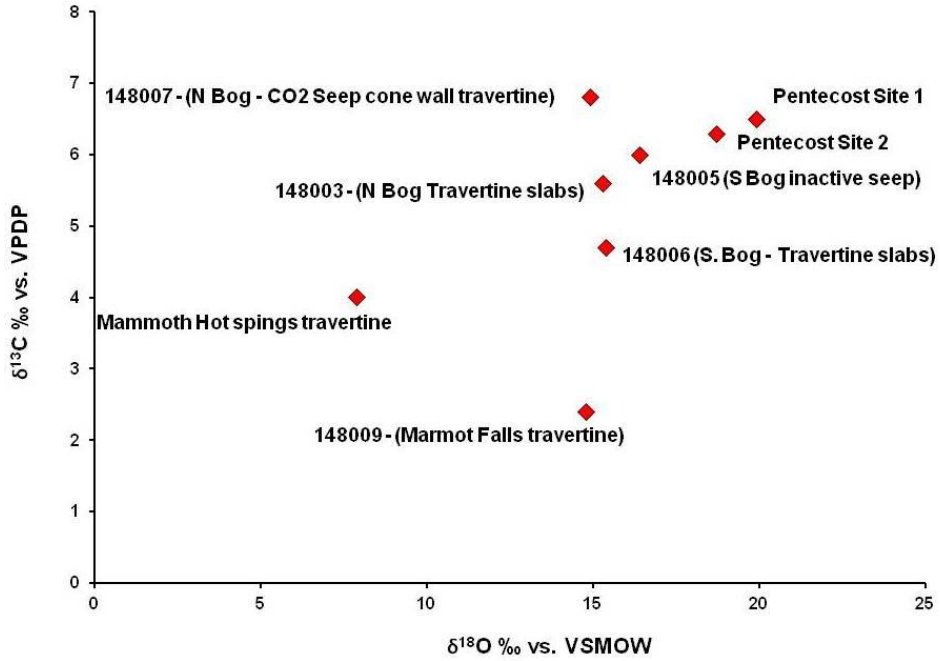

Figure 6.24. Results of δ ^{13}C and δ ^{18}O analyses of travertine samples collected from the North Bog, South Bog, Marmot Falls (Appendix G) and two travertine sites from Italy reported by Pentecost (1995)

8. Seepage gas geochemistry

Figure 6.25 shows the location of the four seepage gas samples collected in duplicate from the North and South Bogs. The duplicate sample ^{3}He/^{4}He ratio, the ^{4}He concentration in ppm (V:V) and the degree of ^{3}He/^{4}He analysis uncertainty reported by Wood Hole Oceanographic Institute (WHOI) isotope laboratory are listed in Table 15. The total ^{4}He concentration reported by the WHOI is converted to ppm (v:v) by correcting the sampled volume of the gas (typically 13 cc) to STP (100 kp, 273^{o}K) based on the atmospheric pressure reported at Quesnel airport and the water temperature on May 29th, 2015 when the samples were collected (101.465 Kp). Figure 6.26 shows the ^{3}He/^{4}He ratio for each sample and the mean ^{4}He concentration of the two ^{4}He determinations.

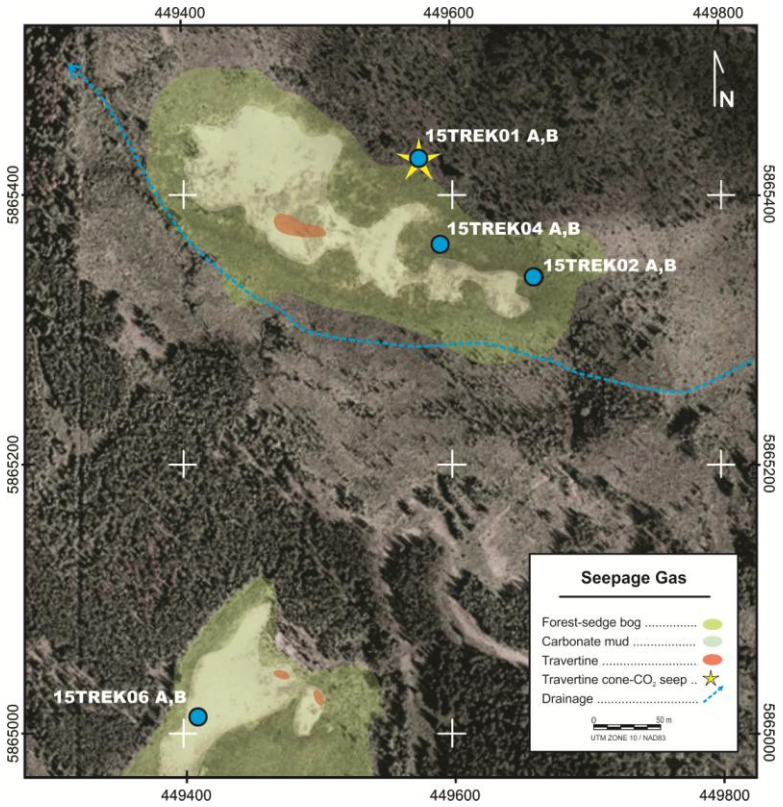

Figure 6.25. Location of seepage gas samples collected for He analysis in 2015.

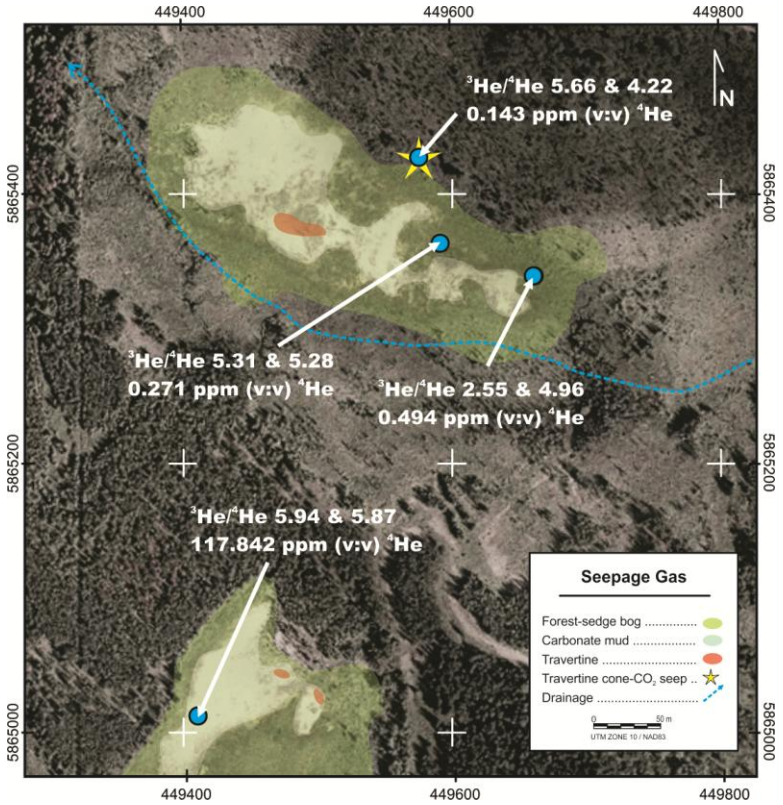

Figure 6.26. Seepage gas $^{3}He/^{4}He$ ratios and ppm (v:v) ^{4}He in gas.

Sample ID	$^3He/^4He$ R/Ra	$^3He/^4He$ uncertainty	^4He (cc STP) total	^4He ppm (STP)
15TREK-GT-1A	5.6598	0.0647	3.7815E-06	0.281
15TREK-GT-1B	4.2200	0.3166	6.9905E-09	0.004
15TREK-GT-2A	2.5513	0.0280	9.4697E-06	0.680
15TREK-GT-2B	4.9582	0.0527	4.2812E-06	0.307
15TREK-GT-4A	5.3124	0.0566	4.0087E-06	0.288
15TREK-GT-4B	5.2809	0.0574	3.5559E-06	0.255
15TREK-GT-6A	5.9392	0.0646	1.6076E-03	114.930
15TREK-GT-6B	5.8698	0.0656	1.6840E-03	120.393

Table 15. Seepage gas $^3He/^4He$ ratios in duplicate samples and uncertainty. Total and corrected for STP sample volume ppm (v:v) ^4He in the gas.

The $^3He/^4He$ ratios and ppm (v:v) ^4He concentrations in the seepage gas at each site are displayed in Figure 6.26. Samples 15TREK-GT-1 A and B are of gas flowing from the travertine-CO_2 vent in the North Bog. Samples 15TREK-GT-2 A and B and 15TREK-GT-4 A and B are of gas seepages in pools towards the center of the bog where, in addition to CO_2, there is detectable smell of H_2S. Samples 15TREK-GT-6 A and B in the South Bog are of a more subdued gas flow in the marshy area shown in Figure 6.27. The highest $^3He/^4He$ ratio (5.94) and mean ^4He concentration (117 ppm) was measured in the CO_2,-rich gas at this site. Similar $^3He/^4He$ ratios measured in the CO_2,-rich gas at sites 15TREK-GT-4 A and B and 15TREK-GT-6 A and B indicate a reliable measurement of the isotopic composition. The lower $^3He/^4He$ ratio for samples 15TREK-GT-2A and 1B may reflect atmospheric He contamination (Kutz , pers comm, 2015).

Figure 6.27. The 15TREK-GT-6 A and 6B sample site in the South Bog.

9 Discussion of the Results

Variations in ground and surface water chemistry could reflect (1) cold water flowing into the Nazko bogs from the surrounding uplands; (2) thermal water upwelling from bedrock; (3) mixing of hot and cold water in bedrock and overburden aquifers. The unusually low temperature of the water in the travertine cone-CO_2 vent on the edge of the North Bog compared to surface and other ground water temperatures suggests absence of a proximal subsurface heat source.

One explanation for the low, relatively constant water temperature over time may lie in the thermodynamics of the water-CO_2 system. The net enthalpy for formation of H_2CO_3 from CO_2 and H_2O is + 1.76 kcal mol^{-1} (Faure, 1995) and this positive heat flow predicts an endothermic reaction. Hence, CO_2 bubbling through the water could absorb heat and lower the water temperature. However, there are several active North Bog CO_2-rich gas seeps sampled in 2015 in pools where water temperature is 15°C and no visible travertine has formed. This would suggest that the cool water in the travertine-CO_2 vent does not, in fact, reflect an endothermic reaction between the CO_2 and the water. However, the net enthalpy for the reaction between Ca^{2+} and CO_3^{2-} forming $CaCO_3$ is - 2.94 kcal mol^{-1} indicating that the reaction is exothermic and generates heat. The bog surface water temperature may therefore be a function of the heat generated from $CaCO_3$ formation balanced by the heat absorbed by the CO_2-H_2CO_3 reaction. Generation of a small amount of heat from the formation of $CaCO_3$ could also explain local anecdotal reports that the Nazko bogs are ice-free in winter.

A reason for the low travertine cone-CO_2 vent water temperature could be that hot, ascending water transferred heat to cooler aquifer rocks as the water flowed from depth along structures and flow paths to the surface. There is, however, no visible evidence for active ground water upwelling and, moreover, the δ^2H, $\delta^{18}O$ values suggest that the water is from a meteoric source. It is, of course, possible that any visible signs of ground water discharge are concealed under the organic sediment along the edge of the bog.

Lithium, B, Mg, Ca, Rb, Si, Cl and Sr in the Nazko bog ground water are lower than those reported in hot spring water from Turkey by Pasvanoğlu (2013), but concentrations are higher than those in the "Volcano" bog and North Bog stream water. Hence, elevated Li, Mg, B, Sr, and Si may reflect the source water chemistry and reaction between rock and water during ascent to the surface. Rocks with a higher Li content include granite pegmatite, rhyolite and evaporite (Eccles and Berhane, 2011). Marine carbonate-evaporite rocks can be another source for the Li, Ca, Mg and CO_2, and the correlation between Li vs Mg in the North Bog water could be a reflection of the reaction between ascending thermal water and carbonates in the geological sequence. For example, Coolbaugh et al. (2011), noted a relationship between the Mg/Li ratio in travertine and that in ground water. There are insufficient water samples from the North Bog

to trace the source of these elements, but clustering of ground water samples with high Li and B near the travertine -CO_2 cone; increased Li and B in organic soil and in tree bark suggests that this area is a possible discharge zone for mineralized water.

High concentrations of Hg have been reported in the hot spring water at Yellowstone National Park (King et al.2006) and other geothermal fields, but no Hg was detected in any of the Nazko area waters despite the high found Hg in mineral soil near the North and South bogs. The very small concentration of Hg extracted by hydroxylamine hydrochloride from a mineral soil with high Hg suggests the most likely Hg mineral form, cinnabar, is resistant to weathering and that Hg has limited mobility in soil and water. Although there are cinnabar grains in till and cinnabar in conglomerate boulders near the bogs, a bedrock Hg source is presently unknown.

Mineral solubility modelling suggests that at a temperature and pH typical of bog water calcite precipitates from an aqueous Ca-CO_3-HCO_3 system in preference to aragonite. However, X-ray diffraction analyses of rock from the wall of the travertine cone-CO_2 vent reveals that aragonite (> 80 percent) is the dominant carbonate mineral. The amount of aragonite in travertine sampled where there are no active CO_2 seeps is smaller and the decrease in aragonite content could reflect maturity and changing carbonate mineralogy of the travertine over time. A higher water temperature and a faster precipitation rate in warm, shallow saline basins where CO_3^{2-} concentrations are higher can also favour the precipitation of aragonite rather than calcite as suggested by Railsback (2014).

Water temperature can be predicted from silica saturation assuming that SiO_2 is in equilibrium with the water. The North Bog saturation indices indicate that chalcedony (SiO2) could precipitate or is close to saturation in water and the XRD analysis detected traces of Si in the travertine. Pasvanoğlu (2013) proposed an equation for predicting temperature from chalcedony equilibrium to be:

$$\text{Log } SiO_2 = 4.69 - (1.32/t^{o}C + 273.15)$$

The SiO_2 geo-thermometer predicted temperatures listed in Table 15 are clearly much higher than those actually measured in the water and are unrealistic since only trace amounts of quartz were detected in travertine by the XRD analysis. However, the model could suggest that water temperatures in the North Bog may be higher in the past.

Analyte	131009	142006	142007	142002	142004	142003
Type	Pool	Stream	Stream	Ground	Ground*	Ground
pH	7.8	7.14	8.12	6.5	6.37	5.76
Temp. ^{o}C	19.3	14.3	11.2	5.8	5.9	11.26
Temp. ^{o}C**	35.2	67.6	47.6	30.6	27.5	66.9
Si ppm	10.4	21.6	14	9.26	9.63	21.3
Chalcedony	-0.14	0.24	0.08	-0.12	-0.04	0.27

Table 16. Chemistry and chalcedony saturation index for ground, surface pool and stream water sites in the North Bog. Ground* (sample 142004) is water from the travertine cone-CO_2 vent water. Temp. ^{o}C** is calculated for chalcedony equilibrium by Log SiO_2 = 4.69-(1.32/t^{o}C +273.15) (Pasvanoğlu, 2013)

Magmatic CO_2 reacting with dissolved Ca^{2+} forms "thermogenic" travertine where the calcite and aragonite are enriched in $\delta^{13}C$ and $\delta^{18}O$ (Ford and Pedley, 1996; Pentecost, 1995). The carbonate from the travertine-CO_2 vent has the highest $\delta^{13}C$ values of all the travertine samples, but no apparent $\delta^{18}O$ enrichment.

Among possible sources for the CO_2 discharging from the Nazko bog seepages are magma degassing, metamorphic decarbonisation and reaction of crustal carbonates with acid ground water. Discrimination between the different sources can be difficult. For example, Giustini et al. (2013) interpreted the results of $\delta^{13}C$ analysis of gases sampled from natural seeps on non-volcanic San Vittorino plain, Italy, to indicate that an average 75 percent of the CO_2 was generated by the thermo-metamorphic reaction of limestone, but less than 6 percent of the CO_2 was magmatic. They found that the $\delta^{13}C$ composition of the CO_2 ranged from - 2 $^{o}/_{oo}$ to 3.8 $^{o}/_{oo}$ compared to $\delta^{13}C$ values between – 6.2 to – 6.9 $^{o}/_{oo}$ PDB measured in the CO_2 from Nazko bog sampled previously by Williams-Jones, (pers comm, 2013).

Helium in the CO_2 -rich gases can also indicate a magmatic and possibly a geothermal origin for the gas. The ^{3}He:^{4}He ratio has been previously used as an indication of a mantle source for magma and related discharging gas or water. ^{4}Helium is produced by the radiogenic decay for U and Th while ^{3}He is assumed to have been incorporated in the earth at the time of its formation and can thus be termed primordial. Because it is an incompatible element, ^{3}He preferentially becomes incorporated in the primitive molten magma forming the mantle. The ^{3}He:^{4}He ratio has been used to interpret the mantle source for hot spring water and geothermal gas in Iceland (Poreda *et al.* 1992), to study the relationship between a mantle plume and mid Atlantic Ridge basalts (Kurz *et al.* 1998) and to study island arc tectonics in Japan (Horiguchi *et al.* 2010). A premise that a high ^{3}He:^{4}He ratio in hot spot magmas is convincing evidence for a primordial mantle source of the ^{3}He has been questioned by Anderson (1993) who argued that ^{3}He may also be in present extra terrestrial dust. He proposed that extra terrestrial dust could have been deposited into ancient oceans, incorporated in pelagic sediments and then returned to the mantle through subduction where ^{3}He would be released.

The Nazko bogs $^{3}He:^{4}He$ ratios for the seep CO_2 range from 2.55 to 5.94R_A (relative to the atmospheric $^{3}He:^{4}He$ ratio) and these compare to $^{3}He:^{4}He$ ratios between 5.9 and 7.3R_A measured by Hulston and Lupton (1996) in gas samples from Wairakei and Ohaaki-Broadlands geothermal fields, New Zealand. The authors found ratios close to 7.2 R_A for the Wairakei field gases compared to ratios between 3 and 6 R_A for the Ohaaki-Broadlands field gases. Hulston and Lupton (1996) interpreted the Wairakei field ratios to reflect ^{3}He predominantly from mantle subduction whereas gases in the Ohaaki-Broadlands field have ^{3}He and ^{4}He from both mantle subduction and from sedimentary rocks being leached by hot ascending fluid containing radiogenic ^{4}He. Snyder *et al.* (2001) attribute the $^{3}He:^{4}He$ ratios of 6.5$\pm$ 0.7 R_A in geothermal gas and water from Central America to be predominantly of mantle origin. Horiguchi *et al.* (2010) demonstrated a clear relationship between tectonics and $^{3}He:^{4}He$ ratio from a measuring He isotopes in gas and water samples collected from hot and mineral springs in northeastern Japan. They interpreted low ratios (< 1 R_A) in the gas and spring water to be from an area underlain by subduction whereas higher ratios (2 to 5 R_A) reflected the area underlain by the volcanic front and the back-arc region.

Hence, the $^{3}He:^{4}He$ range for the Nazko bog seepage gas suggests that the He and CO_2. are from a combination of mantle and crustal sources. Mantle magma sources proposed for the Nazko area have included a hot spot (Bevier *et al.* 1979), the edge-effect of a slab window (Thorkelson and Taylor, 1989) and injection mantle into brittle crustal rocks between 27 and 28 km depth to form a sill/dyke swarm (Hutchinson, 2012). Magma at a relatively shallow depth could be a source of heat, the He and the CO_2 through reaction of hot fluids with crustal rocks. Absence of hot springs in the Nazko bogs may reflect cooling of water rising to the surface and/or change, with time, in the structure transporting the hot fluids to the surface. One indication for structural influence on gas and fluid transport could be the variation of ^{4}He concentration in the CO_2. The highest ^{4}He measured (120 ppm) is from a a seep sampled in the South Bog (Figure 6.27) whereas there is less than 1 ppm ^{4}He in the North Bog seeps. It is probable that there are several, different pathways beneath the Nazko bogs responsible for transporting fluids and gas to the surface.

Today, most commercially available ^{4}He is recovered from natural gas that can have up to 8 percent ^{4}He and 80 percent N_2. Hot geothermal gases (e.g. in India) can have up to 3 percent (V:V) He and are potentially a viable, alternative source for this element (Chaudhuri, 2015). While the Nazko ^{4}He concentration is much lower than that detected in other areas it could be considered as a potentially recoverable resource given the increasing global shortage of this essential element in the medical field and in industry.

10. Conclusions

Conclusions of this study to identify the source for the anomalous geochemical patterns detected in the Nazko bogs water, soil, rock, vegetation and gases are that:

- Carbon dioxide-rich gas sampled from active seepages in the North and South Bogs have $^{3}He/^{4}He$ ratios between 2.55 and 5.94 $_{RA}$ and a ^{4}He content up to 120 ppm. The $^{3}He/^{4}He$ ratios suggest that the source for the He is mantle degassing. The CO_2 could be derived from a reaction between hot fluids and crustal rocks.
- Elevated concentration of Li, Rb, Sr and B in ground water and soil near a travertine cone-CO_2 vent in the North Bog may be a remnant of a deeper, warmer fluid that has cooled during transport to the surface. Although there is no visible upwelling of water in the area the actual discharge may be concealed beneath the bog sediment.
- The high Hg levels in soil and rock samples reflect the presence of cinnabar and do not appear to be related to the recent geothermal activity.
- While there are now only subtle surface geochemical indicators for geothermal activity, the existence of He in seepage gas and $^{3}He/^{4}He$ ratios are evidence for a mantle heat source in the area beneath the Nazko Cone

11 Recommended further studies

The $^{3}He/^{4}He$ ratios in the CO_2-rich gas seepages and the analysis of the water chemistry data increase the probability of a geothermal heat source beneath the Nazko bogs. Depending on the priority for developing geothermal resources in the Nazko area further studies could focus on:

- A closer examination of geophysical and data and other information to identify geological structures in the area around the Nazko Cone that could be responsible for transporting fluids and gases to the surface.
- Re-sampling and re-analysis of the seepage CO_2 to detect other isotopes (e.g. ^{40}Ar, ^{14}C) and other gases (e.g. hydrocarbons).
- Exploratory diamond drilling beneath the Nazko bogs to identify sub-surface geology, confirm existence of structures and to identify a temperature gradient for the area.
- Detection of CO_2-rich gas seepages at other BC sites such as volcanic centers in the Anahim Volcanic belt (e.g. Satah Mountain, Clisbacko). Use of portable He detector (e.g. Agilent PHD-4) could screen seepages for presence of He in the field, and, if detected, seeps would then be sampled and analysis for ^{3}He, ^{4}He and other isotopes.

12. Acknowledgments

This project has been funded by Geoscience BC as part of the 2013 TREK Project. Jamie Constable, Hazel Paul, Trevor Clement, Dave Sacco and Francis Bertoia helped with the authors sampling and data collection during field work 2013 and 2014. Their assistance was invaluable and greatly appreciated. Nathalie Vigouroux, Glyn Williams-Jones and Brent Ward, (Simon Fraser University), and Catherine Hickson, (Alterra Power Corp.), generously shared information about the Nazko wetlands and loaned sampling equipment. Alexei Rukhlov, (BC Ministry of Energy and Mines), is thanked for allowing water testing equipment from the Geological Survey laboratory to be used. Drs. Joshua Curtice and Mark Kurz of the Department of Marine Chemistry and Geochemistry, Woods Hole Oceanographic Institution kindly advised on the gas sampling technique, provided the sampling equipment, analysed the samples and patiently discussed the results with the authors. Their help is very much appreciated. Our thanks to Dr. Colin Dunn for kindly advising on tree bark sampling and the quality control measures for the vegetation sample analysis. A careful and constructive review of this report by Nathalie Vigouroux-Caillibot is very much appreciated.

13. References

Abzalov, M.Z. (2008): Quality Control of Assay Data: A Review of Procedures for Measuring and Monitoring Precision and Accuracy, *Exploration and Mining Geology,* Vol. 17(3-4), pages 1-14.

Anderson, D.L. (1993): Helium-3 from the mantle: Primordial signal or cosmic dust; *Science,* Vol. 261, July 1993, pages 170-176.

Angen, J.J. Westberg, E. Hart, C.J.R. Kim, R. and Rahami, M. (2015): Preliminary Geological Map of the TREK Project Area, Central British Columbia; Geoscience BC Report 2015-10

BC Geological Survey (2013): MINFILE BC mineral deposits database; BC Ministry of Energy and Mines <http://minfile.ca/> [November 2013].

Bellomo, S and Parello, F. (2007): Geochemistry and mineralogy of travertine deposits of the SW flank of Mt. Etna (Italy): Relationship with past volcanoes and degassing activity; *Journal of Volcanology and Geothermal Research*. Volume 165, pages 64-70.

Berkovic, A. M., Gonzalez, M. C., Russo, N., Michelini, M.C., Diez, R.P., and Mártire, D.O., (2010): Reduction of Mercury (II) by the Carbon Dioxide Radical Anion: A Theoretical and Experimental Investigation; *Journal of Physical Chemistry,* A. 2010, December 16; 114(49), pages 12845-50.

Bevier, M. L., Armstrong R.L and Souther, J.G. (1979): Miocene peralkaline volcanism in west-central British Columbia -- Its temporal and plate-tectonics setting; *Geology*, Vol. 7, pages 389-392.

Cassidy, J.F., Balfour, N., Hickson, C., Kao, H., White, R., Caplan-Auerbach, J., Mazzotti, S., Rogers, G.C., Al-Khoubbi, I., Bird, A.L., Esteban, L., Kelman, M., Hutchinson, J., and McCormack, D. 2011. The 2007 Nazko, British Columbia, Earthquake Sequence: Injection of Magma Deep in the Crust beneath the Anahim Volcanic Belt. *Bulletin of the Seismological Society of America*, **101**(4): 732–1741.

Chaudhuri, H. Sinha, B and Chandrasekharam, D. (2015): Helium from Geothermal Sources; *Proceeding of the World Geothermal Congress*, Melbourne, Australia, 19-25 April 2015, pages 1-14.

Coolbaugh, M. Lechler, P.M., Sladek. C. and Kratt, C. (2010): Lithium in tufas of the Great Basin: Exploration implications for geothermal energy and lithium resources; *Geothermal Resources Council Transactions*, 34, p. 521-526.

Dunn, C. E. (2007): Biogeochemistry in mineral exploration, *Handbook of Exploration and Environmental Geochemistry* No 9 (M. Hale, Editor), Elsevier, 459 pages.

Eccles, D.R. and Berhane, H. (2011): Geological Introduction to Lithium-Rich Formation Water with Emphasis on the Fox Creek Area of West-Central Alberta (NTS 83F and 83K), Energy Conservation Resources Board/Alberta Geological Survey Open File 2011-10, 22 pages.

Faure, G. (1998): Principles and applications of geochemistry, *Prentice Hall*, 600 pages.

Ford, T.D and Pedley, H.M. (1996). A review of travertine word wide; *Earth Science Reviews*, 41 pages 117-175.

Fouke, B.W. Farmer, J.D. Des Marais, D.J. Pratt, L. Sturchio, N.C. Burns, P.C. and Discipulo, M. (2000): Depositional facies and aqueous-solid geochemistry of the travertine-depositing hot springs (Angel) Terrace , Mammoth hot springs, Yellowstone national Park, U.S.A., *Journal of Sedimentary Research,* Volume 70, pages 565-585.

Giustini, F. Blessing, M. Brilli, M. Lombardi, S. Voltattorni, N. and Widory, D. (2013): Determining the origin of carbon dioxide and methane in the gaseous emissions of the San Vittorino plain (Central Italy) by means of stable isotopes and noble gas analysis; *Applied Geochemistry, Volume* 34, pages 90-101.

Horigugchi, K. Ueki, S. Sano, Y. Takahata, N. Hasegawa, A. and Igarashi, G. (2010): Geographical distribution of helium isotope ratios in northeastern Japan, *Island Arc*, 19, pages 60-70.

Heberlein, D. R., Dunn C. E. and Hoffman, E. (2015): Investigation of Tree Sap as a Sample Medium for Regional Geochemical Exploration in Glacial Sediment Covered Terrains: A Case History from the Endako area, North-Central BC(NTS map sheets 093F14, 093F15, 093K03 and 093K02), *Geoscience BC* report 2015 - 2.

Hickson, C.J., Kelman, M.C., Chow, E., Shimamura, K., Servranckz, R., Bensimon, D., Cassidy, J., Trusdel, S. and Williams-Jones, G. (2009); Nazko region volcanic hazard map, *Geological Survey of Canada*, Open File 5978, scale 1:650 000.

Hulston, J.R. and Lupton, J.E. (1996): Helium isotope studies of geothermal fields in the Taupo Volcanic Zone, New Zealand; Journal of *Volcanology and Geothermal Research,* Volume 74 (1996), pages 297-321.

Hutchinson J.A. (2012**):** Relocation and analysis of the 2007 Nechako, B.C., seismic swarm: evidence for magmatic intrusion in the lower crust; *University of Western Washington*, Master's Thesis, 73 pages.

King, S.A., Behnke, S., Slack, K., Krabbenhoft, D., Nordstrom, D., Burr , M.D.C., Robert, G. Striegl, R.G. (2006): Mercury in water and biomass of microbial communities in hot springs of Yellowstone National Park, USA; *Applied Geochemistry* 21 (2006), pages 1868–1879.

Kurz, M.D. LeRoex, A.P. and Dick, H.J.B (1998): Isotope geochemistry of the oceanic mantle near the Bouvet triple junction; *Geochimica et Cosmochimica Acta*, Vol. 62, No 5, pages 841-852.

Leybourne, M.I. and Cameron, E.M. (2007). Groundwater in geochemical exploration: Methods, applications and future directions, in "*Proceedings of Exploration 07: Fifth decennial International Conference on Mineral Exploration*" edited by B. Mikereit, pages 201-221.

Jackaman, W. (2014): Regional Geochemical and Mineralogical Data, TREK Project, Interior Plateau, British Columbia, *Geoscience BC Report*, 2014-10.

Lett, R.E. and Jackaman, W. (2014): Geochemical Expression in Soil and Water of Carbon Dioxide Seepages near the Nazko Volcanic Cone, Interior Plateau, central BC, NTS 93B/13, *Geoscience BC* Report, 2014-10.

Lett, R.E. and Jackaman, W. (2015): Tracing the Source of Anomalous Geochemical Patterns in Carbonate-Rich Bog; *Geoscience BC* Report, 2015-1, pages 13-20.

Lott, D.E.(2001): Improvements in noble gas separation methodology: A nude cryogenic trap; *Geochemistry, Geophysics, Systems*, Volume 2, Issue 12, pages 1068-1075.

Pasvanoglu, S. (2013): Hydrogeochemistry of thermal and mineralized water in the Diyadin (Agri) area, Eastern Turkey, *Applied Geochemistry*, 38, pages 70-81.

Parkhurst, D.L. and Appelo, C.A.J. (1999): Users guide PHREEQC (VERSION 2)—a computer program for speciation, batch-reaction, one dimensional transport and inverse calculations, *U.S. Geological Survey*, Water-Resources Investigations Report 99-4259A, 312 pages.

Pentecost, A. (1995): Geochemistry of carbon dioxide in six travertine-depositing springs of Italy, *Journal of Hydrology*, v 167, pages 263-278.

Poreda, R.J. Craig, H. Arnorsson, S and Welhan, J.A. (1992): Helium isotopes in Icelandic geothermal systems: I. 3He, gas chemistry, and 13C relations; *Geochimica et Cosmochimica Acta*, Vol. 56 pages 4221-4228.

Railsback, L.B. (2015): Some Fundamentals of Mineralogy and Geochemistry, *University of Georgia*, http://www.gly.uga.edu/railsback/Fundamentals/

Riddell, J. (2011): Lithostratigraphic and tectonic framework of Jurassic and cretaceous intermountain sedimentary basins of south-central British Columbia; *Canadian Journal of Earth Sciences*, v. 48, pages 870-896.

Souther, J. G. Clague, J.J. and Mathews, R.W. (1987): Nazko cone: a Quaternary volcano in eastern Anahim Belt; *Canadian Journal of Earth Sciences*, v. 24, pages 2477-2485.

Snyder, G. Poreda, R. Hunt, A. and Fehn, H. (2001): Regional variations in volatile composition: Isotopic evidence for carbonate recycling in the Central American volcanic arc; *Geochemistry, Geophysics, Systems*, Vol. 2, pages 263-288.

Talinga, D. and Calvert, A.J. (2014): Distribution of Paleogene and Cretaceous rocks around the Nazko River belt of central British Columbia from 3-D long-offset first-arrival seismic tomography; *Canadian Journal of Earth Sciences*, Vol. 51, pages 358–372.

Thorkelson, D.J. and Taylor, R.P. (1989): Cordilleran slab windows, *Geology*, v. 17, pages 833-836.

Appendix A – Statistics for soil samples collected in 2014

Element	MDL	Mean	Median	3 Quatile	95 pctile	3Q+1.5IQR	Min	Max
Ag ppb ARMS	2	104	83	117	253	212	23	311
Al pct ARMS	0.01	1.84	1.90	2.39	3.99	4.34	0.07	4.54
As ppm ARMS	0.1	4.0	2.7	5.7	8.6	11.8	0.1	17.5
Au ppb ARMS	0.2	0.4	0.1	0.1	1.6	0.1	0.1	2.6
B ppm ARMS	20	15	10	10	51	10	8	68
Ba ppm ARMS	0.5	226.0	179.0	290.6	446.1	517.7	48.0	463.3
Ba ppm LMB	5	630	661	746	820	1042	245	837
Be ppm ARMS	0.1	0.6	0.5	0.8	1.5	1.3	0.0	2.1
Bi ppm ARMS	0.02	0.10	0.08	0.10	0.14	0.15	0.01	0.20
Ca pct ARMS	0.01	2.65	0.31	0.44	20.81	0.70	0.20	25.51
Cd ppm ARMS	0.01	1.20	0.41	0.78	1.98	1.62	0.07	15.49
Ce ppm ARMS	0.1	21.1	18.5	25.8	44.5	42.9	1.0	62.9
Ce ppm LMB	30	36	39	48	61	98	15	72
Co ppm ARMS	0.10	20.01	16.80	19.75	37.47	29.43	0.87	75.30
Co ppm LMB	20	25	23	29	46	58	10	78
Cr ppm ARMS	0.5	46.8	52.9	63.2	68.2	108.9	1.9	70.8
Cs ppm ARMS	0.02	0.75	0.58	0.71	2.46	1.09	0.06	3.45
Cu ppm ARMS	0.01	21.73	16.92	30.97	45.83	57.56	2.68	49.54
Cu ppm LMB	5	33	29	40	54	63	11	56
Fe pct ARMS	0.01	3.72	3.79	4.31	6.34	6.23	0.16	7.90
Ga ppm ARMS	0.1	6.5	6.0	7.8	16.6	13.3	0.2	20.9
Ge ppm ARMS	0.1	0.1	0.1	0.1	0.2	0.1	0.1	0.2
Hf ppm ARMS	0.02	0.29	0.28	0.38	0.57	0.68	0.02	0.86
Hg ppb ARMS	5	244	69	107	736	208	34	2461
In ppm ARMS	0.02	0.03	0.03	0.04	0.05	0.08	0.01	0.06
K pct ARMS	0.01	0.08	0.07	0.10	0.12	0.15	0.02	0.12
La ppm ARMS	0.5	8.7	8.3	11.5	16.0	21.0	0.4	21.2
Li ppm ARMS	0.1	7.0	5.5	8.8	12.9	14.3	0.4	15.2
Mg pct ARMS	0.01	0.58	0.46	0.75	1.02	1.28	0.23	1.22
Mn ppm ARMS	1	674	509	902	1598	1792	219	2067
Mo ppm ARMS	0.01	1.92	1.99	2.62	3.62	5.14	0.34	3.66
Na pct ARMS	0.001	0.032	0.011	0.015	0.134	0.023	0.003	0.187
Nb ppm ARMS	0.02	2.15	1.64	2.59	5.07	5.02	0.18	7.91
Nb ppm LMB	5	17	15	19	45	27	3	46
Ni ppm ARMS	0.1	109.4	82.1	98.0	435.4	157.7	8.2	517.7
Ni ppm LMB	20	126	99	109	451	163	35	516
P pct ARMS	0.001	0.10	0.08	0.1305	0.2403	0.25	0.03	0.27
Pb ppm ARMS	0.01	4.82	5.28	5.95	6.82	8.03	0.59	8.00
Pd ppb ARMS	10	5	5	5	5	5	1	21
Pt ppb ARMS	2	2	1	2	5	2	1	10
Rb ppm ARMS	0.1	7.3	7.2	9.6	12.0	16.0	0.8	12.7

Element	MDL	Mean	Median	3 Quatile	95 pctile	3Q+1.5IQR	Min	Max
Re ppb ARMS	1.0	1.3	0.5	0.5	2.0	0.5	0.5	14.0
S pct ARMS	0.02	0.07	0.01	0.03	0.22	0.06	0.01	0.67
Sb ppm ARMS	0.02	0.43	0.27	0.40	1.44	0.69	0.08	1.49
Sc ppm ARMS	0.1	6.0	4.5	7.9	15.3	14.8	0.5	22.3
Sc ppm LMB	1	15	14	17	24	23	2	38
Se ppm ARMS	0.1	0.7	0.3	0.7	3.2	1.4	0.1	4.9
Sn ppm ARMS	0.1	0.7	0.7	0.8	1.3	1.3	0.1	1.3
Sr ppm ARMS	0.5	552.9	43.3	56.1	3682.8	89.4	30.5	6191.3
Sr ppm LMB	2	554	336	373	1124	477	187	3977
Ta ppm ARMS	0.05	0.04	0.03	0.03	0.10	0.03	0.03	0.14
Te ppm ARMS	0.02	0.02	0.01	0.03	0.07	0.05	0.20	0.16
Th ppm ARMS	0.1	1.4	1.7	1.9	2.5	3.4	0.0	3.0
Ti pct ARMS	0.001	8.225	0.295	0.439	65.819	0.827	0.057	109.0
Tl ppm ARMS	0.02	0.55	0.20	0.66	1.49	1.49	0.04	4.03
U ppm ARMS	0.1	0.6	0.5	0.8	1.5	1.6	0.1	1.9
V ppm ARMS	2	71	83	90	126	138	1	148
Y ppm ARMS	0.01	8.52	4.52	7.80	15.54	14.64	0.39	75.69
Y ppm LMB	3	18	14	17	26	22	2	79
Zn ppm ARMS	0.1	90.5	78.2	120.1	173.6	199.9	22.7	196.6
Zn ppm LMB	5	138	115	160	294	249	41	328
Zr ppm ARMS	0.1	18.2	15.5	24.1	39.3	45.6	1.2	57.8
Zr ppm LMB	5	186	197	224	249	286	29	250

Element	MDL	Mean	Median	3 quartile	95 pctile	1 quartile	3Q+1.5IQR	MIN	MAX
SiO2 PCT LMB	0.01	51.34	58.09	59.79	63.42	53.79	68.79	9.92	64.00
Al2O3 PCT LMB	0.01	13.11	14.51	15.31	16.13	13.54	17.97	2.40	16.42
Fe2O3 PCT LMB	0.04	7.43	7.66	8.06	11.61	7.10	9.50	1.37	11.99
MgO PCT LMB	0.01	1.67	1.51	1.73	2.58	1.35	2.30	1.15	2.65
CaO PCT LMB	0.01	4.10	2.63	2.82	4.74	2.14	3.84	1.96	33.89
Na2O PCT LMB	0.01	1.83	1.91	2.36	2.63	1.51	3.64	0.46	2.68
K2O PCT LMB	0.01	1.23	1.40	1.51	1.59	1.23	1.93	0.26	1.63
TiO2 PCT LMB	0.01	1.67	1.67	1.93	3.30	1.52	2.55	0.27	3.52
P2O5 PCT LMB	0.01	0.30	0.21	0.33	0.85	0.15	0.60	0.07	1.01
MnO PCT LMB	0.01	0.12	0.09	0.14	0.23	0.07	0.25	0.04	0.31
Cr2O3PCT LMB	0.002	0.027	0.029	0.033	0.038	0.026	0.044	0.004	0.046
LOI_PCT_GRAV	0.1	16.93	9.40	13.6	50	8.3	21.55	6.40	66.90
C_PCT_LECO	0.02	5.64	1.76	3.48	23.92	1.33	6.71	0.49	37.85
S_PCT_LECO	0.02	0.06	0.01	0.03	0.17	0.01	0.06	0.01	0.67

Table A 1. The statistics calculated from trace and minor element, minor and major oxide data for 22 North Bog B soil horizon samples collected in 2014. MDL = minimum detection limit. Values below detection limit converted to 1/2 reported detection limit. ARMS = Aqua regia-ICPMS analysis. LMB = Lithium borate-ICPMS analysis. LOI = Loss on ignition. LECO =Leco method for total C and S. pctile - percentile.

Element	MDL	Mean	Median	3 quartile	95 pctil	3Q+1.5IQR	Min	Max
Ag ppb ARMS	2	112	91	166	212	319	30	279
Al pct ARMS	0.01	1.51	1.40	1.81	2.74	3.01	0.17	2.77
As ppm ARMS	0.1	7.3	5.8	9.3	14.5	15.9	0.1	17.7
Au ppb ARMS	0.2	1.3	0.9	1.9	3.6	4.0	0.1	5.6
B ppm ARMS	20	12	10	10	21	10	10	39
Ba ppm ARMS	0.5	163.1	143.4	208.3	265.1	343.8	69.0	314.3
Ba ppm LMB	5	609	598	707	767	928	223	873
Be ppm ARMS	0.1	0.6	0.6	0.6	1.0	0.8	0.1	1.6
Bi ppm ARMS	0.02	0.09	0.08	0.09	0.13	0.12	0.01	0.22
Ca pct ARMS	0.0	1.4	0.4	0.5	1.6	0.8	0.1	20.5
Cd ppm ARMS	0.01	0.65	0.37	0.80	2.38	1.67	0.15	3.11
Ce ppm ARMS	0.1	25.9	27.4	28.6	37.7	39.3	2.6	38.4
Ce ppm LMB	30	35	44	46	52	93	15	54
Co ppm ARMS	0.1	17.5	15.9	19.8	24.4	27.5	6.3	40.6
Co ppm LMB	20	22	24	26	31	34	10	46
Cr ppm ARMS	0.5	50.1	53.9	58.0	66.1	77.8	3.8	74.5
Cs ppm ARMS	0.02	0.95	0.65	0.82	1.32	1.17	0.36	5.86
Cu ppm ARMS	0.01	35.85	35.72	42.60	58.29	63.17	10.67	63.79
Cu ppm LMB	5	47	50	54	65	81	16	73
Fe pct ARMS	0.01	3.68	3.69	4.17	4.68	5.52	0.53	5.48
Ga ppm ARMS	0.1	4.9	4.8	5.9	8.7	9.7	0.4	8.7
Ge ppm ARMS	0.1	0.1	0.1	0.1	0.1	0.1	0.1	0.3
Hf ppm ARMS	0.02	0.37	0.38	0.42	0.56	0.65	0.15	0.60
Hg ppb ARMS	5	455	270	420	1035	863	52	3137
In ppm ARMS	0.02	0.03	0.03	0.04	0.05	0.06	0.01	0.07
K pct ARMS	0.01	0.08	0.08	0.1	0.1	0.13	0.02	0.12
La ppm ARMS	0.5	12.3	11.4	15.3	21.4	25.2	1.2	28.3
Li ppm ARMS	0.1	9.5	5.0	6.2	29.5	9.1	2.2	51.6
Mg pct ARMS	0.01	0.60	0.56	0.68	0.91	0.91	0.22	1.06
Mn ppm ARMS	1	541	450	656	990	1072	246	1064
Mo ppm ARMS	0.01	2.23	2.35	2.77	4.11	5.50	0.57	5.70
Na pct ARMS	0.001	0.029	0.021	0.028	0.096	0.049	0.007	0.097
Nb ppm ARMS	0.02	1.12	0.49	0.91	4.32	1.93	0.07	4.77
Nb ppm LMB	5	14	15	16	18	22	3	19
Ni ppm ARMS	0.1	101.2	82.5	99.5	210.6	164.9	43.1	350.9
Ni ppm LMB	20	113	101	119	203	205	51	370
P pct ARMS	0.001	0.069	0.067	0.080	0.124	0.124	0.015	0.126
Pb ppm ARMS	0.01	5.23	5.48	5.86	6.87	7.47	0.63	6.96
Pd ppb ARMS	10	6	5	5	18	5	5	20
Pt ppb ARMS	2	2	1	2	4	4	1	6
Rb ppm ARMS	0.1	8.5	7.9	10.5	12.8	16.7	1.7	13.3
Re ppb ARMS	1	1	1	1	4	1	1	6
S pct ARMS	0.02	0.05	0.02	0.04	0.11	0.09	0.01	0.58
Sb ppm ARMS	0.02	0.71	0.68	0.90	1.72	1.64	0.25	1.75
Sc ppm ARMS	0.1	6.8	6.6	8.1	8.8	11.9	2.3	12.5
Sc ppm LMB	1	15	15	17	19	20	5	21
Se ppm ARMS	0.1	0.8	0.6	0.8	2.5	1.9	0.1	5.0
Sn ppm ARMS	0.1	0.54	0.50	0.6	0.8	0.90	0.05	1.20

Element	MDL	Mean	Median	3 quartile	95 pctil	3Q+1.5IQR	Min	Max
Sr ppm ARMS	0.5	236.1	45.3	53.2	588.4	74.7	25.7	3339.6
Sr ppm LMB	2	538	372	415	824	562	273	3614
Te ppm ARMS	0.02	0.03	0.03	0.03	0.06	0.06	0.01	0.10
Th ppm ARMS	0.1	1.8	1.8	2.2	2.7	3.3	0.1	2.7
Ti pct ARMS	0.001	0.215	0.235	0.295	0.428	0.589	0.027	0.438
Tl ppm ARMS	0.02	0.67	0.37	0.88	2.50	1.98	0.11	2.51
U ppm ARMS	0.1	0.9	0.6	0.7	1.8	1.0	0.3	4.6
V ppm ARMS	2	72	74	85	92	117	10	94
Y ppm ARMS	0.01	12.68	10.87	11.96	33.16	18.91	1.43	53.42
Y ppm LMB	3	23	21	23	40	29	2	62
Zn ppm ARMS	0.1	83.1	75.4	91.0	134.1	123.1	16.5	165.1
Zn ppm LMB	5	113	107	113	170	139	20	215
Zr ppm ARMS	0.1	21.6	20.1	27.1	31.1	44.4	10.9	36.5
Zr ppm LMB	5	175	181	189	209	224	82	214

Element	MDL	Mean	Median	3 quartile	95 pctil	3Q+1.5IQR	Min	Max
SiO2 PCT LMB	0.01	56.47	59.80	61.98	65.73	71.10	3.63	67.79
Al2O3 PCT LMB	0.01	13.74	14.50	15.13	16.03	16.66	0.89	16.23
Fe2O3 PCT LMB	0.04	7.41	7.53	8.09	9.27	9.44	0.94	9.91
MgO PCT LMB	0.01	1.77	1.74	2.01	2.33	2.64	0.84	2.62
CaO PCT LMB	0.01	4.00	2.58	3.16	3.81	4.53	1.68	31.61
Na2O PCT LMB	0.01	1.88	1.83	2.31	2.72	3.51	0.22	2.77
K2O PCT LMB	0.01	1.39	1.47	1.60	1.69	2.10	0.10	1.96
TiO2 PCT LMB	0.01	1.36	1.37	1.61	1.74	2.14	0.10	1.77
P2O5 PCT LMB	0.01	0.18	0.18	0.21	0.33	0.32	0.07	0.33
MnO PCT LMB	0.01	0.10	0.09	0.12	0.15	0.18	0.06	0.17
Cr2O3PCT LMB	0.002	0.029	0.029	0.034	0.047	0.051	-0.002	0.049
LOI PCT	0.1	11.4	6.8	9.5	28.6	14.3	5.5	59.7
C PCT LECO	0.02	2.49	0.66	0.90	9.17	1.74	0.10	27.14
S PCT LECO	0.02	0.04	0.02	0.04	0.09	0.09	0.01	0.37

Table A 2. The statistics calculated from trace and minor element and major oxide data for 21 North Bog C soil horizon samples collected in 2014. MDL = minimum detection limit. Values below detection limit converted to 1/2 reported detection limit. ARMS = Aqua regia-ICPMS analysis. LMB = Lithium borate-ICPMS analysis. LOI = Loss on ignition. LECO =Leco method for total C and S. pctile - percentile.

Element	MDL	Mean	Median	3 Qtile	95 pctile	3Q+1.5IQR	Min	Max
Ag ppb	2	83	67	111	181	219	4	197
Al pct	0.01	1.25	1.20	1.70	2.12	4.22	0.01	2.55
As ppm	0.1	2.5	2.0	3.0	5.5	7.0	0.1	6.1
Au ppb	0.2	0.2	0.1	0.1	0.7	0.1	0.1	1.0
B ppm	1	5	2	4	12	7	1	41
Ba ppm	0.1	293.3	282.9	344.3	425.9	461.0	110.5	556.2
Be ppm	0.1	0.4	0.3	0.5	0.7	0.8	0.1	0.7
Bi ppm	0.02	0.07	0.07	0.09	0.10	0.11	0.01	0.10
Ca pct	0.01	2.84	0.85	1.54	5.65	3.69	0.39	33.88
Cd ppm	0.01	0.93	0.69	1.19	2.03	2.62	0.06	3.89
Ce ppm	0.01	15.61	14.44	23.35	26.71	58.35	0.13	30.53
Co ppm	0.01	14.10	12.44	15.6	24	20.16	5.21	51.87
Cr ppm	0.1	36.20	34.60	51.3	62.6	127.7	0.50	68.90
Cs ppm	0.005	0.480	0.396	0.616	0.803	1.465	0.060	0.810
Cu ppm	0.01	13.70	12.76	15.75	25.52	30.34	0.83	30.86
Fe pct	0.001	2.436	2.089	3.210	4.210	5.703	0.379	4.658
Ga ppm	0.1	4.6	4.7	6.1	7.7	14.7	0.1	8.3
Ge ppm	0.01	0.05	0.05	0.06	0.09	0.08	0.02	0.14
Hf ppm	0.001	0.230	0.212	0.321	0.437	0.487	0.003	0.470
Hg ppb	1	118	123	145	187	362	15	191
In ppm	0.02	0.02	0.02	0.03	0.04	0.05	0.01	0.04
K pct	0.01	0.13	0.13	0.14	0.20	0.28	0.02	0.21
La ppm	0.01	5.88	5.84	7.79	10.16	11.41	0.06	12.03
Li ppm	0.01	5.29	5.46	6.43	8.54	14.56	1.87	10.13
Mg pct	0.001	0.410	0.372	0.451	0.836	0.566	0.158	0.894
Mn ppm	1	1150	1306	1441	1634	3599	206	2281
Mo ppm	0.01	3.16	3.34	4.04	4.86	5.30	0.11	5.38
Na pct	0.001	0.028	0.009	0.011	0.159	0.013	0.004	0.175
Nb ppm	0.01	3.74	4.09	5.13	5.54	7.62	0.03	6.46
Ni ppm	0.1	60.9	43.0	56.0	114.7	121.0	14.8	329.7
P pct	0.001	0.101	0.104	0.124	0.132	0.160	0.035	0.157
Pb ppm	0.01	6.00	6.23	7.20	8.66	8.73	0.11	8.78
Pd ppb	2	2	1	1	5	2	1	7
Pt ppb	1	1	1	1	1	1	1	2
Rb ppm	0.1	7.4	8.3	9.8	12.7	23.6	0.5	14.5
Re ppb	1	1	1	1	1	1	1	4
S pct	0.01	0.16	0.10	0.15	0.26	0.23	0.06	1.06
Sb ppm	0.02	0.33	0.27	0.44	0.58	0.98	0.04	0.85
Sc ppm	0.1	3.6	3.1	4.8	6.4	11.8	0.1	7.1
Se ppm	0.1	0.4	0.3	0.5	0.9	1.2	0.1	1.8
Sn ppm	0.02	0.51	0.52	0.70	0.83	1.75	0.01	0.84
Sr ppm	0.5	659.1	109.8	169.8	1663.9	423.3	54.7	9700.5
Ta ppm	0.001	0.002	0.001	0.002	0.008	0.004	0.001	0.014
Te ppm	0.02	0.01	0.01	0.01	0.02	0.01	0.01	0.02
Th ppm	0.01	0.82	0.73	1.29	1.57	2.12	0.01	1.58
Ti pct	1	1790	1701	2666	3142	6660	12	3423
Tl ppm	0.02	0.27	0.14	0.34	0.68	0.73	0.05	1.64
U ppm	0.01	0.27	0.25	0.29	0.53	0.58	0.04	0.94
V ppm	2	31	29	45	57	111	1	62
Y ppm	0.001	3.605	3.495	4.483	6.273	6.602	0.131	9.819
Zn ppm	0.1	100.7	109.9	136.2	146.3	250.0	6.0	179.7
Zr ppm	0.01	13.33	11.58	19.94	24.10	45.25	0.17	25.48

Table A 3. The statistics calculated from trace and minor element data for 19 North Bog B Ah horizon humus samples collected in 2014 and analysed by ARMS = Aqua regia-ICPMS. MDL = minimum detection limit. Values below detection limit converted to 1/2 reported detection limit.

Element	MDL	Mean	Median	3 quartile	95 pctile	3Q+1.5IQR	MIN	MAX
Ag ppb	2	14.53	13.00	14.50	34.80	22.75	7.00	39.00
Al pct	0.01	0.02	0.02	0.02	0.03	0.03	-0.01	0.03
B ppm	1	4	4	5	6	8	2	7
Ba ppm	0.1	37.6	8.7	11.5	200.8	17.6	5.5	251.3
Ca pct	0.01	0.44	0.26	0.35	1.37	0.52	0.18	1.46
Cd ppm	0.01	0.30	0.22	0.46	0.60	0.88	0.03	0.61
Ce ppm	0.01	0.20	0.17	0.20	0.36	0.26	0.12	0.55
Co ppm	0.01	0.12	0.10	0.13	0.17	0.16	0.08	0.24
Cr ppm	0.1	2.1	2.1	2.3	2.5	2.6	1.8	2.6
Cs ppm	0.005	0.01	0.01	0.01	0.01	0.01	-0.01	0.02
Cu ppm	0.01	3.52	3.29	3.47	5.56	4.29	2.34	7.27
Dy ppm	0.02	0.01	0.01	0.01	0.02	0.01	0.01	0.03
Fe pct	0.001	0.017	0.014	0.016	0.034	0.019	0.009	0.050
Gd ppm	0.02	0.02	0.01	0.02	0.04	0.04	0.01	0.06
Ge ppm	0.01	0.01	0.01	0.02	0.02	0.03	0.01	0.03
Hf ppm	0.001	0.006	0.005	0.006	0.013	0.008	0.002	0.016
Hg ppb	1	39	31	39	79	60	16	95
K pct	0.01	0.06	0.05	0.06	0.10	0.09	0.03	0.15
La ppm	0.01	0.08	0.07	0.08	0.15	0.11	0.05	0.23
Li ppm	0.01	0.03	0.02	0.02	0.07	0.02	0.01	0.07
Mg pct	0.001	0.032	0.028	0.034	0.050	0.043	0.024	0.051
Mn ppm	1	87	69	79	184	108	32	369
Mo ppm	0.01	0.07	0.06	0.08	0.12	0.10	0.04	0.18
Na pct	0.001	0.001	0.001	0.001	0.002	0.001	0.001	0.004
Nb ppm	0.01	0.03	0.02	0.03	0.05	0.05	0.01	0.06
Nd ppm	0.02	0.09	0.08	0.09	0.19	0.14	0.05	0.29
Ni ppm	0.1	0.6	0.5	0.7	0.9	1.2	0.3	1.0
P pct	0.001	0.018	0.016	0.018	0.027	0.023	0.012	0.032
Pb ppm	0.01	0.17	0.16	0.19	0.35	0.30	0.07	0.43
Pr ppm	0.02	0.01	0.01	0.01	0.04	0.01	0.01	0.06
Rb ppm	0.1	0.5	0.4	0.6	1.1	0.9	0.2	1.2
S pct	0.01	0.02	0.02	0.03	0.03	0.04	0.01	0.04
Sb ppm	0.02	0.01	0.01	0.02	0.02	0.04	0.01	0.03
Sc ppm	0.1	0.3	0.3	0.4	0.4	0.6	0.2	0.5
Sm ppm	0.02	0.02	0.01	0.02	0.04	0.04	0.01	0.05
Sn ppm	0.02	0.02	0.01	0.02	0.03	0.04	0.01	0.03
Sr ppm	0.5	26.9	15.8	25.7	75.1	47.1	7.2	89.9
Ta ppm	0.001	0.001	0.001	0.001	0.002	0.001	0.001	0.002
Th ppm	0.01	0.01	0.01	0.01	0.01	0.01	0.01	0.02
Ti pct	1	14	12	14	27	18	7	29
Tl ppm	0.02	0.01	0.01	0.01	0.02	0.01	0.01	0.03
Y ppm	0.001	0.07	0.06	0.07	0.14	0.09	0.04	0.21
Yb ppm	0.02	0.01	0.01	0.01	0.01	0.01	0.01	0.02
Zn ppm	0.1	38.6	29.7	35.4	85.4	48.6	20.5	105.1
Zr ppm	0.01	0.21	0.18	0.18	0.44	0.21	0.11	0.53

Table A 4. Statistics from trace and minor element data for 15 North Bog lodge pole pine (*Pinus contorta)* bark samples collected in 2014 and analysed by ARMS = Aqua regia-ICPMS. MDL = minimum detection limit. Values below detection limit converted to $^{1}/_{2}$ reported detection limit.

Appendix B.1 - Stable Isotope Analysis.

250uL of water is placed with a Hokko bead stick into a Exetainer vial (Labco p/n: 038W), then capped and flushed with either a 0.5% CO_2 + balance helium or 2% H_2 + balance helium gas mix respectively. Vials are flushed for ~10minutes at ~70ml/min then placed in the heated block of the GasBench at 25ºC and left to react for ~20 and 1 hour for CO_2 and H_2 respectively. The CO_2 or H_2 headspace is then sampled automatically by the Gas Bench using a sample loop (typically 50uL) and inlet to the ion source of a DeltaV^{Plus} stable isotope ratio mass spectrometer for analysis of $^{2}H/^{1}H$ and $^{18}O/^{16}O$ ratios. The headspace of each vial is sampled 6 times by loop injection and the first peak is discarded and the subsequent 5 injections are acquired. If the first peak is > 30 [V], the subsequent 5 injections are automatically diluted by ~ 1/3. Measurement of ^{2}H and ^{18}O are made in two separate sequences, optimizing the ion source first for HD and then for ^{18}O respectively. Raw data is corrected for drift and normalized to the international VSMOW-VSLAP scale using LIMs (USGS). Final results are expressed in the usual per mil notation.

Exetainers (Labco p/n: 038W) are loaded with 250 uL of 85% H_2PO_4, capped and flushed with UHP helium at ~70ml/min for 10minutes. Based on the alkalinity, an amount of sample equal to ~0.250mg of pure $CaCO_3$ is injected into the vial. Vials are placed in the heated block of the GasBench at 25^{o}C and left to react for ~5 hours. The evolved CO_2 headspace is then sampled automatically by the Gas Bench using a sample loop (typically 50uL) and inlet to the ion source of a DeltaV^{Plus} stable isotope ratio mass spectrometer for analysis of $^{13}C/^{12}C$ ratios. The headspace of each vial is sampled 6 times by loop injection. The first peak is discarded and the subsequent 5 injections are acquired. If the first peak is > 30 [V], the subsequent 5 injections are automatically diluted by ~ 1/3.

Appendix B.2 -Helium Isotope Analysis

Copper tubes (~ 13 cc volume)were attached to a custom built Ultra-High-Vacuum (UHV) line via viton o-ring and introduced into the extraction line via a 0.75cc stainless steel aliquot, so multiple aliquots could be taken if necessary. Only one sample had measurable water (2015-TREK-GT-1B, 11.94 grams) and the remaining samples were entirely gaseous. The gas was purified using charcoal at liquid nitrogen temperature, followed by active metal (SAES ST707) gettering at high and low temperature. Helium was cryogenically separated from the other noble gases (e.g., Lott, 2001). The gas samples were automatically split on the extraction line, using pre-measurement with a quadrupole mass spectrometer, by a factor varying between 1 and ~ 1000, to ensure that appropriate amounts were inlet into the mass spectrometer.

Splitting volumes were calibrated manometrically and were used to calculate total gas abundances. Helium concentrations and isotopic compositions were analyzed via magnetic sector mass spectrometry by comparison to air standards ($^{3}He/^{4}He$ = 1.384 x 10^-6). The full procedural blank is typically less than 1 x 10^-10 cc STP 4He, and is insignificant relative to sample helium contents in all cases, except possibly 2015-TREK-GT-1B.Uncertainties for ^{4}He abundances are approximately 5% due to the variability in copper tube volume along with the splitting procedures.

Appendix G - Location of Samples from Marmot Falls and Redwater Creek